UNIVERSITY OF CALIFORNIA
SANTA CRUZ

# KELP AND CARBON: PATHWAYS AND BARRIERS TO ACQUISITION AND TRANSPORT

A dissertation submitted in partial satisfaction
of the requirements for the degree of

DOCTOR OF PHILOSOPHY

in

ECOLOGY AND EVOLUTIONARY BIOLOGY

by

**Sarah Tepler Drobnitch**

December 2016

The Dissertation of Sarah Tepler Drobnitch is approved:

_____
Professor Jarmila Pittermann, chair

_____
Professor Mark H. Carr

_____
Professor Peter Raimondi

_____
Professor Matthew Edwards

_____
Tyrus Miller
Vice Provost and Dean of Graduate Studies

**Table of Contents**

## List of Figures and Illustrations

**Abstract**

KELP AND CARBON: PATHWAYS AND BARRIERS TO ACQUISITION AND TRANSPORT

Sarah Tepler Drobnitch

Large brown algae in the class Phaeophyceae (Heterokontophyta) form the structural and energetic foundation of temperate and subtropical nearshore marine forests of high productivity and ecological diversity. This dissertation examines the carbon uptake and transport physiology of large brown algae with a particular focus on the plastic or adaptive responses of these physiological traits to their abiotic environment. Chapter 1 takes an anatomical and modeling approach to investigate the structure and function of photosynthate transport networks (analogous to phloem) in diverse members of the Laminariales. To evaluate the existence of scaling and optimization of the kelp vascular system, a model of optimized transport anatomy was developed and tested with a diverse suite of kelp species in the Laminariales. Results revealed a surprising lack of universal scaling in the kelps and the presence of optimized transport anatomy in the giant kelp (*Macrocystis pyrifera*) only. Chapter 2 focuses on the dynamics of carbon uptake in *M. pyrifera*, which can acquire both carbon dioxide and bicarbonate as carbon substrates for photosynthesis. To evaluate whether the proportion of carbon dioxide and bicarbonate utilized by *M. pyrifera* is constant or a variable function of their fluctuating environment, oxygen evolution experiments were carried out on entire blades from several targeted populations in the

Monterey Bay. Results indicated that *M. pyrifera* possesses a plastic carbon uptake physiology in which proportionally more bicarbonate is used in high irradiance and high flow conditions, but that local populations have not yet developed fixed genetic differences. Chapter 3 investigates the mechanism and patterns of carbon stable isotope discrimination in *M. pyrifera*. Results of a dual field and laboratory incubation approach indicate that $^{13}C$ discrimination patterns are determined by a complex interaction of light intensity, dissolved inorganic carbon limitation, and fractionation occurring during transport of polysaccharides. Overall, this dissertation informs patterns and mechanisms of carbon uptake and transport in kelps, and highlights the many ways in which kelps may impact and structure their ecosystems.

I dedicate this dissertation to my grandparents Arlene, Wesley, Sylvia, and Ephraim, trailblazers in all directions.

## Acknowledgements

*Publications.*

Chapters 1 and 2 are lightly edited versions of the following publications:

Drobnitch, S.T., Nickols, K.J., and M. Edwards. 2016. Abiotic influences on bicarbonate use in the giant kelp, *Macrocystis pyrifera*, in the Monterey Bay. *Journal of Phycology.* In press.

Drobnitch, S.T., Jensen, K.H., Prentice, P., and J. Pittermann. 2015. Convergent evolution of vascular optimization in kelp (Laminariales). *Proceedings of the Royal Society B* 282: 20151667.

I gratefully acknowledge my coauthors. In Drobnitch et al. 2015, Kaare developed the model of optimal vascular transport in macroalgae and contributed methods and Paige acquired micrographs and analyzed data. In Drobnitch et al. 2016, Kerry gathered and analyzed all in situ flow velocity data at the Hopkins Marine Station.

*Advisors of all kinds.*

I seriously thank Dick Zimmermann for his indulgent moonlighting as an unofficial technical physiology advisor. Michael Knoblauch for his incredible enthusiasm, expertise, and generosity. Jan Knoblauch, for patiently teaching me fine techniques despite my advanced age. Matt Edwards for his support, interest, and technical

knowledge. Pete Raimondi for his statistical advice, life advice, and generous spirit. Mark Carr for his bold and decisive advice and his willingness to machete through the weeds of kelp physiology. Finally, Jarmila Pittermann, for promoting creativity and practicality in all of my work, and extending so willingly into an alien seaweed world.

*Interns.*

First, thank you to the indefatigable Taylor Pochron, who did a huge amount of work helping to build, maintain, and collect data from FLAVI, all the while entertaining me with stories of Growing Up Greek. Thank you also to Celine Miranda, who did an almost equally huge amount of work on FLAVI. Thank you to Olga Johnson, Marilyne Allietta, Jose Ayala, and Zachary Benavidez for incredible amounts of experimental and analytical lab work, without which I would have nothing.

*Specimen Collection.*

As everyone full well knows, I am a terrible, fearful, suspicious, highly un-accredited diver. I could not have done any of my work without the incredible kelp collection missions organized and mounted by Mike Fox, Mark Readdie, Emily Saarman, Dan Malone, Jose Ayala, Kate Vylet, Tristan McHugh, Colin Gaylord, Todd Van Natta, Rudy Raimondi, and many more PISCO volunteers, past and present. Thanks to all of you for dragging your exhausted bodies and boats around the Monterey Bay every damn day.

*Building experiments.*

I profusely thank Erick Sturm and the NOAA Southwest Fisheries Science Center for providing access to a Loligo respirometer, as well as support, infrastructure, advice, and large periodic doses of skepticism and science-related nihilism. Chapter 2 would not exist without him.

I profusely thank Mark Carr, Todd Van Natta, Randolph Skrovan, Nate Moore, Betsy Steele, and Danny Drobnitch (Sexiest Field Assistant Alive, 2011-2016, *People Magazine*) for their dedicated help in designing, assembling, and troubleshooting FLAVI and all of my other seawater-based experimental setups. They are a fount of knowledge, dexterity, and strength. I always wear my safety glasses and never mix seawater and electricity.

*Pittermann Lab Members.*

I am eternally grateful to Alex Baer, Kate Cary, Jim Wheeler, Jenn Mahley, Leah Smyth, and Helen Holmlund for their careful advice, frequent help, and cathartic commiseration. May we be reunited during the second coming of the Ferns and the Fern Allies.

*Raimondi-Carr Lab Members.*

To my great distress, I am pretty sure I will never have a scientific family like this again. I appreciate and love the friendship, advice, and logistical support freely

given by Emily Saarman (Angry Den Mother just wants to be understood), Dan Malone (Will work for food), Kendra Karr, Ann-Marie Osterback, Don Profesor Rodrigo Beas (Surfing sucks, don't try it), Kim Brewitt, Dan Brumbaugh, Brenna Mahoney, Brent Hughes, Mary Young, Kristin DeNesnera (Marshalls model and champion of justice), Maya Friedman-Simler (Weariest and First Jew), Monica Moritsch (time traveler), Kate Melanson (Most Upbeat and Third Jew), Gina Contolini (Fellow angry snail-wrangler), Roy Qi (Reels. I need Reels.), Kat Beheshti (Lady Who Lunches in Marshes), Josh Smith (who is he really), Mark Morales (cries every Taco Time), Ellen Willis-Norton (most dignified lab member), Taylor White (Poster child for Wild Alaska), Casey Sheridan (Least judgemental lab member) and especially Rachel Zuercher (morally superior cubicle mate for life).

*Funding sources.*

Funding for this work was provided by an NSF GRFP stipend, an NSF REU (NSF 1157090), the UCSC Chancellor's Fellowship, the Department of Ecology and Evolutionary Biology, the Botanical Society of America, the Phycological Society of America, the California Native Plant Society, and the Earl and Ethel Myers Oceanographic Trust. I sincerely thank each of these institutions for their investment and hope I have put it to good use.

## Introduction

Plant ecophysiology is the interaction between physiology—the cellular- and trait-level functions of a plant, and ecology—how the plant responds and adjusts its physiology in response to its biotic and abiotic environment. Ecophysiology can also be taken a step further, asking how these plant physiological adjustments impact the other members of its community.

As largely sessile organisms, most macrophytes are strongly affected by abiotic factors, but in turn affect many of the abiotic factors experienced by associated biota. In particular, plants and macroalgae that function as autogenic ecosystem engineers (*sensu* Jones et al. 1994) have far-reaching impacts on their community. Ecosystem engineers may create biogenic habitat or facilitate community assembly by modifying existing habitat features (Bruno and Bertness 2001, Crain and Bertness 2006). For example, early successional bacteria, fungi, algae, and plants colonize novel mineral environments and support the colonization of late successional organisms (Berner 1997, Walker et al. 2003, Pointing and Belnap 2012, Gowell et al. 2015). Sessile invertebrates can create biogenic habitat and temperature-mediated microenvironments in which particular communities may thrive in an otherwise harsh environment (Helmuth 1998, McAfee et al. 2016). Macrophytes may also facilitate juveniles of other species; mature shrubs often serve as obligate nurse plants for juvenile cacti in arid regions (Franco and Nobel 1989). Macrophytes that form marine and terrestrial forests both create biogenic habitat and create a climate-controlled

space, facilitating the development of diverse communities (Campbell and Coxson 2001, Badano and Marquet 2009, Rambo and North 2009). Finally, forests of canopy-forming marine macrophytes can chemically mediate surrounding fluids, dictating the pH and carbon availability of the local environment (Lee and Dunton 2000, Fritz et al. 2004, Delille et al. 2009, Cornwall et al. 2013).

Large brown algae in the Laminariales (Phaeophyceae, Heterokontophyta), or kelps, are a relatively under-studied but ecologically-important group of autotrophic ecosystem engineers. Kelp-dominated ecosystems are widespread along the temperate coasts of all seven continents (Steneck et al. 2002, Graham et al. 2007, Carr and Reed 2015). These kelp forests are incredibly productive, in some cases outstripping the primary productivity of terrestrial tropical forests (Reed and Brzezinski 2009). They support large and economically important populations of vertebrate and invertebrate species and may contribute substantially to long-term deep sea carbon burial (Duarte et al. 2004, Tokoro et al. 2014).

While different "kelp forests" are dominated by different canopy-forming species in different regions (e.g. *Ecklonia* sp. in Australia, *Macrocystis* in the Eastern Pacific, *Laminaria* on the coasts of the Atlantic Ocean), they function in remarkably similar ways. The physiology and distributions of kelps are affected by many simultaneous factors—the severity of hydrodynamic forces, light availability, seasonal oceanographic nutrient conditions (e.g. upwelling), temperature, dissolved inorganic carbon (DIC) availability, N and trace nutrient availability, and grazing (Gerard 1982, Utter and Denny 1996, Graham 1997, Nielsen et al. 2006, Graham et

al. 2007, Brown et al. 2014). However these brown algae form dense stands (forests) which in turn modify the local ecosystem. Kelp forests control and attenuate wave forces, reduce light availability, and mediate carbon and nitrogen availability (Komatsu et al. 1982, Gerard 1984, Lee and Dunton 2000, Wernberg et al. 2005, 2011, Gaylord et al. 2007, Delille et al. 2009, Cornwall et al. 2013). In this way, they create true forest microhabitats that are protected from broader oceanographic conditions, in which gradients of energy and nutrients are maintained. In particular, it is increasingly clear that kelp canopies, in conjunction with respiring heterotrophic benthic communities, create a vertical gradient of $CO_2$ availability within the water column (Raven and Hurd 2012). In total, the kelp forest ecosystem, especially the chemical environment, is the result of the push and pull of multiple actors. It is the intersection of the combined inputs and outputs of autotrophic and heterotrophic assemblages and larger abiotic climatic forces.

This dissertation represents an effort to understand how key physiological traits of brown algae respond to their abiotic environment, and how those traits, in turn, affect the kelp forest ecosystem. In particular I chose to focus on the physiology of DIC uptake and photosynthate transport in *Macrocystis pyrifera*, the giant kelp, as well as other members of the Laminariales, which are abundant on the west coast of California.

In Chapter 1, I took an anatomical and modeling approach to understanding how photosynthate transport networks function in diverse members of the Laminariales. The Laminariales are as distantly related to terrestrial plants as fungi

yet have convergently evolved a plant-like body plan and a specialized phloem-like transport network. This kelp "phloem" is recognized but poorly studied, particularly in regards to vascular scaling and integration with whole thallus function. In plants and mammals, universal allometric scaling relationships constrain vascular anatomy and key functional traits, suggesting that optimal resource transport has evolved in these phyla. To evaluate possible scaling and optimization in the kelp vascular system, I co-developed a model of optimized transport anatomy and tested it with measurements from *M. pyrifera* and a diverse sampling of five other kelps (Laminariales). Within the Laminariales, only *M. pyrifera* displays strong scaling relationships between all tested vascular parameters and agrees with our model; other species display weak or nonexistent vascular allometries and are in poor agreement with the model. The lack of universal scaling in the kelps and the presence of optimized transport anatomy in *M. pyrifera* raised important questions about the evolution of optimization and the possible competitive advantage conferred by optimized vascular systems to multicellular phyla. Have ecological factors driven *M. pyrifera* to possess a scaled and tapered vascular system? Do all canopy-forming kelps possess optimized vascular tissues? This is still an open question, but has interesting implications. It would indicate that the unique microclimates supported by kelp forests have been enabled by the evolution of optimized cellular transport networks.

In Chapter 2, I focused on the dynamics of carbon uptake in *M. pyrifera*. In the Monterey Bay region of Central California, the giant kelp *Macrocystis pyrifera*

experiences broad fluctuations in wave forces, temperature, light availability, nutrient availability, and seawater carbonate chemistry, all of which may impact their carbon uptake physiology. In particular, current velocities and light intensity may strongly regulate the supply and demand of dissolved inorganic carbon (DIC). *M. pyrifera* can acquire and utilize both $CO_2$ and bicarbonate ($HCO_3^-$) as DIC substrates for photosynthesis and growth; given the variability of carbon supply (due to current velocities and nutrient availability) and demand (in the form of saturating irradiance), I hypothesized that the proportion of $CO_2$ and bicarbonate utilized is not constant for *M. pyrifera,* but a variable function of their fluctuating environment. I further hypothesized that populations acclimated to different wave exposure and irradiance habitats would display different patterns of bicarbonate uptake. To test these hypotheses, I carried out oxygen evolution trials in the laboratory to measure the proportion of bicarbonate utilized by *M. pyrifera* via external carbonic anhydrase under an orthogonal cross of velocity, irradiance, and acclimation treatments. Monterey Bay populations of *M. pyrifera* exhibit proportionally higher external bicarbonate utilization in high irradiance and high flow velocity conditions than in sub-saturating irradiance or low flow velocity conditions. However, there was no significant difference in proportional bicarbonate use between deep blades and canopy blades, nor between individuals from wave-exposed vs. wave-protected sites. This study demonstrated that *M. pyrifera* possess a plastic carbon uptake physiology in which proportionally more bicarbonate is used in high irradiance and high flow conditions, but that local populations have not yet developed fixed genetic

differences. The implications for the development of pH and DIC gradients within kelp forests are profound; the surface and protected inner areas of kelp beds are likely significantly more acidic and DIC-poor than benthic and offshore edges of kelp beds. These dynamic seawater conditions may determine where other macroalgae, phytoplankton, and invertebrates thrive, and where they cannot.

Chapter 3 applies the findings of bicarbonate use patterns in Chapter 2 to a study of patterns of carbon stable isotope discrimination in *M. pyrifera*. The signature of the relative abundance of $^{13}C$ in autotroph tissue, $\partial^{13}C$, is a critical tool for assessing the role of *M. pyrifera* in the kelp forest food chain. $\partial^{13}C$ may also be an accurate diagnostic for carbon uptake strategy in macroalgae. However there is growing recognition that, contrary to theory, $\partial^{13}C$ can vary widely in different individuals of a single species of autotroph, greatly complicating the designation of a primary producer within a food chain. *M. pyrifera* is an acute example of this issue—$\partial^{13}C$ signatures of kelp tissue can differ up to 6‰ *within a single individual*. Abiotic factors such as irradiance, [DIC], water motion, and water temperature can drive $\partial^{13}C$ variation, either by altering the supply of total DIC available to individual tissues, or by inducing facultative carbon concentrating mechanisms. In this study, I sought to understand and predict the abiotic drivers of $\partial^{13}C$ signatures in *M. pyrifera* tissues, using both a field survey and experimental approach. To test whether tissue $\partial^{13}C$ is driven by DIC limitation or an induced carbon concentrating mechanism, I incubated meristematic tissue in an outdoor mesocosm for 2 weeks in 4 fully-crossed treatments intended to induce the extremes of DIC supply and limitation. To test our ability to

predict tissue $\partial^{13}C$ in the field, I carried out targeted sampling from extreme irradiance and wave exposure microhabitats around the Monterey Peninsula in Central California, USA. I observed that the $\partial^{13}C$ of incubated tissue was driven by irradiance level, but was not correlated with flow velocity or growth rate (a proxy for DIC consumption). This indicates that enrichment in *M. pyrifera* tissue is the result of a light-induced metabolic process as opposed to abiotic or biotic DIC limitation. Field-collected samples supported the strong correlation between irradiance habitat and $\partial^{13}C$ signatures, but also indicated that DIC limitation (via oceanographic or biotic forces) played a role. I also confirmed a physiological $\partial^{13}C$ enrichment process associated with photosynthate transport. These data inform ongoing questions regarding the mechanisms of $^{13}C$ discrimination in macroalgae, and account for much of the variation in $\partial^{13}C$ observed in the field. This study may thus yield a predictive framework for tracking microhabitat use of grazers and higher predators in the kelp forest ecosystem.

# Chapter 1:
# Convergent evolution of vascular optimization in kelp (Laminariales)

## Introduction

Biological transport networks are a key innovation in the evolution of modern complex organisms. Across the tree of life, there is evidence that vascular transport networks are optimized, balancing maximum speed and integrity of resource delivery with minimal resource investment in transport and infrastructure. West, Brown, and Enquist (1999) posited that the observed universal allometric scaling relationships between key anatomical traits and metabolism were attributable to optimization in biological resource networks (West et al. 1999). Their work fueled a flurry of inquiry into the mechanisms and implications of vascular scaling relationships. In the plant kingdom, robust and universal allometric scaling between functional and anatomical properties of transport cells has been observed, from angiosperms to gymnosperms to bryophytes (Niklas 1993, Savage et al. 2010). Even the simplest "one-dimensional" conifer leaves display size scaling of xylem vessel elements, achieving a modeled 10% reduction in transport energy loss relative to a structure with size-invariant vessels(Zwieniecki et al. 2006). In mammals, strong power law relationships have been observed between vascular path length and body size across multiple venous and arterial networks of different skeletal muscles and organs(Kassab 2006). The universality of the scaling exponents within each of these phyla suggests that both

terrestrial plants and animals have separately arrived upon a similar optimal strategy for delivering resources to support structure, function, and metabolism.

This idea that diverse kingdoms have independently evolved optimized allometric scaling of their vascular networks led us to examine organisms of another kingdom altogether—the Chromista, in which the brown algae (Phaeophyceae, Ochrophyta) reside. Kelps (Laminariales) are as distantly related to plants as metazoans; the basal clades of the Ochrophyta are flagellated unicellular eukaryotes such as diatoms(Baldauf 2008, Riisberg et al. 2009). Despite this evolutionary distance, they possess a remarkable convergent physiology. On a macroscopic level, brown algae are often plant-like, bearing specialized analogs of plant organs such as blades (leaves), stipes (stems), and sporangia (reproductive organs). At the cell and tissue level, a few orders of the brown algae also possess a phloem-like long distance transport network of trumpet-shaped sieve elements (SE) separated by perforated sieve plates (Figure 1). This long distance transport system moves carbohydrates (mannitol, glucose, mannose), amino acids, heavy metals, and perhaps signaling compounds(Schmitz 1981, Manley 1983). A survey of translocation velocities in the Laminariales found that transport rates of radiolabeled $C^{14}$ range from 50 to 780 mm/hr(Schmitz and Lobban 1976). While macroalgal SE's resemble those of plants, they have no structures analogous to xylem or companion cells, and the mechanism of SE loading is still unclear.

Like terrestrial plants, brown macroalgae play a critical role in the ecology of nearshore marine systems and in the global carbon cycle (Mann 1982, Huston and

Wolverton 2009, Reed and Brzezinski 2009). Despite the ecological importance of kelps in the Laminariales, the structure, function, and scaling of their vascular system has been minimally explored. In this chapter, I ask the following question: do members of the Laminariales display allometric power-law scaling of their SE's indicative of optimal resource allocation?

I approached this by co-developing a model for optimized resource transport in brown macroalgae. The model is based on the concept that optimized phloem transport occurs when the osmotic pressure gradient required to drive translocation is minimized, as is the volume of the SE's required to serve the entire organism. Such a network is characterized by the tapering of phloem area in terminal branching units and unloading zones. I then tested the quantitative scaling predictions of the optimal model using the giant kelp, *Macrocystis pyrifera*, a species whose translocation patterns have been carefully studied. Furthermore, I investigated whether the classic vascular plant allometric relationships (SE diameter vs. conduit packing, vascular fraction, stipe diameter, biomass, and metabolic area) could be observed in *M. pyrifera* as well as five other members of the family Laminariales.

## Methods

*Study species:*

The six species chosen for this study spanned a broad size range (Figure 2). Three individuals each of *Nereocystis luetkeana* and *Macrocystis pyrifera* (large; >10 m tall), *Egregia menziesii* (intermediate; between 2 and 5 m tall), and *Laminaria*

*setchellii, Pterygophora californica,* and *Alaria marginata* (small; < 2m tall) were sampled. These species represent the diversity of macroalgal habits and include taxa that are annual, perennial, upright, prostrate, subtidal and intertidal. Each species possesses a unique body plan (placement of reproductive sporophylls, meristems, etc.). Such ecologically and morphologically diverse species were chosen to thoroughly test the hypothesis that observed vascular scaling relationships would be common to all members of the Laminariales. Species were collected intertidally or on SCUBA from the Monterey Bay region of Central California (Davenport Landing, Davenport (37.024663, -122.217210); Lover's Point, Pacific Grove (36.626419, -121.915837); Stillwater Bay, Carmel (36.626419, -121.915837); and Big Creek, Big Sur (36.068229, -121.600362). 3-5 individuals of each species were collected, and individuals of each species were collected from the same site. Collections were carried out in summer of 2012 and 2013, as well as November 2013.

*Sampling methods:*

Each individual was collected, brought to the lab, and immediately refrigerated with seawater-soaked paper towels in a closed container for the duration of their dissection. Each individual (or individual frond, if from multi-frond species *M. pyrifera* and *E. menziesii*) was cut into 15-25 segments, each representing <10% of total thallus length. For each segment, segment length, stipe diameter, and attached blade length were measured, as was total photosynthetic area, measured with a LiCOR Li-3100C Area Meter (Lincoln, NE). A subsample of 2-3 cm was reserved in refrigerated seawater for sectioning and microscopic examination; the remaining

tissue was dried for biomass analysis. Each sub-sample was hand sectioned using a razor blade or manual microtome, stained with toluidine blue to provide contrast, and photographed on a Motic BA210 microscope mounted with a Moticam digital camera (JH Technologies, San Jose, CA).

Individual SE areas and total medulla (vascular tissue) areas were measured from digital micrographs using Fiji (ImageJ) software (Schindelin et al. 2012). I measured only cells that exhibited the classic "trumpet hyphae" morphology in longitudinal section, identifiable by hallmark swelling of the cell wall in cross section (Knoblauch et al. 2016). I did not measure the interconnected cells known as "hyphae" in the periphery of the medulla; they failed to transport carboxyfluorescein diacetate (CFDA) in preliminary trials and lack the swelling mechanism of pressurized true sieve elements. At least 100 SE's were measured per segment; a total of 37,751 individual SE's were measured in this work. Each segment of each individual sampled alga was assigned a transport status: "loading", a section of tissue assumed to be only loading photoassimilate into the phloem; "unloading" a section assumed to be only unloading transported sap from the phloem; and "both", a segment in which bi-directional transport might be occurring. Assignments were based on published $C^{14}$ tracer studies of study species or congeners sharing their body plans (arrangement of meristems, reproductive tissues, and vegetative blades)(Schmitz and Lobban 1976, Lobban 1978). Average SE diameter, conduit packing, vascular fraction, and total estimated phloem area were calculated for each segment.

*Model development:*

In this optimal model of phloem functional anatomy, phloem area is expected to taper from large conduits at the start of a loading or unloading zone to smaller conduits at the terminus of transport (distal meristem or storage tissue). This total phloem area taper can manifest as a reduction in the number of SE's (N*)* or a reduction in individual SE area (*A)*. In the majority of sampled species, N was invariant; thus I formulated the model to predict variation in *A* (see *Appendix 1*).

Below I develop a one-dimensional phloem transport model for the relationship between SE area and height for macroalgal tissue that exclusively loads or unloads from the phloem conduits. For the full model derivation, see the *Appendix 1*.

Briefly, I assume conservation of carbohydrate mass

$$c\frac{d}{dx}(Au) = qc,$$

where $A(x)=N(x)a(x)$ is the conductive phloem area, $N(x)$ is the number of conduits, $a(x)$ is the individual conduit area, $u(x)$ is the translocation speed, $c$ is the sap carbohydrate concentration, and $q$ is the unloaded volume of sap per unit length. The coordinate $x$ is measured from the start of the unloading zone ($\ell = 1$ m from the apex), and we write it as $x = \ell + x^* - H$, where $H$ is the organism height, and $x^*$ is the distance from the holdfast. Using Darcy's law for the relationship between

velocity and pressure *p:* $dp/dx = -\eta u/k(x)$, where *k* is the conductivity, I arrive at an expression for the pressure drop across the unloading zone

$$\Delta p = 8\pi \frac{\eta q}{N} \int_0^{\ell} \frac{\ell - x}{a(x)^2} dx$$

Minimizing the pressure drop subject to a constant volume constraint leads to the prediction $a = \bar{a}(1 - x/\ell)^{1/3}$, where $\bar{a}$ is the area at $x = 0$. Compared to a uniform collection of pipes ($a(x)$ = const), the optimum area distribution requires approximately 20% less pressure to drive the same flow. Both this optimal slope (1/3) and the suboptimal slope (0, representing size-invariant SE's) were used as null hypotheses to test for optimality in *M. pyrifera*, the only brown algal species in which we have observed unidirectional transport (Lobban 1978). A similar approach was previously used to study architecture of xylem (Zwieniecki et al. 2006) and phloem (Ronellenfitsch et al. 2015) in needles.

*Testing for allometric relationships:*

I tested three fundamental relationships observed in plant xylem and theoretically expected for phloem. Although xylem and phloem operate under different mechanisms for fluid transport and hydraulic safety, I expected them to exhibit similar allometric trends. Fundamentally, both systems are fluid transport conduits driven by pressure gradients and both are theoretically optimized by the minimization of this gradient.

*Relationship 1:* SE diameter vs. stipe diameter. As in terrestrial plant xylem, I hypothesized that conduit diameter would increase log-linearly as stem diameter increased (Enquist and Biology 2003, Hölttä et al. 2009, Savage et al. 2010, Jensen et al. 2012, Petit and Crivellaro 2014). This relationship is primarily a developmental phenomenon, and indicates a programmed genetic algorithm for growth. This relationship is universal in angiosperm and gymnosperm trees with an average exponent of 0.27 (Savage et al. 2010).

*Relationship 2:* SE area vs. conduit packing (transport cells per unit area). We hypothesized that the total conduit area of vascular tissue should remain roughly constant throughout the entire sporophyte of an alga. With this requirement, tapering of individual SE area must be balanced by a denser packing of these small conduits into the medulla to transport the same volume of photoassimilate. In short, small SE's should be more numerous than large SE's in the same medulla area (*the Packing Rule*,18, 22). In the xylem of angiosperm and gymnosperm trees, this relationship is again universal with a scaling exponent of ~2.0(Savage et al. 2010). In kelps, we predicted a similar log-linear relationship where conduit packing decreases with increasing conduit size.

*Relationship 3:* SE area vs. biomass, cumulative blade (photosynthetic) area, and path length (*L-trans*, the distance that photosynthate must move from the observed SE). I hypothesized that the diameter of a transport conduit at any given point along the sporophyte would scale exponentially with the photosynthetic area that conduit must support (a proxy for metabolic function). Cumulative blade area is

defined as the total blade area "supported" by each dissected segment; this includes any tissue that potentially sends photoassimilate through the segment. Maximum cumulative blade area is usually supported by segments of a macroalga that engage in bi-directional transport (not exclusively sink or source tissue).

The values and universality of the scaling exponents of these log-linear relationships for each study species were analyzed using a reduced major axis approach in R (SMATR package) and are fully reported in *Appendix 1*.

**Results**

The model for optimized phloem transport in brown algae describes an optimal distribution of total phloem area along the length of an individual sporophyte in tissue that is exclusively loading or unloading from the phloem. The model predicts a slope of 1/3 for the linear allometric log-transformed relationship between average SE area ($\mu m^2$) and distance from the terminus of the unloading zone (m). However, scaling exponents in the range $0.15 < n < 0.5$ are within 5% of the efficiency of the optimum value. Macroalgae adhering to this optimization mechanism theoretically conserve 20% of their transport energy expenditure by tapering conduits in this manner (see *Appendix 1)*.

Of the six study species, *M. pyrifera* was the only species for which I had sufficient physiological data to test the model. N is invariant as a function of sporophyte height for *M. pyrifera* (Figure 3A). However we detected a strong positive relationship between $A$ and $1 - x/l$ (inverse height along the sporophyte) for the distal

"unloading" zone in *M. pyrifera*. The slope of this relationship falls within the 95% confidence intervals for the predicted optimal slope of 1/3 (slope ($m$) = 0.45, p = 0.0003, $R^2$ = 0.276) (Figure 3B, C). This slope is significantly different from the sub-optimal hypothesis of a zero slope ($p < 0.0001$).

In general, the distribution of individual SE areas was normal within each segment of each sporophyte across all species examined. In *M. pyrifera,* however, segments from the distal 0.5 m of each frond are distinctly skewed towards smaller values. Additionally, when the coefficient of variation is calculated for individual segments of *M. pyrifera*, it is clear that variance in SE areas increases linearly with increasing height along the sporophyte (i.e. youngest tissue displays the most cell area variance, $p< 0.0001$, $R^2 = 0.33$) (Figure 4).

Moving beyond the allometry predicted by the model, I explored three additional functional relationships that I would expect to display allometric scaling (and thus optimization).

*Relationship 1:* In kelps, there is no single universal scaling relationship observed in the log-log plot of stipe diameter vs. average SE diameter. Those that do scale, however, do so in a manner similar to terrestrial plants, where SE diameter increases proportionally with stipe diameter. *L. setchellii* and *P. californica* are not statistically different from one another ($m = 0.15$, $p = 0.0003$, $R^2 = 0.28$; and $m = 0.20$, $p= 0.03$, $R^2 = 0.11$, respectively). *N. luetkeana* also displays a significant relationship ($m = 0.30$, $p = 0.0006$, $R^2 = 0.23$). These three species have low $R^2$

values, indicating high variability around the slope, whereas *M. pyrifera* displays a much stronger positive relationship ($m = 0.87$, $p<0.0001$, $R^2$ of 0.81) (Figure 5A).

*Relationship 2:* Of my six species, only *M. pyrifera* displays a significant relationship in the log-log plot of average SE diameter vs. conduit packing ($m = 0.67$ ($p< 0.0001$) (Figure 5B).

*Relationship 3.* The relationship between average SE diameter and cumulative blade area (Figure 5C) is highly significant and explains substantial portions of the variation in SE diameter for both *M. pyrifera* ($m = 0.19$, $p< 0.0001$, $R^2 = 0.78$) and *L. setchellii* ($m = 0.23$, $p< 0.0001$, $R^2 = 0.46$). *A. marginata* also displays a significant relationship ($m = 0.11$, $p< 0.0001$, $R^2 = 0.37$).

**Discussion**

Several surprising results emerge from my analysis of scaling relationships in kelp phloem. The first such result is the lack universal allometric scaling between SE area and stipe diameter, path length, or metabolic area among study species. Despite morphological diversity, basic uniform allometric relationships have been observed between anatomical parameters of vascular networks and body size/metabolic rate in both terrestrial plants and mammals(Kassab 2006, Savage et al. 2010). The theory of metabolic scaling is fundamentally based on the idea that body size and metabolism are constrained by the network that delivers resources to active metabolic tissue(West et al. 1997, 1999, Banavar et al. 2010).There is no *a priori* reason to assume that brown macroalgae should possess vascular allometries similar to either terrestrial

plant xylem, plant phloem, or mammalian cardiovascular systems; however if these other phyla are any example, I did expect that if an advantageous optimized architecture had sufficiently strong evolutionary drivers and time to emerge in one member of the Laminariales, it would have been adopted throughout the order.

Instead, I observe that members of the Laminariales possess significantly different scaling exponents, as is exemplified by the relationship between SE diameter and stipe diameter (Figure 5). These differences are even more dramatic in other tested allometric relationships, yielding a strong dichotomy between *M. pyrifera* and the majority of my study species (*A. marginata, E. menziesii, L. setchellii, N. luetkeana, P. californica*). For every relationship tested, *M. pyrifera* displays significant allometric relationships indicative of optimal network design, whereas the remaining species display weaker or inconsistent covariation. The data indicate that most kelps possess SE networks that vary little in diameter, and that their vascular anatomy is driven by selective forces other than optimization of carbohydrate transport. These findings lead us to question what ecological and life history drivers produce the consistent and predictable scaling of *M. pyrifera*. Is there a body size or sink size threshold over which carbohydrate transport must be optimized? Do smaller kelps retain an ancestral function of the brown algal SE cell network different than that of carbohydrate transport? Finally, is there directionality to the evolution of vascular function within the Laminariales?

The members of the Laminariales that do not display strong vascular allometry may instead possess body plans optimized for other ecologically relevant

functions, such as spore dispersal, resistance to hydrodynamic forces, or herbivory. Furthermore, most of these macroalgae are less than 2 m tall, so their body size may constrain their maximum SE size and thus variance and detectable allometric scaling. Even in terrestrial plants, smaller plants may not display as broad a range of conduit sizes as large plants(Jensen et al. 2011). Plant and algal transport pathways may be very complicated, with bidirectional activity and possible relays(Hölttä et al. 2009); it is conceivable that robust scaling of vascular anatomy exists on scales much smaller than those measured in my whole-sporophyte approach. The strength and isolation of carbohydrate sources and sinks is not as extreme in small macroalgae as it is in large *M. pyrifera* or terrestrial plants. With the exception of *A. marginata*, these small species co-locate their reproductive tissue with vegetative tissue, minimizing the need for transport. Small kelps have diverse meristem types and placement, and photosynthesize in all parts of the sporophyte. Perhaps ecological drivers have favored a flexibility of resource generation over energy-optimized transport in some species.

It is also possible that the ancestral function of the SE's is not to transport energetic subsidies, but rather to facilitate signaling for development or defense. Signaling and development in macroalgae is poorly understood, but there have been studies showing that the intercalary meristem of *Laminaria japonica* releases a "sporification inhibitor" to mature tissues, preventing tissue from becoming catastrophically reproductive before the proper season(Skriptsova and Titlyanov 2003). If molecules of this kind are being transported via the SE's, this could provide

an alternate view on early evolutionary role of non-optimized transport networks in brown algae and terrestrial plants.

Evolutionary drivers of optimization are suggested by the unique traits and phenology of *M. pyrifera.* It is the most plant-like of the Laminariales, with multiple stipes bearing alternately branching blades, and true apical meristems. It is an order of magnitude larger than all but four species in the Laminariales. It is unique among canopy-forming algae in that it has basal meristems and reproductive tissue (i.e. new fronds arise at the base of the alga in a light-limited environment), which require carbon subsidies from surface fronds (Figure S4, *Appendix 1*). Increased size, specialization, or spatial organ could have driven the evolution of transport optimization in giant kelp.

It must be addressed that the observed scaling relationships between SE cells and gross anatomy could be an artifact of development in *M. pyrifera*. The smallest conducting cells are located in the distal immature apical tissue, and could simply be immature, not genetically programmed to be smaller in order to optimize resource transport. This interpretation is unlikely to be correct for two reasons. The first is that the largest SE's and the largest stipes are located not at the oldest point of each mature frond (the base), but rather mid-frond, the most productive portion of the sporophyte (Figure 3B). This association of large SE's with productivity instead of age indicates that there is a developmental program for SE size *M. pyrifera*, possibly triggered by light availability. Secondly, there is increased variance in the area of individual SE's in distal tissues. In these tissues, we observed many small SE's (5-10

μm in diameter), but also large SE's, which are an order of magnitude larger in area than the average. Thus these immature, small-diameter stipes support "disproportionately" large SEs, which in turn have the capacity to support exponentially higher phloem conductivity and velocity(Jensen et al. 2011). Apical meristems may be laying down these larger SE's for later transport as the stipe elongates, while primarily conducting transport more appropriate to their loading rates through the more numerous, smaller SE's.

The Laminariales and other phloem-bearing brown macroalgae are evolutionarily younger than terrestrial plants. The first vascular tracheophytes emerged 419 to 454 Ma, whereas the common Phaeophycean ancestor of the phloem-bearing lineages is estimated to have evolved 189 Ma, and the Laminariales 84 Ma(Silberfeld et al. 2010, Clarke et al. 2011). It is conceivable that the evolution of a functional long-distance transport network is in its infancy in brown algae; in this way my study of scaling and simple functional anatomy is not only an exploration of algal biology, but also an exploration of the broader process of the evolution of transport structures and network optimization in any phylum.

**Table 1.** Scaling parameters for the log-log relationship between average SE diameter and various functional anatomy traits. Only significant relationships ($p < 0.05$) are shown; for all species, see *Appendix 1*.

| Independent variable | species | slope | intercept | $R^2$ |
|---|---|---|---|---|
| Stipe diameter (cm) | *L. setchellii* | 0.147 | 1.128 | 0.28 |
| | *M. pyrifera* | 0.871 | 1.660 | 0.89 |
| | *N. luetkeana* | 0.302 | 1.448 | 0.23 |
| | *P. californica* | 0.197 | 1.137 | 0.11 |
| Conduit packing (SE/$\mu m^2$) | *M. pyrifera* | -0.676 | -0.955 | 0.95 |
| Vascular fraction | *A. marginata* | 0.346 | 1.346 | 0.40 |
| | *E. menziesii* | 0.558 | 1.503 | 0.22 |
| | *L. setchellii* | 0.526 | 1.517 | 0.32 |
| | *M. pyrifera* | 1.597 | 2.608 | 0.68 |
| | *N. luetkeana* | 0.735 | 1.991 | 0.46 |
| | *P. californica* | 0.601 | 1.568 | 0.49 |
| Cumulative blade area (cm^2) | *A. marginata* | 0.108 | 0.833 | 0.37 |
| | *L. setchellii* | 0.229 | 0.366 | 0.46 |
| | *M. pyrifera* | 0.193 | 0.803 | 0.88 |
| Path length (m) | *M. pyrifera* | 0.280 | 1.427 | 0.85 |
| Cumulative biomass (g) | *L. setchellii* | 0.239 | 0.747 | 0.25 |
| | *M. pyrifera* | 0.188 | 1.204 | 0.89 |

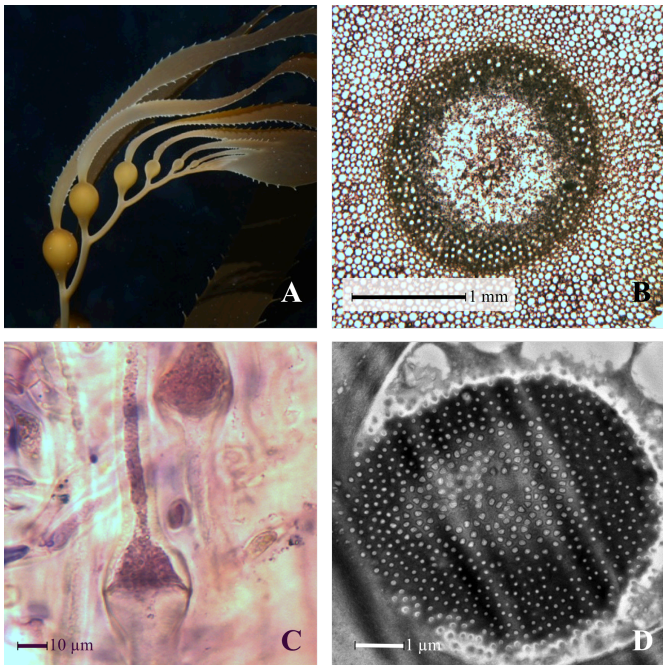


**Figure 1.** (A) *N. luetkeana* sporophyte. Credit: J. Hildering. (B) Cross-section of *N. luetkeana* medulla (dark circle) containing sieve elements. (C) Occluded *A. marginata* sieve element in longitudinal section. (D) *A. marginata* sieve plate (TEM micrograph). Credit: S. T. Drobnitch.

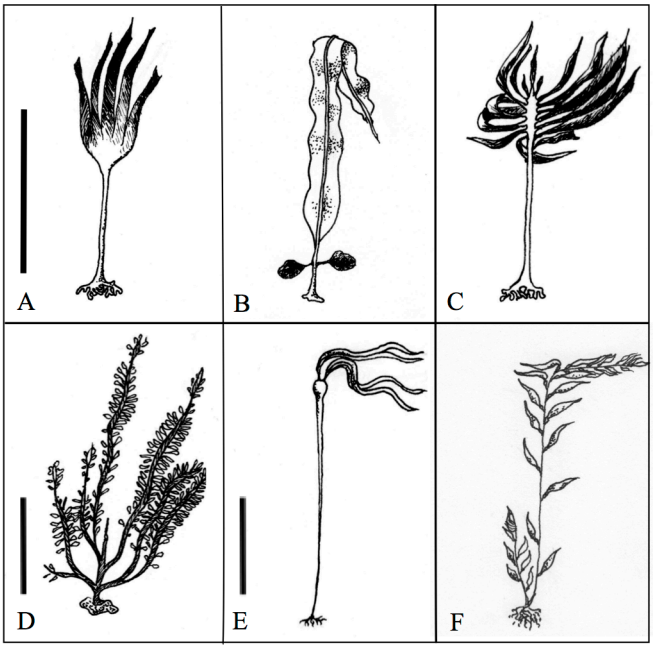


**Figure 2.** Illustration of the six study species. (A, B, C, D) *Laminaria setchellii*, *Alaria marginata, Pterygophora californica, Egregia menziesii*. Scale = 1 meter. (E, F) *Nereocystis luetkeana, Macrocystis pyrifera*. Scale = 5 meters. Credit: S.T. Drobnitch.

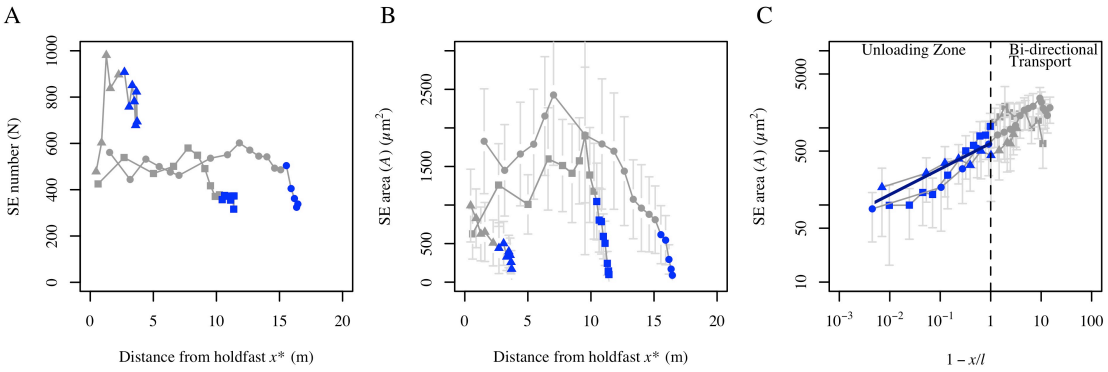


**Figure 3**. **(A)** Number of conduits *N* and **(B)** average sieve element (SE) cross-sectional area *a* vs. distance from the holdfast $x^*$ in *M. pyrifera*. Segments (points) from a single *M. pyrifera* frond are joined by a line; three individual fronds (symbols) are shown. Points in each frond that purely unload from the phloem are blue; segments engaging in bi-directional transport are grey. **(C)** Relationship between *a* and $1 - x/l$ (inverse height). The data fall along the predicted optimum scaling slope (solid blue line) within a 5% confidence interval. All error bars represent SD.

**Figure 4.** Axes are log-transformed. Each point represents a segment of an individual sporophyte. (A) The developmental scaling relationship between sieve element (SE) diameter and stipe diameter in six kelp species. Four of the six species display significant relationships: for *M. pyrifera*, $m = 0.87$; for *N. luetkeana*, $m = 0.30$; *P. californica* and *L. setchellii* are indistinguishable with an $m$ of 0.20 and 0.15, respectively. (B) The packing rule in kelp. Average SE diameter is plotted as a function of conduit packing (number of SE per $\mu m^2$); only *M. pyrifera* displays a significant relationship, $m = -0.53$). (C) The allometry of SE size and supported metabolic tissue. Average SE diameter is plotted as a function of cumulative blade area supported by each segment. Three species scale: *A. marginata*, $m = 0.11$; *L. setchellii* and *M. pyrifera* are statistically indistinguishable with $m = 0.23$ and 0.19, respectively.

A

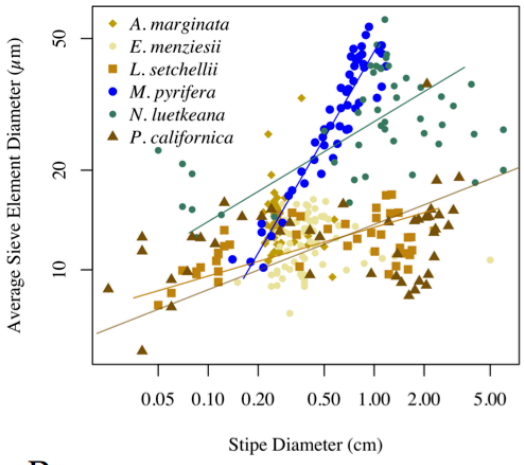
A. marginata
E. menziesii
L. setchellii
M. pyrifera
N. luetkeana
P. californica
Average Sieve Element Diameter (μm)
10
20
50
0.05
0.10
0.20
0.50
1.00
2.00
5.00
Stipe Diameter (cm)

B

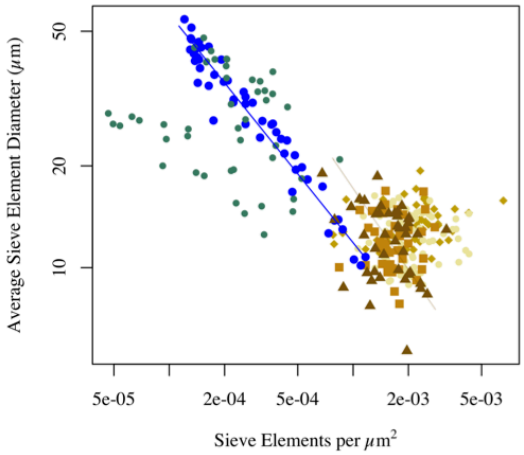
Average Sieve Element Diameter (μm)
10
20
50
5e-05
2e-04
5e-04
2e-03
5e-03
Sieve Elements per μm²

C

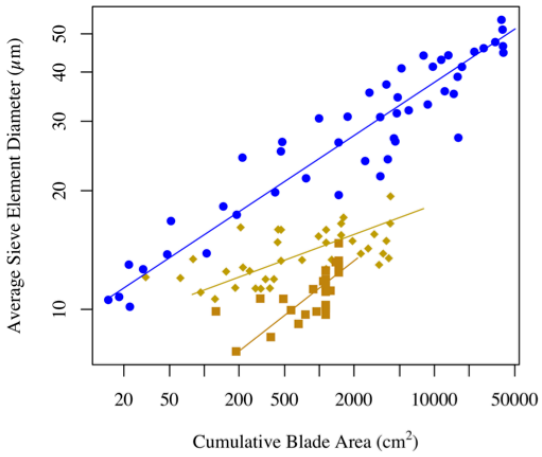
Average Sieve Element Diameter (μm)
10
20
30
40
50
20
50
200
500
2000
10000
50000
Cumulative Blade Area (cm²)

## Chapter 2:
## Abiotic influences on bicarbonate use in the giant kelp, *Macrocystis pyrifera*, in the Monterey Bay

### Introduction

The organisms that inhabit nearshore and intertidal marine ecosystems must cope with fluctuations in wave forces, temperature, light availability, nutrient availability, and seawater carbonate chemistry. Kelps are no exception, and experience this stressful variability in shallow temperate waters around the world. For example, kelp forests along the central coast of California experience water temperature fluctuations of 4˚C on a daily basis due to tidal bores and internal waves propagating inshore, and seasonal fluctuations of up to 7˚C due to upwelling vs. relaxed oceanographic conditions (Storlazzi et al. 2003, Woodson et al. 2007). Irradiance varies with depth—for example, irradiance at 12 m depth is only ~10% of surface values and macroalgal canopies further reduce irradiance at depth by 75% (Gerard 1984, Edwards 1998). Wave force and current velocities also vary seasonally and geographically; kelp forest communities at exposed sites frequently experience current velocities in excess of 30 cm/s while velocities lower than 2 cm/s occur in nearby protected embayments (Gaylord et al. 2003, Storlazzi et al. 2003).

In Chapter 1, I demonstrated that the giant kelp, *M. pyrifera,* is an efficient and possibly unique kelp optimized for carbon allocation in the nearshore water column, which contains regions of very low and very high irradiance levels. As is evident from its worldwide distribution on temperate rocky coastlines (Graham et al. 2007), *M. pyrifera* also thrives in a broad range of temperatures, nutrient availability, and

hydrodynamic stress (Gerard 1982, Alonso Vega et al. 2005, Graham et al. 2007, Schiel and Foster 2015, Carr and Reed 2016). Further, *M. pyrifera* is known to acclimate to these abiotic factors by altering its sporophyte morphology and photosynthetic physiology (Brostoff 1988, Colombo-Pallotta et al. 2006, Hurd and Pilditch 2011, Kopczak et al. 1991, Stewart et al. 2009, Utter and Denny 1996). We lack, however, a clear understanding of how environmental factors impact carbon acquisition physiology in *M. pyrifera* and other large brown macroalgae. Recent work has focused on the effects of variable pH environments on carbon acquisition (Brown et al. 2014, Fernández et al. 2015) , but we have little information regarding the effects of variable irradiance and current velocities on carbon uptake dynamics in *M. pyrifera.*

*M. pyrifera* can utilize both $CO_2$ and $HCO_3^-$ (bicarbonate) as substrates for photosynthesis and growth. These two species of inorganic carbon differ strongly in availability and ease of uptake by photosynthetic organisms at current ocean pH. $CO_2$ is a small nonpolar molecule that diffuses easily across cell membranes and requires no costly active uptake mechanism, but comprises only 1% of seawater Ci at pH 8.1. In contrast, bicarbonate is strongly polar and requires active transport or external catalysis to $CO_2$ to be utilized as a photosynthetic substrate, yet is abundantly available (91% of Ci) (Royal Society 2005). Consequently, the ability to utilize bicarbonate as a substrate in photosynthesis is beneficial but may not always be cost-effective for marine algae (Raven et al. 2014).

Environmental variation in irradiance and current velocities may strongly affect patterns of carbon uptake. Current velocity can control supply of inorganic carbon (Ci) to *M. pyrifera.* Low current velocities (< 3 cm/s) have been shown to induce boundary layer formation that limits the nutrient influx to and efflux from kelp blades (Wheeler 1980), whereas velocities greater than 3 cm/s saturate gas exchange rates. Irradiance, on the other hand, regulate Ci demand. High irradiance experienced by canopy blades stimulates increased photosynthesis (Sharkey et al. 1986) and demand for Ci unlike that experienced by deeper understory blades.

In this study, I ask the following questions: Does *M. pyrifera* use a constant proportion of bicarbonate relative to $CO_2$, or does relative bicarbonate utilization vary? Further, is the proportion of bicarbonate use influenced by abiotic conditions that alter Ci supply (current velocities) and/or photosynthetic demand (irradiance levels)? Finally, do local populations of *M. pyrifera* display acclimation of carbon uptake physiology to local physical conditions?

If *M. pyrifera* upregulates bicarbonate uptake in response to low ambient [Ci], I would hypothesize that in low flow velocities (diffusion-limited Ci supply) and high irradiance (high photochemical demand), *M. pyrifera* would exhibit the highest proportional bicarbonate use. On the other hand, I would hypothesize that *M. pyrifera* would utilize the smallest proportion of bicarbonate when photosynthesizing in high flow velocities and low irradiance (saturating Ci supply coupled with low photochemical demand). Previous studies have demonstrated that bicarbonate utilization is up- and down-regulated by light-mediated processes, and that

bicarbonate utilization is down-regulated in very high [Ci] (Johnston and Raven 1990, Kubler and Raven 1995, Zou et al. 2003, Mcginn et al. 2004, Raven and Hurd 2012, Fernández et al. 2015, Hennon et al. 2015, Young et al. 2015). However no study has observed induction of increased bicarbonate uptake in response to exposure to low [Ci]. If low ambient [Ci] does not actively up-regulate bicarbonate utilization, low flow velocities would instead limit the supply of both $CO_2$ and bicarbonate, resulting in proportionally lower bicarbonate utilization relative to tissues photosynthesizing in high flow velocities.

I further hypothesized that *M. pyrifera* blades acclimate their bicarbonate utilization mechanism, thus altering proportional bicarbonate use, in response to microhabitats characterized by consistent high and low irradiance and flow velocity levels. If acclimated, consistently light-limited blades should exhibit lower proportional bicarbonate use than light-replete canopy blades when exposed to high irradiance in the laboratory. Similarly, if blades from high wave exposure habitats were acclimated to greater ambient current velocities and thus higher rates of gas exchange, they should exhibit lower ability to utilize bicarbonate when incubated in low current velocities as compared to blades accustomed to low flow environments.

To evaluate these hypotheses, I carried out a set of laboratory experiments to estimate the relative utilization of bicarbonate in support of photosynthesis as a function of orthogonal combinations of irradiance, flow velocity, and blade origin treatments. To assess relative utilization of bicarbonate vs. $CO_2$, I used acetazolamide, (AZ), a potent inhibitor of the enzyme carbonic anhydrase (CA). AZ,

which must be dissolved in NaOH, and thus acts as a slight carbonate buffer, inhibits external utilization of bicarbonate both via CA activity and acidification of the extracellular space (Drechsler et al. 1993, Larsson and Axelsson 1999, Klenell et al. 2004, Mercado et al. 2006). When actively photosynthesizing tissue is inhibited by AZ, removing their external utilization of bicarbonate, photosynthetic rates decrease. These lower, inhibited photosynthetic rates are thus a measure of metabolism supported only by $CO_2$ uptake and an unknown fraction of active bicarbonate uptake (via anion-exchange channels, which do not respond to AZ).

## Methods

### *Experimental Approach*

To test my predictions of carbon uptake of *M. pyrifera* to in response to the levels of irradiance and flow velocity experienced in the field, I measured the contribution of external bicarbonate utilization to photosynthetic rates in two experiments. In 2014, I measured the effect of irradiance, flow velocity, and blade origin from different irradiance habitats on the proportion of bicarbonate uptake during photosynthesis. I orthogonally tested the separate and combined effects of two levels of irradiance (1000 or 80 μmoles photons/$m^2$/s), two levels of flow velocity (30 or 4.5 cm/s), and two levels of blade origin (blades from the surface or 10m depth) on uninhibited photosynthesis (PS) and acetazolamide-inhibited photosynthesis rates (AZPS). Since acetazolamide inhibits the utilization of bicarbonate via extracellular catalysis, PS represents full $CO_2$ + bicarbonate utilization and AZPS represents only

$CO_2$ uptake and an unknown proportion of active bicarbonate uptake. Biologically relevant saturating and non-saturating irradiance levels were selected by consulting previous studies of *M. pyrifera* in the field (Stewart et al. 2009, Edwards and Kim 2010).

In 2015, I again measured the effect of irradiance and flow velocity, but examined the effect of blade origin from different wave exposure habitats on relative bicarbonate uptake during photosynthesis. I tested orthogonally for the separate and combined effects of two levels of irradiance (800 or 100 μmoles photons/$m^2$/s), two levels of flow velocity (10 or 3 cm/s), and two levels of blade origin (from protected or exposed hydrodynamic populations) on PS and AZPS. Flow velocity treatments were lowered in 2015 to reflect velocities frequently encountered by blades at the Hopkins Marine Station, where we carried out detailed depth-stratified current velocity measurements (see *Results*). Light levels were slightly different in 2015, but remained below and above the irradiance threshold for photosynthesis (200 μmoles photons/$m^2$/s) in *M. pyrifera* (Gerard 1984).

*Collection of M. pyrifera fronds for photosynthesis experiments*

To explore the possibility that the carbon uptake physiology of *M. pyrifera* is acclimated to high and low irradiance microenvironments, I collected individual frond segments from sporophytes growing in the McAbee kelp bed (Monterey Bay, California; N 36.61485 W 121.89706) in March 2014. Light-replete frond segments containing at least six entire and non-epiphytized blades were collected 2 m distal to

the apical scimitar of the frond. Light-limited frond segments were collected at 10 m depth from mature fronds that reached the surface. Each frond segment was taken from a separate sporophyte. These segments were transferred in a cooler of cold seawater back to Long Marine Laboratory (University of California, Santa Cruz). There, each blade of each segment was trimmed to a length of 35cm to fit in the working section of the respirometer and held for 24-72 hours indoors in a flow-through seawater table away from a shaded window (light level ~5 μmoles photons/$m^2$).

To explore the possibility that the carbon uptake physiology of *M. pyrifera* is acclimated to high and low wave exposure habitats, I collected meter-long segments from the surface fronds of wave-protected kelp beds (McAbee, Hopkins Marine Station, Stillwater Cove) and wave-exposed kelp beds (Otter Pt., Pt. Piños, and Sunset Pt.) in the Monterey and Carmel bays in February 2015 (coordinates in Table S1, *Appendix 3*). These sites represent the extremes of possible wave-exposed and wave-protected conditions in Central California, yet are located along a single peninsula. The exposed sites experience significantly higher wave heights and forces in empirical and modeled datasets (USGS SWAN wave force model, Table S1, one-tailed T-test, $p = 0.011$, $DF = 2.81$, $t\text{-ratio} = 4.63$) (Graham et al. 1997, Figurski 2010, Erikson et al. 2014). While the relationship between wave exposure and unidirectional (current-driven) velocity magnitudes is complex and unknown for most of my sites, increased wave exposure is empirically associated with higher velocity magnitudes throughout the water column in a recent study near the Hopkins Marine

Station kelp forest (Koweek et al. in prep.). In general, since high wave exposure sites in the Monterey Bay are also oriented toward the open ocean, one would expect unidirectional current velocities to increase with wave exposure at all my sites. After collection, frond segments were immediately transported to the NOAA SWFSC adjacent to Long Marine Lab where they were trimmed and held in a shaded outdoor flow-through tank (maximum ~ 100 μmoles photons/$m^2$) for 24 – 72 hrs. During both study periods, filtered seawater ranged between 13 and 16˚C.

*Oxygen evolution experiments*

To measure photosynthetic rates of entire *M. pyrifera* blades in response to irradiance and velocity treatments, I carried out oxygen evolution experiments in a Loligo swim tunnel respirometer 10L (Loligo Systems, Denmark). While flow velocity is an important determinant of boundary layer thickness, studies have shown that blade structure and rugosity also strongly influence boundary layer thickness in *M. pyrifera* (Hurd and Pilditch 2011). Furthermore, while the use of tissue discs subsampled from entire blades is prevalent in recent studies, it is well established that there is significant variability of photosynthetic rates within single blades, and that tissue wounding impacts photosynthetic studies (Arnold and Manley 1985). Thus I used the Loligo respirometer with a 10 L working volume instead of traditional BOD bottles to accommodate entire *M. pyrifera* blades. The respirometer was comprised of a sealed rectangular working section (40 x 10 x 10 cm) and collimator surrounded by a recirculating seawater jacket. The working section was fitted with a self-sealing

silicone injection port and an oxygen sensor port. The oxygen meter (Firesting $O_2$, Pyro Science, Germany) was fitted with an optical sensor and thermocouple, and measured temperature-corrected dissolved oxygen concentrations once per second. The oxygen meter was calibrated daily. Rates of respiration and photosynthesis were calculated as the slope of linear decrease and increase, respectively, of the $[O_2]$ in the sealed respirometer. Photosynthesis was stimulated by two artificial light fixtures (Artificial light (200 W sodium halide bulb in combination with a GE 65 W blue Plant Grow Light). When combined, the fixtures produced measurable light at all wavelengths relevant to photosynthesis (Figure S1, *Appendix 2*).

For each oxygen evolution trial, a healthy, mature blade was chosen haphazardly from the collected *M. pyrifera* segments (after at least 24 h incubation) and tethered in the working section of the respirometer. The respirometer was then filled with 2 micron filtered seawater and sealed, and photosynthesis was measured in four phases. First dark respiration (R1) was measured under complete darkness using a custom fabric-draped shade box. Then uninhibited photosynthesis (PS) was measured under artificial light. After this, 3.3 mL of 25 mM acetazolamide (AZ) in 0.05 M NaOH (final concentration = 100 μM) was injected to inhibit external use of bicarbonate; with the light level unaltered, photosynthesis under this constraint (AZPS) was measured. Finally, the trial was completed with a second measurement of respiration (R2) in complete darkness. Each illuminated phase of measurement was carried out for 15-20 minutes, resulting in a maximum of 40 minutes of photosynthetic activity in 10 L of seawater. After oxygen measurements were

completed, the kelp blade was refrigerated in the dark at 4˚C and reserved for pigment extraction within 24 hours. I conducted a set of controls for one full replicate of each Treatment (1, 2, 3, and 4) on light-acclimated blades by injecting 0.05 M NaOH solution instead of the NaOH-based AZ solution. These controls confirmed that a) injection of this weak base had no impact on photosynthetic rates and b) AZ was responsible for observed reductions in photosynthetic rates post-injection.

The measurement of oxygen evolution is potentially problematic at very low flow velocities. Since I hypothesized that flow velocities less than 3 cm/s may drive photosynthetic limitation via boundary layer formation, photosynthetically-produced oxygen may be trapped in the boundary layer, delaying or reducing detection in the bulk flow by the oxygen sensor. To qualitatively assess the completeness of fluid mixing in the respirometer, I injected saturated Rhodamine B dye solution onto the blade at each flow treatment level. At 10 cm/s, dye mixed almost immediately (< 3 seconds). At 3 cm/s, dye remained on the blade for much longer, but did eventually fully mix in ~ 30 s. Trials run at 3cm/s indeed generated much more variable oxygen evolution traces than trials run at 10 cm/s and faster. Since, however, rates of oxygen production were integrated over several minutes, it is likely that $O_2$ sensor detected accurate levels of oxygen production for the two different flow velocities.

For each measurement period of the oxygen evolution trials (R1, PS, AZPS, and R2), [$O_2$] data were trimmed by visual inspection to the most stable 2 - 5 minutes of measurement duration. The relationship between [$O_2$] and time (s) was always linear in these durations. Linear regression was then used to estimate the slope each

measurement period in R (R Core Team, 2013). Gross photosynthesis was calculated as R1 + PS, whereas AZ-inhibited gross photosynthesis was calculated as AZPS + R2. Photosynthetic rates were normalized to blade wet weight. To calculate the proportion of external bicarbonate utilization (EBU) during each trial, I used the following equation:

$$\text{Proportion EBU} = ((PS + R1) - (AZ + R2)) / (PS + R1)$$

*Monitoring of seawater [Ci] during experimentation*

Ci is highly variable along the coast of California (including the Monterey Bay) due to tidal, upwelling, and stratification events (Frieder et al. 2012, Kapsenberg and Hofmann 2016). In a representative kelp forest at the Hopkins Marine Station, pCO2 ranges between 260-770 µatm at the benthos yearly (pH = 7.78-8.20 (total scale)), and between 175-540 µatm at the surface (pH: 7.92-8.33 (total scale)) (Koweek et al. in prep.). Variation in pH, water temperature, and salinity are all driven by upwelling processes within the Monterey Bay, which has little to no freshwater input. During upwelling relaxation, temperatures range from 11-16 ˚C, whereas they drop significantly (9-10˚C) during upwelling (Drake et al. 2005). Salinity varies between 33.1 and 33.9 ppt on a yearly basis (Ward 2005).

To monitor for variation in seawater [Ci] supply at Long Marine Lab, water samples were collected at the start and end of a subsample of oxygen evolution trials in 2014 (16 runs), and for all trials in 2015. Water samples were fixed with 200 µL saturated $HgCl_2$ and stored in 120 mL borosilicate glass bottles sealed with parafilm

at 4˚C until total alkalinity and pH could be measured. To determine [DIC] of the seawater samples, I measured the pH and total alkalinity (TA) within eight months of $HgCl_2$ fixation. pH was measured in triplicate on a spectrophotometer using the indicator dye m-cresol purple (pH of solution = 7.9 $\pm$ 0.01) in a temperature-controlled measurement cell set to 25˚C. Absorbances of the dyed and un-dyed sample were measured at three wavelengths: a non-absorbing wavelength (730 nm for m-cresol purple) and at the wavelengths corresponding to the absorption maxima of the base (I2–) and acid (HI–) forms of the dye, respectively (578 and 434 nm). TA was measured in duplicate or singly using open-cell titration with HCl on the Titrando automatic titrator (MetroOhm Inc.) in a jacketed flask maintained at 25˚C. The titrator was calibrated daily with certified reference material from the Dickson Laboratory at the Scripps Institute of Oceanography. TA was calculated from the second (i.e. highest) integral endpoint calculated by the Tiamo (MetroOhm Inc.) software. TA and pH for each sample were then entered into the CO2SYS Excel macro (v.2, Pierrot et al. 2006) to calculate [DIC] and $pCO_2$ at 15˚C (the temperature at which the oxygen evolution experiments were run). Boxplot distributions of $pCO_2$ and pH measurements for each experiment are presented in Figure S2 (*Appendix 2)*.

*Measurement of pigment content in incubated blades*

To assess possible local adaptation of tissue pigment content to my collection sites, relative pigment concentrations were measured within 24 hours of each oxygen evolution trial. Fucoxanthin, chlorophyll a, and chlorophyll c were extracted from

fresh (refrigerated) tissue discs (2.5 cm diameter) with acetone, methanol, and dimethyl sulfoxide in 30 mL glass test tubes capped with parafilm. Tissue discs were first extracted with dimethyl sulfoxide and water (4:1) on ice for 15 minutes; the disc was then transferred to a new test tube for further extraction with a 4:1:1 mixture of acetone, methanol, and water in a dark chamber for 2 hours. Absorbance of extracts was measured on a Thermo-Scientific GENESYS 10S UV-VIS spectrophotometer at 665, 631, 582, and 480 nm and converted to g pigment/ kg kelp tissue using the calculations detailed in Seely et al. 1972.

*Measurement of within-kelp forest current velocity*

The flow velocities that limit gas exchange in *M. pyrifera* blades are known from laboratory studies (Wheeler 1980), but we have no detailed knowledge of the velocities experienced by *M. pyrifera* within the water column of a mature kelp forest. To parameterize the unidirectional velocities used in my oxygen evolution experiments, I measured unidirectional background current velocities within a low wave exposure kelp forest.

Water column velocity was measured in July and October 2013 with a bottom-mounted Acoustic Doppler Current Profiler (ADCP; RD Instruments 1200 kHz). The instrument was deployed in the middle of a kelp bed offshore of Hopkins Marine Station in southern Monterey Bay, CA (36.6216 N, 121.90176 W) at a depth of 10 m. Instantaneous velocity measurements were recorded every 3 minutes in 0.5 m vertical bins that extended from ~1.5 m above the bottom to ~1.5 m below the

surface. Velocity magnitudes were calculated as the square root of the sum of the east-west velocity component squared and the north-south velocity component squared. These velocity magnitudes quantify the unidirectional background currents experienced by kelp plants, as they do not capture wave orbital velocity, oscillatory flow, or the movement of the kelp tissue itself relative to the adjacent water mass.

*Statistical analysis*

I removed outliers representing instrument or operator error from each photosynthetic rate dataset using JMP Pro 12 (SAS Institute, Inc.). Type I ANOVA was performed separately for each experiment (2014 and 2015) to test the hypothesis that light level, flow velocity, and blade origin influence the proportion of externally-utilized bicarbonate used to support photosynthesis. I also tested for the interaction between irradiance and blade origin in 2014, and between flow velocity and blade origin in 2015. I did not test for any other interactions because they were not relevant to my hypotheses. The proportion of externally utilized bicarbonate was normally distributed, not binomial, and so I did not transform the data.

Gross photosynthetic rates were square root transformed for analysis to correct for slight non-normality and heteroscedasticity. In 2014, I performed a type I ANOVA to test for the fixed effects of irradiance, flow velocity, blade origin, and irradiance x blade origin on AZPS and PS as separate dependent variables. To account for the possible influence of fluctuating $CO_2$ concentrations in experimental seawater, I carried out a least squares regression analysis on a subset of my PS and

AZPS datasets. In 2014, $pCO_2$ had no correlation with gross photosynthetic rates, whereas $pCO_2$ was significantly correlated with gross photosynthesis magnitude in 2015. Thus in 2015, I used an ANCOVA approach on PS and AZPS with $pCO_2$ as a continuous variable to examine the fixed effects of irradiance, flow velocity, blade origin (wave exposure) and the interaction between flow velocity and blade origin. Again, I did not test for any other interactions because they were not relevant to my hypotheses.

## Results

*Measurement of flow velocities within a protected kelp forest*

ADCP measurements indicated that unidirectional background current velocities slower than 3 cm/s persistently occur in the protected Hopkins Marine Station kelp forest, especially at depth (5+ meters deep). At 8.5 m depth, these low velocities occur continuously for 15 minutes for 40 - 80% of each day (top two panels, Figure 1 and S3 (*Appendix 2*)). Longer duration periods of slow flow also occur at depth, but less frequently; velocities slower than 3 cm/s can occur continuously for 60 minutes 10 - 40% of the time (bottom right panels, Figure 1 and S3). These critically low flow velocities occur rarely, if at all, at the upper part of the water column (surface to 1.5 m depth, Figures 1 and S3, top right). These data indicate that kelp at protected sites regularly experience currents that can limit gas exchange, but mostly near the seafloor. As such, kelp tissues that experience low flows also must experience low light; thus the experimental conditions in which kelp

are photosynthesizing at high light levels but low flow levels (Treatment 3) are unlikely to occur in the field. Nonetheless, it was important to manipulate these two factors orthogonally to fully evaluate their relative effects on bicarbonate use.

*Oxygen evolution experiments: Proportion of external bicarbonate uptake under irradiance and velocity treatments*

In 2014, the mean proportion of photosynthesis supported by external bicarbonate utilization (EBU) clearly differed in response to irradiance exposure level, but not blade origin or flow velocity (ANOVA Table 2, Fig. 2). Blades photosynthesizing at low irradiance levels (analogous to irradiance levels at 10m depth beneath a full canopy) used only an average 27 $\pm$ 3.7% external bicarbonate whereas blades experiencing high irradiance (analogous to surface canopy conditions) used an average of 53 $\pm$ 3.8% external bicarbonate.

In 2015, irradiance and flow velocity both influenced the proportion of photosynthesis supported by EBU, but blade origin (differing exposure habitats) did not (ANOVA, Table 2, Fig. 3, blade origin not shown). Proportional EBU was reduced in low irradiance treatments (mean = 33 $\pm$ 3.4%) relative to high irradiance treatments (mean = 43 $\pm$ 3.7%). Kelp blades experiencing flows below 3 cm/s (limiting Ci supply) used an average 30 $\pm$ 3.4% external bicarbonate whereas those blades experiencing flows of 10 cm/s used an average 46 $\pm$ 3.7% external bicarbonate to support photosynthesis. There was no interaction between flow velocity and blade origin.

*Oxygen evolution experiments: Patterns of gross photosynthesis in response to irradiance and velocity treatments in blades from different populations*

In 2014, both AZ-inhibited (AZPS) and uninhibited photosynthetic rates (PS) varied as a function of blade origin (ANOVA Table 3, Figures S5 and S6 in *Appendix 2*). Surface blades photosynthesized at greater rates (15.30 $\pm$ 0.105 µmoles $O_2$ $g^{-1}$ FW $hr^{-1}$) than 10 m deep blades (12.16 $\pm$ 0.109 µmoles $O_2$ $g^{-1}$ FW $hr^{-1}$). Acetazolamide inhibited photosynthesis was also much greater in surface blades (9.25 $\pm$ 0.107 µmoles $O_2$ $g^{-1}$ FW $hr^{-1}$) than 10 m deep blades (6.19 $\pm$ 0.110 µmoles $O_2$ $g^{-1}$ FW $hr^{-1}$, Figure 4). As expected, high irradiance increased both PS ($p < 0.0001$) and AZPS ($p = 0.0173$) relative to the low irradiance treatment. There was a significant interaction of blade origin with irradiance treatment on PS ($p = 0.0101$) and AZPS ($p = 0.0256$); 10m deep (light-limited) blades showed reduced PS in response to the high irradiance treatment but were indistinguishable from light-replete canopy blades under the low irradiance treatment. It is possible, therefore, that the light-limited blades expressed lower rates of photosynthesis under my high light treatment because of photoinhibition (Cabello-Pasini et al. 2000). $pCO_2$ was not correlated with PS or AZPS in my subsample of oxygen evolution trials (Least Squares Regression, $p = 0.496$ and 0.6403, respectively).

In 2015, samples from low wave exposure habitats demonstrated increased PS ($p = 0.0088$) and AZPS ($p = 0.0451$) relative to those from high wave exposure habitats, but there was no interaction with flow velocity treatments (ANOVA Table

4). This result, however, is likely a Type I error. The significance is driven by high PS in a single treatment cross (low exposure origin, high irradiance, high velocity), and is likely a site effect of high PS rates in blades from the Breakwater and Hopkins Marine Station. $pCO_2$ was strongly correlated with PS rates ($p = 0.0035$) and AZPS rates ($p = 0.0013$).

No differences were detected in the above treatments when normalized either to blade wet weight or total pigment concentration. Photosynthetic rates of long incubation duration (5-6 days) did not significantly decrease relative to mid (3-4 d) or short incubation duration (1-2 d) as measured in oxygen evolution trials in 2014 (Least Squares Means Contrast, $p = 0.8968$) or in 2015 (LSMC, $p = 0.8969$). R2 was significantly greater than R1 in 2014 (t-test, means = -1.14, -1.93, $p = 0.0053$), indicating possible thermal stress or osmotic shock during oxygen evolution (Lapointe et al. 1984, Henkel and Hofmann 2008). In 2015, however, R2 and R1 were not significantly different (t-test, $p = 0.2541$). Overall, respiration rates remained low during oxygen evolution trials. In 2014, the average ratio of PS:R1 was $18.45 \pm 3.23$; in 2015, the average ratio of PS: R1 was $12.41 \pm 2.33$ (see Figure S4 in *Appendix 2* for graphical representation of PS vs. AZPS vs. R1 vs. R2).

*Relative pigment concentrations of experimental samples*

In 2014, blades from 10m depth at McAbee had a higher ratio of fucoxanthin to chlorophyll a ($0.62 \pm 0.021$) than surface blades ($0.51 \pm 0.024$, t-test, $p = 0.0008$), supporting the possibility that the two blade types possess acclimated photosynthetic

physiology to their respective microhabitats. Pigment composition was not related to incubation duration of each blade (least squares mean contrast test); however we lack pigment composition data prior to the incubation, so there is still the possibility of an incubation effect. In 2015, there were no significant differences between the pigment compositions of surface blades collected from different sites or exposure categories. The average ratio of fuc:Chl a in blades collected in 2015 was $0.5 \pm 0.05$. Additional pigment data for both years are given in Table 1.

**Discussion**

My results are the first to demonstrate that patterns of EBU-supported photosynthesis in *M. pyrifera* are influenced by irradiance and flow velocity. In both experiments, high irradiance increased the proportion of photosynthesis supported by external bicarbonate use. In the field, this means that canopy blades likely utilize significantly more bicarbonate than light-limited blades at depth. Contrary to my hypotheses, however, decreasing flow velocity below a saturation threshold greatly *decreased* the proportion of external bicarbonate use in *M. pyrifera* blades. Kelp blades experiencing flows below 3 cm/s used, on average, 30% less external bicarbonate utilization to support photosynthesis than blades experiencing flows of 10 cm/s. This indicates that EBU is not stimulated by limiting [Ci], but is rather a passive function of Ci supply. It is certainly possible that active (ion exchange channel-mediated) bicarbonate utilization, which I did not measure in this study, may respond to limiting [Ci]; this requires further work.

Most studies that have observed photosynthetic limitation of aquatic autotrophs at low flow velocities (0 – 3 cm/s) attribute this pattern to nutrient limitation; very low flows generate thick boundary layers through which Ci and other nutrients must diffuse, potentially restricting productivity (Koehl and Alberte 1988, Nishihara and Ackerman 2009). Another mechanism has been proposed, however, in which the diffusive boundary layer may restrict efflux of $O_2$, resulting in high extracellular oxygen concentrations. $O_2$ retention could then restrict photosynthesis by promoting photorespiration or the production of reactive oxygen species (Mass et al. 2010). Flow velocity treatments in 2014 did not impact the proportion of external bicarbonate utilization, but this is likely because nutrient influx/efflux as a function of boundary layer thickness is maximized at velocities greater than 3 cm/s (Wheeler 1980, Hansen et al. 2011).While it is already clear that canopy-forming kelps locally increase seawater pH as they photosynthesize during the day, especially in the upper portion of the water column (Delille et al. 2009, Britton et al. 2016), this study adds yet another example of how *M. pyrifera* may chemically structure and stratify the water column via changes in carbon uptake physiology.

The second finding of this work is the lack of EBU acclimation in different tissues in *M. pyrifera*. In both irradiance treatments canopy blades and deep blades utilized the same percentage of bicarbonate via external catalysis (Table 2). In all other respects, however, canopy blades and deep blades exhibited expected photosynthetic acclimation. Light-replete canopy blades at McAbee possess a lower ratio of accessory pigments (fucoxanthin and chlorophyll c) relative to chlorophyll a than

deep light-limited blades, as has been observed in *M. pyrifera* in Southern California and Chile (Smith and Melis 1987, Colombo-Pallotta et al. 2006). My data also corroborate the finding that light-limited blades possess significantly lower photosynthetic rates than light-replete blades in Southern Californian and Chilean populations of *M. pyrifera* (Arnold and Manley 1985, Smith and Melis 1987, Colombo-Pallotta et al. 2006); this pattern has been attributed to the greater efficiency and photosystem turnover in light-acclimated blades. In my study, this observation may also have been due to photoinhibition in blades from deep waters, which were likely not acclimated to the high irradiance to which they were subjected. Regardless, there is no evidence that deep and canopy blades differ in their carbon uptake dynamics. This result supports the conclusion that *M. pyrifera* tissue does not up-regulate external bicarbonate utilization in response to limiting [Ci].

Across all years and treatments, I find that *M. pyrifera* in the Monterey Bay utilize bicarbonate via external catalysis to support an average 40% of photosynthesis, corroborating the findings of Brown et al. (2014). The remaining 60% of photosynthesis is supported by dissolved $CO_2$ and an unknown proportion of active bicarbonate uptake via ion exchange proteins. This finding differs from the report that *M. pyrifera* from New Zealand use less than 20% external bicarbonate uptake at pH 7.65 (Fernández et al. 2014). My experiments were carried out in seawater of varying pH, which prevents direct comparison to the more controlled approach of Fernandez et al. It is, however, remotely possible that there is a genetic divergence between carbon uptake in northern and southern hemisphere populations of *M. pyrifera*.

Although *M. pyrifera* is a monotypic species (Coyer et al. 2001), strong ecotypic variation has been observed in holdfast, habit, and blade morphology (e.g. *integrifolia* vs. *pyrifera* morphs). On the California coast, for example, local adaptation of nitrate uptake physiology in different populations of *M. pyrifera* has occurred despite the fact these populations likely still exchange genetic material via long-distance dispersal (Kopczak et al. 1991).

The results of this research indicate that utilization of different Ci species ($CO_2$ and bicarbonate) is a plastic process regulated by persistent abiotic variables in the nearshore marine system. This work contributes to our understanding of the impact of the abiotic environment on *M. pyrifera*, but also give us a sense of how *M. pyrifera* may in turn structure carbonate chemistry in kelp forest microhabitats.

**Table 1.** Mean (± one standard deviation) grams of pigment (chlorophyll a, fucoxanthin, and chlorophyll c) per gram of fresh *Macrocystis pyrifera* tissue. In 2014, blade tissue was sampled at the surface and at depth (10m) at McAbee. In 2015, blade tissue was sampled from the surface from three protected (low wave exposure) and three exposed (high wave exposure) sites.

| Blade origin | g Chl a $g^{-1}$ FW | g fx $g^{-1}$ FW | g Chl c $g^{-1}$ FW | Fuc:Chl a (by mass) | Year Sampled | Habitat |
|---|---|---|---|---|---|---|
| McAbee (surface) | 0.32 ± 0.070 | 0.16 ± 0.028 | 0.063 ± 0.015 | 0.51 ± 0.094 | 2014 | Protected |
| McAbee (10m) | 0.30 ± 0.064 | 0.18 ± 0.033 | 0.095 ± 0.015 | 0.62 ± 0.084 | 2014 | Protected |
| Sunset Pt. | 0.20 ± 0.037 | 0.084 ± 0.029 | 0.037 ± 0.010 | 0.41 ± 0.057 | 2015 | Exposed |
| Pt. Pinos | 0.20 ± 0.051 | 0.10 ± 0.052 | 0.046 ± 0.023 | 0.47 ± 0.17 | 2015 | Exposed |
| Otter Point | 0.25 ± 0.065 | 0.12 ± 0.033 | 0.060 ± 0.019 | 0.52 ± 0.11 | 2015 | Exposed |
| Hopkins | 0.27 ± 0.14 | 0.12 ± 0.084 | 0.056 ± 0.043 | 0.44 ± 0.086 | 2015 | Protected |
| McAbee | 0.19 ± 0.088 | 0.086 ± 0.051 | 0.041 ± 0.023 | 0.43 ± 0.12 | 2015 | Protected |
| Stillwater | 0.21 ± 0.062 | 0.10 ± 0.050 | 0.047 ± 0.021 | 0.49 ± 0.14 | 2015 | Protected |

**Table 2**. Effect of experimental treatments on the fraction of photosynthesis supported by external bicarbonate utilization (EBU). ANOVA, DF = 1.

| Year | Fixed Effect | F Ratio | Prob > F |
|---|---|---|---|
| 2014 | Blade origin (irradiance) | 3.16 | 0.0873 |
| 2014 | Light | 23.12 | <.0001*** |
| 2014 | Flow velocity | 0.27 | 0.6103 |
| 2014 | Blade origin x light | 0.04 | 0.8413 |
| 2015 | Blade origin (exposure) | 0.04 | 0.8413 |
| 2015 | Light | 4.40 | 0.0436* |
| 2015 | Flow velocity | 10.73 | 0.0025** |
| 2015 | Blade origin x flow velocity | 0.05 | 0.822 |

**Table 3**. Effect of experimental treatments on uninhibited photosynthesis (PS, square root transformed) or AZ-inhibited photosynthesis (AZPS, square root transformed). 2014 data: ANOVA, DF = 1. 2015 data: ANCOVA, DF = 1, continuous variable = $pCO_2$ of experimental incubation seawater. Graphical representation of mean PS and AZPS in response to these treatments can be found in Figure S5 and Figure S6 (*Appendix 2)*.

| Data | Year | Fixed Effect | F Ratio | Prob > F |
|---|---|---|---|---|
| PS | 2014 | Blade origin (irradiance) | 7.88 | 0.0093** |
| PS | 2014 | Light | 75.64 | <.0001*** |
| PS | 2014 | Flow velocity | 3.91 | 0.0588 |
| PS | 2014 | Blade origin x Light | 7.70 | 0.0101* |
| AZPS | 2014 | Blade origin (irradiance) | 13.02 | 0.0013** |
| AZPS | 2014 | Light | 6.47 | 0.0173* |
| AZPS | 2014 | Flow velocity | 0.68 | 0.4164 |
| AZPS | 2014 | Blade origin x flow velocity | 5.61 | 0.0256* |
| PS | 2015 | $pCO_2$ | 10.08 | 0.0035** |
| PS | 2015 | Blade origin (wave exposure) | 7.85 | 0.0088** |
| PS | 2015 | Light | 12.75 | 0.0012** |
| PS | 2015 | Flow velocity | 76.31 | <.0001*** |
| PS | 2015 | Blade origin x flow velocity | 0.16 | 0.6908 |
| AZPS | 2015 | $pCO_2$ | 12.52 | 0.0013** |
| AZPS | 2015 | Blade origin (wave exposure) | 4.37 | 0.0451* |
| AZPS | 2015 | Light | 0.41 | 0.529 |
| AZPS | 2015 | Flow velocity | 9.29 | 0.0048** |
| AZPS | 2015 | Blade origin x flow velocity | 0.21 | 0.6536 |

**Figure 1.** Proportions of 15 minute periods (A,B) and 60 minute periods (C,D) each day in July 2013 when velocities were less than or equal to 3 cm $s^{-1}$ (dark blue), between 3 and 10 cm $s^{-1}$ (medium green) or greater than 10 cm $s^{-1}$ (light yellow) at the closest ADCP bin to the bottom (1.5 m above bottom; A,C) and the closest ADCP bin to the surface (8.5 m above bottom; B,D). October 2013 data can be found in figure S3 in *Appendix 2.*

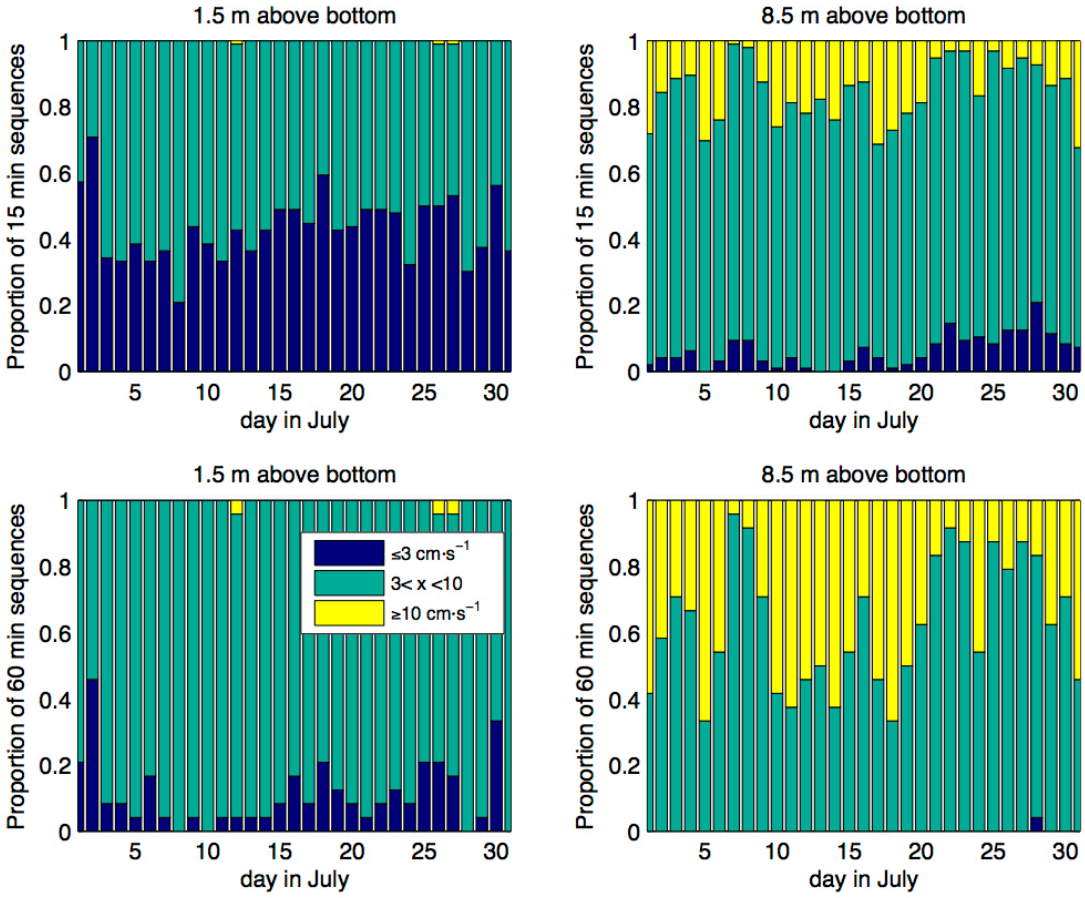

**Figure 2.** Fraction of photosynthesis supported by external bicarbonate uptake as a function of irradiance level and blade origin (surface and 10 m). Fractions were calculated from rates of gross PS and AZPS from the 2014 experiment. Error bars represent SE.

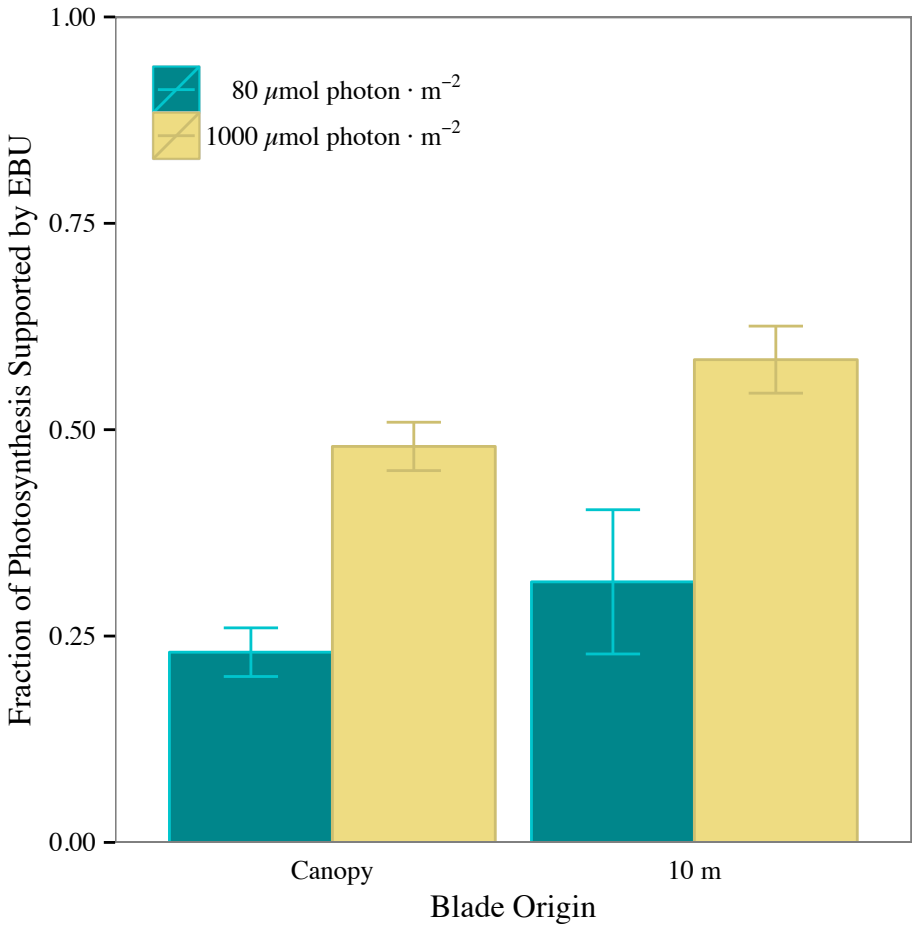

**Figure 3.** Fraction of photosynthesis supported by external bicarbonate uptake as a function of irradiance level and flow velocity. Fractions were calculated from rates of gross PS and AZPS from the 2015 experiment. Error bars represent SE.

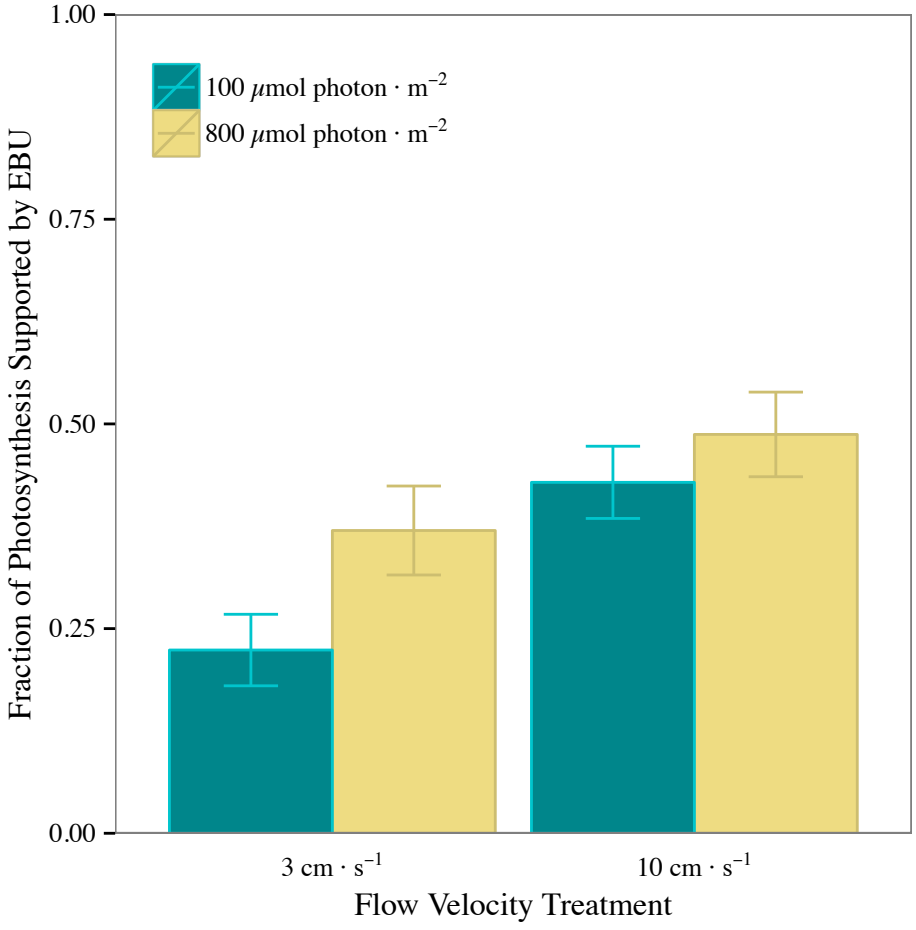

**Figure 4.** Gross photosynthetic rate of uninhibited photosynthesis (PS) and AZ-inhibited photosynthesis (AZPS) grouped by blade origin (surface and 10 meter depth). Each bar represents 4 replicate trials. Error bars represent SE. Data are from the high irradiance treatment only (1000 µmoles photons/$m^2$) in the 2015 experiment.

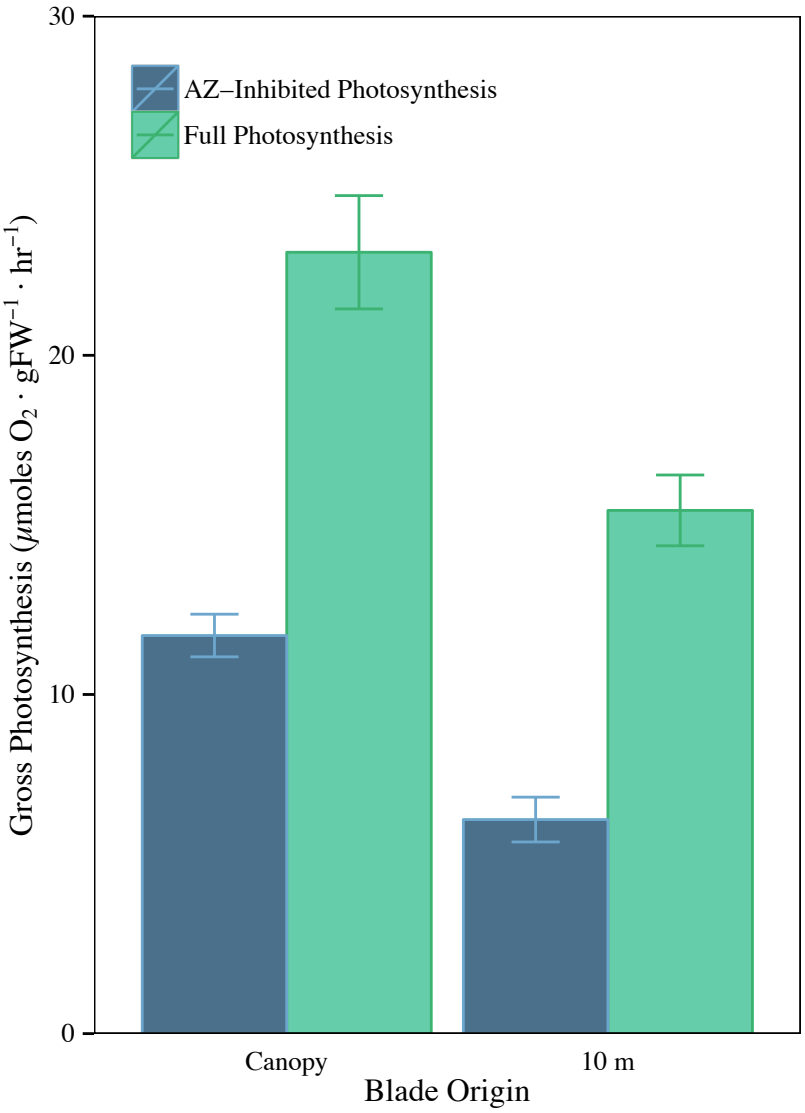

## Chapter 3:

## Patterns and Drivers of $\partial^{13}$C Variation in the Giant Kelp, *Macrocystis pyrifera*

### Introduction

The enormous productivity of *M. pyrifera* means that it is a major source of energy at the base of the nearshore food chain (Miller and Page 2012, Miller et al. 2015). As with many other dominant canopy-forming macroalgae, *M. pyrifera* has extremely variable $\partial^{13}$C values – up to 6‰ different tissue signatures within a single individual (Foley and Koch 2010). The stable isotope of carbon ($\partial^{13}$C) is an information-rich biomarker that can be used to infer the autotrophic source of food webs (O'Leary 1988, Post 2002). In nearshore marine habitats, $\partial^{13}$C signatures of heterotrophic organisms should directly reflect the relative contributions of various primary producers (macroalgae, phytoplankton, or seagrasses) to a given food web (Duggins et al. 1989, Fredriksen 2003, Kaehler et al. 2006). It has become increasingly clear, however, that $\partial^{13}$C can vary widely within macroalgal species, populations, and even individuals, confounding the attempts of straightforward end-member designation in trophic studies (Phillips and Gregg 2003, Cornelisen et al. 2007, Miller and Page 2012, Dethier et al. 2013).

In other species of marine autotrophs, patterns of $\partial^{13}$C variation have been correlated with key abiotic factors that regulate dissolved inorganic carbon (DIC) supply and usage. Variation in irradiance and seawater [DIC] are the strongest observed drivers of $\partial^{13}$C signatures, followed by water velocity and temperature

(Wefer and Killingley 1986, Wiencke and Fischer 1990, Grice et al. 1996, Hemminga and Mateo 1996, MacLeod and Barton 1998, Burkhardt et al. 1999, Trudeau and Rasmussen 2003, Mackey et al. 2015, McPherson et al. 2015). In the Monterey bay, these abiotic factors vary geographically but also seasonally, as coastal upwelling (a wind-forcing oceanographic phenomenon) injects cold, saline, and high $pCO_2$ water into kelp forests during the spring and summer months (Drake et al. 2005, Kapsenberg and Hofmann 2016). With a 6‰ variation in tissue $\partial^{13}C$, *M. pyrifera* is an extreme example of a hyper-variable foundational primary producer. How does the $\partial^{13}C$ of *M. pyrifera* co-vary with abiotic forces in the Monterey Bay, and what physiological mechanisms drive these diverse signatures in *M. pyrifera?*

There are several possible mechanisms driving within-individual and within-species variation of $\partial^{13}C$ in *M. pyrifera*. In Central California, *M. pyrifera* displays some seasonal and upwelling-driven $\partial^{13}C$ variation, but shows no response to differing carbon source end members (i.e. freshwater-derived vs. upwelling-derived) (Foley and Koch 2010). Since, as demonstrated in Chapter 2, *M. pyrifera* is capable of utilizing both dissolved $CO_2$ and bicarbonate, $\partial^{13}C$ may be driven by the differential use of $CO_2$ and bicarbonate within a given source pool. Macroalgae exclusively using bicarbonate exhibit a $\partial^{13}C$ of +5 to -15‰, whereas individuals relying only on diffusive $CO_2$ are depleted in $^{13}C$, with values lower than -25‰ (Mook et al. 1974, Giordano et al. 2005, Marconi et al. 2011, Raven et al. 2012). Kelp may use more or less bicarbonate due to upwelling-driven changes in seawater pH and seawater [DIC] (Fernández et al. 2015) or as a function of light intensity and

water velocity (Drobnitch et al. in press). Alternatively, $\partial^{13}C$ variation could be caused by differences in maximum productivity of kelps from different microhabitats. In phytoplankton, increasing enrichment of $\partial^{13}C$ is linearly correlated with growth rates and exhaustion of the available pool of DIC (Laws et al. 1995, Popp et al. 1998, Vanderklift and Bearham 2014). When local DIC supply becomes critically limiting, enzymes cannot continue to discriminate against $^{13}C$, resulting in tissue enrichment as the total pool is assimilated. This limitation is most extreme in conditions of low water circulation or very high irradiance. Finally, kelp tissue $\partial^{13}C$ could be driven by fractionation during carbohydrate storage or transport. The $\partial^{13}C$ of emerging frond initials of large *M. pyrifera* sporophytes experience marked enrichment as biomass is translocated to them by adult canopy blades (Fox 2013).

In this study, I seek to gain a mechanistic understanding of the abiotic variables that determine $\partial^{13}C$ in *M. pyrifera* in Central California. To assess whether differential bicarbonate use or productivity-driven DIC limitation drive $\partial^{13}C$ variation in *M. pyrifera*, I experimentally incubated meristematic tissue in velocity-limited and irradiance-limited conditions. To evaluate the influence of DIC supply as a function of flow velocity and irradiance on $\partial^{13}C$ discrimination in *M. pyrifera* in the field, I carried out a targeted sampling of kelp tissue from a range of microhabitats in the Monterey Bay. Finally, to quantify the impact of translocation on kelp $\partial^{13}C$, I took paired samples of vegetative blade and adjacent sap tissue from different depths on *M. pyrifera* fronds at two different sites in the Monterey Bay.

Overall, I seek to uncover consistent patterns underlying the variation in $\partial^{13}C$ signature of *M. pyrifera* tissue. Establishment of such patterns, particularly if they are associated with discrete seasons and microhabitats, will add new descriptive power to $\partial^{13}C$ as an ecological biomarker.

**Methods**

*Hypotheses: Mechanisms of $\partial^{13}C$ discrimination in* M. pyrifera

I hypothesized that increased bicarbonate use (up to 50% bicarbonate) in higher irradiance and higher flow velocities would lead to enriched meristems relative to those relying mostly on $CO_2$ (up to 80% $CO_2$ usage) in low irradiance and low flow velocity conditions (Drobnitch et al. in press). Alternatively, productivity (growth rate) could solely drive enrichment of *M. pyrifera* tissue via exhaustion of available DIC supply, in which case I would hypothesize that there would be a significant correlation between growth rate and $\partial^{13}C$ signatures in incubated meristems regardless of abiotic treatment.

*Hypotheses: Patterns of ∂13C in kelp forest microhabitats in the Monterey Bay*

I hypothesized that kelp tissue growing at ≥ 10 meter depth (where irradiance levels are sub-saturating for photosynthesis) would primarily utilize dissolved $CO_2$ and furthermore experience no DIC limitation, resulting in depleted $\partial^{13}C$ signatures that closely reflect Rubisco discrimination (-27‰). On the other hand, canopy blades (which consistently experience high irradiance) should use a larger proportion of

bicarbonate (Drobnitch et al. in press) and also largely deplete ambient DIC, yielding enriched $\partial^{13}C$ signatures up to -11‰. I acknowledge that depth can be a proxy for several abiotic factors; pH levels and flow velocities are generally greater in the surface canopy, while $pCO_2$ is greatest in the kelp forest benthos. Irradiance, however, has the strongest gradient with depth. At 12 m depth, irradiance is only ~10% of surface values, and the presence of a kelp canopy further reduces irradiance by 75% (Gerard 1984, Edwards 1998). Thus I chose to treat depth primarily as a proxy for irradiance.

In wave-protected kelp beds, where current velocities may consistently remain between 0.0 and 3.0 cm/s, *M. pyrifera* tissue should use a reduced proportion of bicarbonate, leading to depleted tissue $\partial^{13}C$ (Drobnitch et al. in press). This source of depletion, however, may be canceled out by DIC limitation in these slow-moving currents, which would lead to *enriched* signatures relative to blades growing in high wave-exposure sites. Thus, the direction and magnitude of $\partial^{13}C$ variation in response to different wave exposure environments is difficult to predict.

Finally, I hypothesize that during upwelling periods (April – July in the Monterey Bay), higher ambient concentrations of DIC in kelp beds should lead to depleted $\partial^{13}C$ signatures relative to periods of upwelling relaxation, in which waters can become warmer, stratified, and nutrient-limited (August – March, with the exception of winter storm activity).

*Hypotheses: Fractionation of transport tissues in* M. pyrifera

I hypothesized that sap $d^{13}C$ would be enriched relative to vegetative tissue, yet might become depleted with depth in tandem with adjacent vegetative tissues as irradiance becomes limiting.

*Experimental incubation of kelp meristems in light and velocity treatments*

To test the hypotheses that differential bicarbonate use or productivity drive $\partial^{13}C$ signatures, I incubated *M. pyrifera* meristems in an orthogonal cross of irradiance and flow velocity treatments in a custom built Flowthrough Light and Velocity Incubator (FLAVI, Figure 1). I carried out three repetitions of this incubation experiment, for a total of 12 replicates of each orthogonal cross of water velocity and irradiance. Each repetition of the experiment was initiated with kelp from a single site, but the collection sites varied between incubations. Apical meristems of individual *M. pyrifera* fronds were collected by boat from three following three sites in the Monterey Bay: July 17, 2015, Pleasure Pt.; July 8, 2015, Monterey Harbor; February 28, 2016, Monterey Breakwater (coordinates in Table S1). Collected meristems were transferred in cool seawater to UCSC's Long Marine Lab within two hours and immediately placed into FLAVI. Each meristem was basally trimmed to ~20 cm length and tethered in an incubation flume; trimmed blades immediately proximal to the incubated distal meristem were removed, patted dry, and frozen for stable isotope analysis.

FLAVI was a closed recirculating network of incubation tanks and unidirectional flumes containing four experimental blocks (Figure 1). Natural seawater was maintained at constant temperature (11 or 16°C) with an AquaLogic 1 HP Marine Chiller. Each block contained a dedicated reservoir flowing to four experimental flumes, each containing one meristem. Each block of four experimental flumes subjected the meristems to an orthogonal cross of two levels each of flow velocity (10 cm/s and 0.5 cm/s) and irradiance (ambient sunlight and 7% sunlight). Each flume was a hemispheric elongated trough with a 3 L working section (43.2 cm x 11.3 cm x 6 cm); seawater flow through each flume was evenly distributed by a collimator consisting of two PVC directing fins, 18x16 wires/inch mesh fiberglass screening, and 10 cm long honeycomb aeronautics blocks (Plascore, Inc).

A total of 16 meristems (1 per flume, 4 flumes per block, 4 blocks per repetition) were incubated under experimental conditions for 2 - 3 weeks—long enough to triple the area of meristems in high light treatments. Throughout the incubation period, seawater temperature and incident illuminance were recorded every 30 minutes by HOBO sensors (1 per light level per block). Water samples for total alkalinity were taken bi-weekly, fixed with 150 μL of saturated $HgCl_2$, sealed with parafilm and refrigerated until analysis. $NO_2$, $NO_3$ and $NH_4$ content of the recirculating seawater within FLAVI was measured weekly during Incubation 3 on a Lachat QuikChem 8000 analyzer.

Health and photosynthetic capacity of the incubated meristems was assessed weekly, at dawn and mid-afternoon, using an Opti-Sciences OS1p pulse amplitude-modulated fluorometer (PAM; data in *Appendix 3*). Growth of incubated meristems was tracked with weekly length measurements and tissue area measurements from photographs analyzed using Fiji in incubations 2 and 3 (Schindelin et al. 2012). At the conclusion of each incubation in FLAVI, the apical scimitar of each meristem was collected and frozen for stable isotope analysis.

*Analysis of FLAVI seawater samples*

Bi-weekly water samples from FLAVI were measured for pH and total alkalinity (TA) within four months of collection. pH was measured in triplicate on a Shimadzu UV 1800 spectrophotometer using the indicator dye m-cresol purple (pH of solution = 7.9 $\pm$ 0.01)(Dickson 2010). TA was measured in duplicate using open-cell titration with HCl on the Titrando automatic titrator (MetroOhm Inc.). The titrator was calibrated daily with certified reference material. TA was calculated from the second (i.e. highest) integral endpoint calculated by the Tiamo (MetroOhm Inc.) software. [DIC] and $pCO_2$ were calculated using the CO2SYS Excel macro (v.2, Pierrot et al. 2006).

*Stable isotope analysis*

Frozen tissues from the start and end of each incubation in FLAVI were dried using a Labconco lyophilizer, homogenized to a powder, and weighed prior to analysis. Carbon and nitrogen isotopic and elemental composition was determined by

Dumas combustion using a Carlo Erba 1108 elemental analyzer coupled to a ThermoFinnigan Delta Plus XP isotope ratio mass spectrometer at the University of California, Santa Cruz Stable Isotope Laboratory. Analytical precision of internationally calibrated in-house standards was better than 0.2 permil for $\partial^{13}C$. Sample isotopic values are corrected for size, drift and source stretching effects. Carbon and nitrogen elemental composition was estimated based on standards of known elemental composition. Precision of these known compounds is determined to better than 1%.

*Assessing patterns of ∂13C in kelp forest microhabitats in the Monterey Bay*

To test the hypothesis that $\partial^{13}C$ partitioning in the field occurs as a function of DIC supply and demand, I collected *M. pyrifera* tissues from a set of carefully chosen microhabitats. I designated 3 field sites as "protected" (Stillwater Cove, Hopkins Marine Station, and McAbee kelp beds) and 3 sites as "exposed" (Otter Pt., Pt. Piños, and Cypress Pt. beds) based on wave force data from Figurski 2010 and wave height predictions from the SWAN model (Erikson et al. 2014) (Table S1). At each site, I designated four microhabitats; a surface canopy and a 10 m deep zone in the center of the kelp bed (i.e. dense vegetation, attenuated water flow), and a surface canopy and deep zone on the offshore edge of the kelp bed (i.e. sparse vegetation, un-attenuated water flow)(Stewart et al. 2009). A majority of the blades located at 10 m depth are mature or senescent; thus I were careful to sample both juvenile and mature tissues from each depth level to avoid confounding the abiotic covariates of "depth" with

tissue age. I sampled three mature blades and three juvenile meristems from each microhabitat at each site. Blades were collected on SCUBA, patted dry, and transferred on ice to the Long Marine Lab, where they were frozen for later analysis. Frozen tissues from field collections were dried using a Labconco lyophilizer, homogenized to a powder, and weighed prior to analysis. Carbon and nitrogen isotopic and elemental composition was determined as described above. This sampling program was carried out twice in 2015; once in April during strong upwelling conditions and once in September during a period of upwelling relaxation.

*Fractionation of transport tissues*

Paired sap and blade samples were harvested in a randomized block design. Mature, entire, non-epiphytized blades and adjacent sap were harvested at three points (base, mid-frond, and 3 m from the canopy) along an entire frond (the block). Five fronds from different sporophytes were sampled from holdfasts of at least 10 m depth at each of our sites (Hopkins, wave-protected; Pt. Piños, wave-exposed). To collect phloem sap, the stipe was severed, blotted, and the phloem sap collected using a sterile 1 mL syringe. Sap was then ejected directly into pre-weighed 5x9 mm tin capsules for elemental analysis and kept on ice. Phloem sap was collected from the stipe located directly distal to sampled blade. Sampled sporophytes were chosen from the offshore edge of the kelp bed to reduce environmental/conspecific effects. All tissue was then returned to Long Marine Lab, where blades were frozen, lyophilized, and homogenized and sap was dried in a dehydrator at 60˚C. Finally, all tissue samples were analyzed for stable isotope content as above.

*Statistical analysis:*

To evaluate the drivers of $^{13}C$ discrimination in *M. pyrifera* tissue, I carried out several analyses of data from FLAVI incubations. **1)** To confirm my assumption that my low irradiance treatment and low flow velocity treatment were sufficient to affect meristem productivity, I ran a mixed model ANOVA to test the interactive effects of Irradiance Level (categorical) and Flow Velocity (categorical) on Growth rate ($cm^2$/day) from only incubations 2 and 3 (in which growth rate was measured). Temperature and pH varied in each incubation, so Incubation was included as a random effect to account for this temporal variance. Tukey's HSD test was used for post-hoc analysis of significant interactions. **2)** To evaluate the degree of nitrogen limitation in our incubated meristems under our different treatment levels, I ran a mixed-model ANCOVA to test the interactive effects of Irradiance level (categorical) and Flow velocity (categorical) on Final C:N ratio with Incubation as a random effect. Initial C:N was the covariate, but was only included in the statistical model as a source of variance, not an explanatory variable; thus I did not evaluate any interactions between Initial C:N and the other fixed effects in the model. **3)** To further assess the drivers of nitrogen limitation in our incubations, I performed two-factor ANOVA to test the interactive effects of Mean illuminance level (categorical) and Flow velocity (categorical) on final Tissue %N. Post-hoc LSM Contrast analysis was carried out on Mean illuminance levels. To investigate the possibility that nitrogen limitation occurred in meristems with high growth rates I also performed a least squares regression test of final Tissue %N by Growth rate ($cm^2$/day). **4)** I ran a mixed

model ANCOVA to evaluate the interactive effect of Flow Velocity (categorical) and Irradiance (categorical) on the Final $\partial^{13}C$ of incubated with Incubation as a random effect. Initial $\partial^{13}C$ (the covariate) was treated as a source of variance, not as an explanatory variable, in the statistical model. Experimental block was non-significant ($p = 0.3110$) when run as a random effect in preliminary analyses; thus we removed it to recover degrees of freedom. **5)** Finally, to test the hypothesis that productivity drives enrichment of $\partial^{13}C$ in incubated meristems, I ran a multiple regression analysis of Final $\partial^{13}C$ by Growth rate ($cm^2$/day, continuous) with Incubation as a random effect on data from incubations 2 and 3. Initial $\partial^{13}C$ (continuous) was also included as a covariate in the statistical model as a source of variance, not as an explanatory variable.

To test my hypotheses regarding $^{13}C$ patterns in the field, I used a Mixed Model ANOVA to test the interactive effects of a full factorial cross of Tissue Depth, sporophyte location (Location within kelp bed), Collection Month, and site Exposure Level on Tissue $\partial^{13}C$ with site as a random effect nested within exposure. To recover degrees of freedom, I did not include the four-way interaction, which was not significant ($p = 0.1721$) in the full orthogonal model. To better understand the influence of upwelling and nutrient availability on kelp $\partial^{13}C$ in the field, I evaluated tissue C:N ratios using the exact same statistical model as above, replacing $\partial^{13}C$ with C:N ratio as the response variable. Again, I did not include the four-way interaction, which was not significant ($p = 0.3117$) in the full orthogonal model. Tukey's HSD test was used for post-hoc analysis of significant interactions in all field data.

To assess the relative explanatory power of the four fixed effects on $\partial^{13}C$ discrimination, we additionally ran a mixed model ANOVA including only the following main effects: site (nested within Exposure Level), Exposure Level, Tissue Depth, Position within kelp bed, and Collection Month. All main effects were treated as random variables in order to produce a variance component output. This analysis was done to provide an estimate of the relative contribution of each term to the overall variance explained by the model. Note that treating fixed effects as random effects is unorthodox.

To test my hypothesis that *M. pyrifera* sap is significantly more enriched than vegetative tissue, I ran a two-way ANOVA testing the interactive effects of Tissue Depth (3 levels) and Tissue Type (Sap or Blade) on Tissue $\partial^{13}C$ with individual fronds as each block. Tukey's HSD test was used for post-hoc analysis of the significant interaction.

**Results**

*Experimental incubation of kelp meristems in light and velocity treatments*

Flow velocity and irradiance treatments significantly affected meristem growth rate (productivity, **Analysis 1**). Low flow velocity and low irradiance both individually reduced growth rate of meristems ($p = 0.009$ and $<0.0001$, respectively); they also had interactive effects ($p = 0.0205$). At high irradiance but low velocity levels, growth rate was reduced (9.2 $cm^2$/day) relative to the high irradiance/high velocity treatment (27.6 $cm^2$/day, Tukey HSD test, Table 1, Figure 2).

C:N ratios were driven by the combined effects of irradiance and flow velocity (**Analysis 2**, Table 2). Ratios increased in high light ($p < 0.0001$) with an additive effect of low flow velocity ($p = 0.0011$); the interaction term was not significant. Tissue %N decreased when incubated at low velocity relative to high velocity ($1.66 \pm 0.059\%$ vs. $2.05 \pm 0.059\%$, ANOVA, $p < 0.0001$, Table 3, **Analysis 3,** Figure 3). High illuminance levels also decreased tissue %N relative to low illuminance levels (ranging from 2.26 to $1.15 \pm 0.103\%$, LSM Contrast, DF = 1, F = 42.08, $p < 0.0001$, Figure 3). The interaction between illuminance level and velocity level was not significant. However, growth rate ($cm^2$/day) was not correlated with %N ($F = 1.0054$, DF = 1, $p = 0.3213$).

Irradiance level explained 71% of variation in final incubated $\partial^{13}C$ when initial $\partial^{13}C$ was accounted for (**Analysis 4**, Table 4, Figure 4). Meristems incubated in low irradiance were depleted (-18.55 + 0.77) relative to those incubated in high irradiance (-15.33 + 0.77, $p < 0.0001$). Flow velocity level, however, had no significant impact on final incubated $\partial^{13}C$. Initial $\partial^{13}C$ explained a significant portion of variation in final $\partial^{13}C$ ($p = 0.0168$). Finally, the results of my incubation experiment indicated that growth rate ($cm^2$/day) does not significantly explain any variation in incubated $\partial^{13}C$ ($p = 0.2365$, $R^2 = 0.13$, **Analysis 5**).

*Assessing patterns of $\partial^{13}C$ in kelp forest microhabitats in the Monterey Bay*

The results of the targeted sampling of *M. pyrifera* blades from different temporal and spatial scales on the Monterey peninsula showed that 64% of the

variation in field tissue $\partial^{13}C$ was explained by tissue Depth, tissue Location within the kelp bed, and Collection month (ANOVA, Table 5). In September, blades were much more enriched (-15.59 $\pm$ 0.51‰) than in April (-17.96 $\pm$ 0.53‰, $p < 0.0001$, Figure 5). 10 m deep blades were on the whole much more depleted (-18.63 $\pm$ 0.52‰) than surface blades (-14.93 $\pm$ 0.52‰, $p < 0.0001$, Figure 5). Location within the kelp bed also had a significant effect on $d^{13}C$; blades collected from inside each kelp bed (across all sites and depths) were more enriched (-16.47 $\pm$ 0.51‰) than those collected outside each kelp bed (-17.08 $\pm$ 0.51‰, $p = 0.0173$, Figure 5). Finally, there was a significant 3-way interaction between collection month, site exposure, and depth ($p = 0.0012$). In April, tissue from low exposure sites was more depleted (-20.54 $\pm$ 0.81‰) than kelp in high exposure sites (-19.23 $\pm$ 0.80‰), but only at 10 m depth. At the surface, kelp from high exposure sites was more depleted (-16.61 $\pm$ 0.80‰) than at low exposure sites (-15.45 $\pm$ 0.80‰). Overall, low exposure sites displayed a larger range of $\partial^{13}C$ values than high exposure sites in April. In September, however, there was no difference in the response of kelp from different exposure sites to depth (Tukey HSD). Overall, variance component estimates indicate that tissue depth alone explained 47% of tissue $\partial^{13}C$ variation, followed by collection month (19%), collection site (8%), location within kelp bed (1%), and exposure (0%) (Table 6).

Similar to patterns observed for $\partial^{13}C$, C:N ratio varied significantly on both temporal and spatial scales (ANOVA, Table 7). Since tissue %N declines in my samples as C:N ratio increases, higher C:N ratios likely indicate nitrogen limitation.

C:N ratio is higher in tissues collected in September than in April. The interaction between the location within the kelp bed and collection month was marginally significant ($p = 0.458$). In April, C:N ratios were identical inside and offshore of the kelp bed, whereas in September, tissues collected inside the kelp bed had greater C:N ratios ($14.45 \pm 0.39$) than those collected outside the bed ($13.32 \pm 0.40$, Tukey HSD). There was a significant interaction between collection month and depth ($p = 0.0066$); in April, tissue C:N did not differ with depth, whereas in September, surface tissue C:N was significantly higher ($14.44 \pm 0.39$) than 10 m deep tissue ($13.32 \pm 0.39$, Tukey HSD). There was a significant interaction between site exposure and depth ($p < 0.001$) and between exposure, depth, and location within the kelp bed ($p = 0.0154$). These interaction terms indicate that, at the inside of kelp beds at low exposure sites, C:N was lower at depth ($11.26 \pm 0.58$) than at the surface ($13.97 \pm 0.58$). At the inside of kelp beds at high exposure sites, however, C:N was lower on the surface ($12.41 \pm 0.58$) than at depth ($13.69 \pm 0.58$). On the offshore edge of kelp beds, this interaction is not observed; C:N is lower at low exposure ($11.47 \pm 0.59$) sites than at high exposure ($13.06 \pm 0.59$) sites at 10 m depth only (Tukey HSD).

*Fractionation of transport tissues*

Sap $\partial^{13}C$ was significantly more enriched than blades, regardless of position on the sporophyte (ANOVA, DF = 1, F-ratio = 83.8769, $p < 0.0001$). In agreement with field survey data, blades exhibited $\partial^{13}C$ depletion with depth, whereas sap $\partial^{13}C$

was invariant with depth (~12‰), resulting in a significant interaction between tissue depth and tissue type (ANOVA, DF = 2, F-ratio = 3.3862, p = 0.0427, Figure 6).

**Discussion**

My proposed mechanisms of $^{13}C$ fractionation were not supported by the results of the manipulative experiment. Incubations in FLAVI did not support the hypotheses that productivity (measured both as length and area increases) or DIC limitation (as a function of low flow velocity) drive patterns in $\partial^{13}C$ enrichment, although it was clear that low flow velocity limited growth rates and nutrient delivery (Figs. 2 and 3). Nor did bicarbonate use appear to drive $\partial^{13}C$, since flow velocity treatments had no impact on $\partial^{13}C$ but clearly influenced bicarbonate use in a previous study (Drobnitch et al. in press). In the incubation experiment, the sole driver of $\partial^{13}C$ enrichment was irradiance (Fig. 4), but the mechanism by which irradiance alone drives enhanced $^{13}C$ uptake is unclear.

There are several possible mechanisms that could drive $\partial^{13}C$ enrichment under high irradiance conditions, but with no effect of flow velocity or growth rates. While I expected bicarbonate use to be an additive function of flow velocity and irradiance, this hypothesis was based on a study of the dynamics of passive external uptake of bicarbonate (via extracellular carbonic anhydrase). Since *M. pyrifera* can also take up a substantial proportion of bicarbonate via *active* trans-membrane uptake (via ion-exchange channels, Fernández et al. 2014), it is possible that high irradiance strongly up-regulates active bicarbonate uptake regardless of DIC supply. If this is the case,

tissues exposed to high irradiance would display characteristic enrichment as a greater fraction of enriched bicarbonate-derived $^{13}C$ atoms were preferentially fixed.

Using a similar mechanism, irradiance could drive $\partial^{13}C$ enrichment via increased recycling of respired and transported $CO_2$. $CO_2$, a small non-polar molecule, diffuses easily into algal cells, but just as easily diffuses out. Under high metabolic and photosynthetic rates, many macroalgae may fix respired carbon before it can leak out of cells, leading to decreased discrimination against heavy $^{13}C$ and subsequent enrichment (Surif and Raven 1990).

N-limitation could also play a strong role in the enrichment of high-irradiance incubations because high C:N ratios are diagnostic of N-limitation. N-limitation was especially marked in high irradiance x low velocity treatments (C:N = 20+, Wheeler and North 1981, Fig. 3). Previous studies have observed that under limiting nitrogen conditions, green algae take steps to curtail nitrogen lost as ammonia during photorespiration, which is often acute in high irradiance conditions. In these high irradiance/low N conditions, the alga *Chlamydomonas* up-regulates the enzyme glutamine synthase to scavenge $NH_3$. The alga *Chlorella*, however, instead up-regulates its carbon concentrating mechanism (CCM), which increases $CO_2$ concentrations at the site of Rubisco and prevents photorespiration (Beardall et al. 1982). In *Chlorella*, this N-conservation strategy results in tissue enrichment, since their CCM interferes with RUBISCO discrimination against $^{13}C$. If a similar mechanism is operating in *M. pyrifera*, this could explain irradiance-driven enrichment.

My field study also supported the hypothesis that high irradiance environments yield enriched *M. pyrifera* tissue, exhibiting a strong correlation between $\partial^{13}C$ enrichment and blade depth (and vice versa). Blades from 10 m depth, regardless of tissue age, were an average 3‰ more depleted than canopy blades, with maximal differences of ~ 6‰ (Fig. 5). While irradiance itself is the likeliest driver of canopy $\partial^{13}C$ enrichment and deep blade $\partial^{13}C$ depletion, there is another possible driver. DIC concentrations would be greater at depth because of a lower kelp biomass (most biomass is in the canopy) and a substantial subsidy of respired $CO_2$ from the benthic community (Middelburg et al. 2007, Frieder et al. 2012). Higher DIC concentrations could also result in depletion of kelp tissue, since it can effectively discriminate against $^{13}C$, whereas canopy tissue would become enriched as DIC becomes limiting.

DIC limitation via kelp drawdown of the $CO_2$ pool in dense surface canopies is also suggested by differences in the $\partial^{13}C$ signature of kelp from within vs. outside the kelp bed (Fig. 5). Field data indicate a relationship between $\partial^{13}C$ enrichment and blade residence within the kelp bed (as opposed to on the offshore edge of the bed). Since site exposure had no bearing on $\partial^{13}C$ signatures, it is unlikely that this is a direct effect of flow velocity or boundary layer formation. It is likely, however, given marked pH increases within dense *M. pyrifera* canopies (Delille et al. 2009), that the DIC pool becomes limiting inside the bed relative to outside the bed. Again, this DIC limitation could lead directly to $\partial^{13}C$ enrichment (an average 1‰ more enriched

within the bed relative to the edge), as kelp tissues might not be able to fully discriminate against $^{13}C$ in limiting conditions.

My field study also indicated that kelp tissue is significantly depleted during upwelling season in the Monterey Bay (April – July, Fig. 5). It is possible that increased DIC supply and pH decrease allow kelp tissues to fully discriminate against $^{13}C$, yielding depleted values diagnostic of their carbon uptake and fixation physiology. A related possibility stems from the fact that canopy biomass is generally much greater in September (the end of the growing season) than in April. Again, this increased biomass could draw down much more of the available DIC within the kelp bed, resulting in more enriched signatures. It is also possible, as mentioned above, that N-limitation in non-upwelling seasons drives enrichment; however C:N ratios indicate that N-limitation was not severe. It is also possible that the lower temperatures associated with upwelling result in depletion, but I did not assess temperature as a possible influence of $\partial^{13}C$ signatures.

Finally, my study confirms that there is marked enrichment of transported photosynthate relative to structural tissue carbon in vegetative blades, and that this sap $\partial^{13}C$ signature does not change with depth (unlike tandem vegetative tissues, Fig. 6). This either indicates that sieve tube sap is coming largely from one source (i.e. canopy to base) or that the carbon pool available for transport is always saturating, leading to uniform sap $\partial^{13}C$ via loading or transport. This may result in a dilution effect, in which in the deeper tissues always appear less depleted than expected from their carbon acquisition physiology. Such transport fractionation may prevent deep

kelp tissue from achieving $\partial^{13}C$ signatures of -25‰ or less, which I would expect from tissue relying mostly on dissolved $CO_2$ uptake.

Overall, there is strong evidence that a light-mediated process and DIC limitation drive enrichment of *M. pyrifera* $\partial^{13}C$. In the field, I observed that depth, location within to the kelp bed, and upwelling are strong predictors of $\partial^{13}C$. Resolving these fine spatial and seasonal drivers of $\partial^{13}C$ variation could give us power similar to that of compound-specific stable isotope analyses, allowing us to relate $\partial^{13}C$ signatures to microhabitats (Finlay et al. 1999, Gillies et al. 2011, Connolly and Walthan 2015, Mcmahon et al. 2015, McPherson et al. 2015). There are many species of young fishes and larval/adult invertebrates that exclusively inhabit the kelp forest canopy; conversely there are also a substantial subset of species that live their adult lives strictly near or on the seafloor (Ebeling et al. 1978, Bernstein and Jung 1979, Coyer 1979, Watanabe 1984, Demartini and Roberts 1990, Hartney 1996). I suggest that the next steps in understanding and effectively using $\partial^{13}C$ as a biomarker should be to test kelp forest ecosystems for isotopic differences within seasonally- or depth- stratified communities. As a physiological marker, there is still a great deal of uncertainty as to which specific enzymatic pathways control $\partial^{13}C$ discrimination in *M. pyrifera* and other kelps. It still remains unclear whether or not discrimination is driven by a certain process—up-regulation of a CCM, or a phloem-loading process—or simply by external DIC limitation, which can be the result of many biotic and abiotic factors.

**Table 1**. Results of a Mixed Model ANOVA testing the effect of irradiance and flow velocity on the growth rate ($cm^2$/day) of incubated meristems.

| Source | Nparm | DF | DFDen | F Ratio | Prob > F |
|---|---|---|---|---|---|
| Flow Velocity Treatment | 1 | 1 | 42 | 15.0967 | 0.0004*** |
| Irradiance Treatment | 1 | 1 | 42 | 65.1152 | <0.0001*** |
| Irradiance * Flow Velocity | 1 | 1 | 42 | 13.3697 | 0.0007*** |

**Table 2**. Results of a Mixed Model ANCOVA testing the effect of irradiance and flow velocity on the Final C:N ratio of incubated meristems. Initial C:N is included as a covariate to account for this significant source of variation in Final C:N.

| Source | Nparm | DF | DFDen | F Ratio | Prob > F |
|---|---|---|---|---|---|
| Irradiance | 1 | 1 | 42 | 47.5796 | <0.0001*** |
| Flow Velocity | 1 | 1 | 42 | 12.2784 | 0.0011** |
| Irradiance * Flow Velocity | 1 | 1 | 42 | 0.7334 | 0.3966 |
| Initial_CN | 1 | 1 | 42.04 | 13.8899 | 0.0006*** |

**Table 3.** Results of a two-way ANOVA to test for the influence of mean illuminance level and flow velocity treatment on the Tissue %N of incubated meristems.

| Source | Nparm | DF | Sum of Squares | F Ratio | Prob > F |
|---|---|---|---|---|---|
| Mean Illuminance | 5 | 5 | 7.14 | 16.861 | <0.0001*** |
| Flow Velocity | 1 | 1 | 1.81 | 21.3393 | <0.0001*** |
| Flow velocity * mean illuminance | 5 | 5 | 0.58 | 1.3728 | 0.2575 |

**Table 4.** Results of a Mixed Model ANCOVA to evaluate the effect of flow velocity and irradiance on the final $\partial^{13}C$ of incubated meristems. Initial $\partial^{13}C$ is included as a covariate to account for this significant source of variation in final $\partial^{13}C$.

| Source | Nparm | DF | DFDen | F Ratio | Prob > F |
|---|---|---|---|---|---|
| Initial meristem $\partial^{13}C$ | 1 | 1 | 31.17 | 6.3821 | 0.0168* |
| Irradiance | 1 | 1 | 41.58 | 53.8928 | <0.0001*** |
| Flow velocity | 1 | 1 | 41.58 | 0.514 | 0.4774 |
| Flow velocity * irradiance | 1 | 1 | 41.38 | 0.2796 | 0.5998 |

**Table 5.** Results of a Mixed Model ANOVA with $\partial^{13}C$ as the response variable and Site as a random effect nested within Exposure.

| Source | N | DF | DFDen | F Ratio | Prob > F |
|---|---|---|---|---|---|
| Location within kelp bed | 1 | 1 | 217.8 | 5.7566 | 0.0173* |
| Collection month | 1 | 1 | 222 | 68.1599 | <.0001*** |
| Depth | 1 | 1 | 217.8 | 200.3034 | <.0001*** |
| Exposure | 1 | 1 | 3.827 | 0.0068 | 0.9386 |
| Location within kelp bed * Collection month | 1 | 1 | 217.8 | 1.7769 | 0.1839 |
| Location within kelp bed * Exposure | 1 | 1 | 217.8 | 0.0171 | 0.896 |
| Collection month * Exposure | 1 | 1 | 222 | 0.0002 | 0.9888 |
| Location within kelp bed * Depth | 1 | 1 | 217.8 | 2.1228 | 0.1466 |
| Collection month * Depth | 1 | 1 | 217.8 | 0.3828 | 0.5368 |
| Exposure * Depth | 1 | 1 | 217.8 | 2.0111 | 0.1576 |
| Location within kelp bed * Collection month * Exposure | 1 | 1 | 217.8 | 0.52 | 0.4716 |
| Collection month* Exposure* Depth | 1 | 1 | 217.8 | 10.7791 | 0.0012** |
| Location within kelp bed * Collection month * Depth | 1 | 1 | 217.8 | 0.4408 | 0.5074 |
| Location within kelp bed * Exposure * Depth | 1 | 1 | 217.9 | 0.1601 | 0.6894 |

**Table 6.** Variance components for main effects on kelp tissue $\partial^{13}C$ from a mixed model ANOVA in which all fixed effects were treated as random factors.

| Component | Variance Comp. Estimate | Percent of Total |
|---|---|---|
| Site (nested within Exposure) | 1.028429 | 7.286 |
| Location within kelp bed | 0.203769 | 1.444 |
| Collection Month | 2.615599 | 18.532 |
| Exposure | -0.37764 | -2.676 |
| Depth | 6.652935 | 47.136 |
| Residual | 3.991099 | 28.277 |
| Total | 14.11419 | 100 |

**Table 7.** Results of a Mixed Model ANOVA with C:N ratio as the response variable and Site as a random effect nested within Exposure.

| Source | Nparm | DF | DFDen | F Ratio | Prob > F |
|---|---|---|---|---|---|
| Location within kelp bed | 1 | 1 | 218 | 4.1987 | 0.0417 |
| Collection month | 1 | 1 | 214 | 74.6559 | <.0001*** |
| Exposure | 1 | 1 | 3.905 | 1.0415 | 0.3665 |
| Depth | 1 | 1 | 218 | 1.5258 | 0.2181 |
| Location within kelp bed * Collection month | 1 | 1 | 218 | 4.0343 | 0.0458 |
| Collection month * Depth | 1 | 1 | 218 | 7.511 | 0.0066** |
| Exposure * Depth | 1 | 1 | 218 | 22.0726 | <.0001*** |
| Location within kelp bed * Exposure | 1 | 1 | 218 | 0.7649 | 0.3828 |
| Collection month * Exposure | 1 | 1 | 214.1 | 0.294 | 0.5882 |
| Location within kelp bed * Depth | 1 | 1 | 218 | 1.7094 | 0.1924 |
| Location within kelp bed * Collection month * Exposure | 1 | 1 | 218 | 0.601 | 0.439 |
| Location within kelp bed * Collection month * Depth | 1 | 1 | 218 | 0.45 | 0.503 |
| Location within kelp bed * Exposure * Depth | 1 | 1 | 219 | 6.0442 | 0.0147* |
| Collection month * Exposure * Depth | 1 | 1 | 218 | 0.0015 | 0.9688 |

**Figure 1**. Design of the Flowthrough Light and Velocity Incubator (FLAVI)

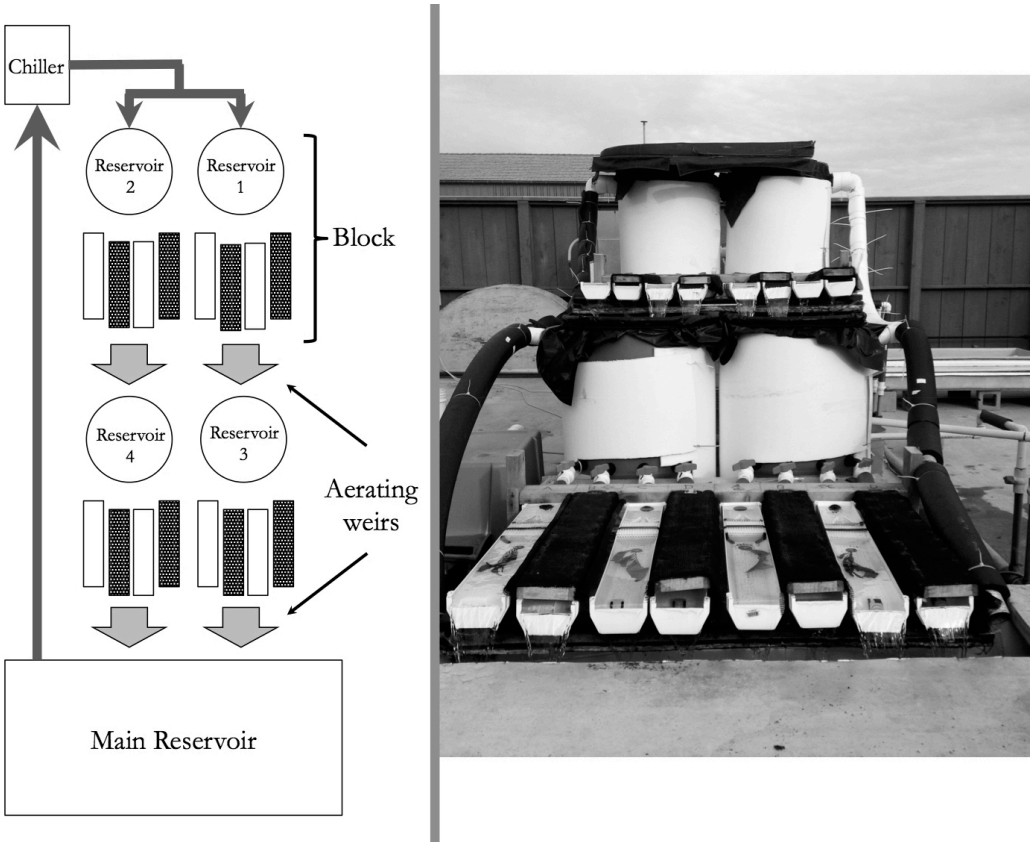

**Figure 2**. Growth rate ($cm^2$/day) of incubated meristems in response to irradiance treatment and flow velocity treatment. Significance of treatments is indicated by letters (Tukey HSD).

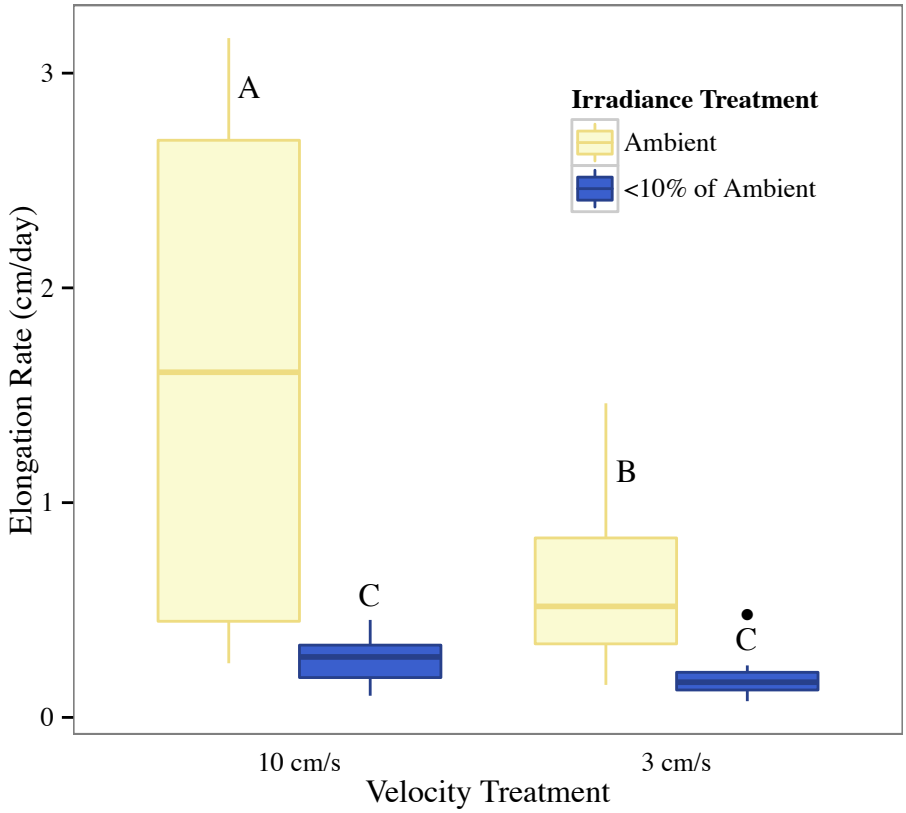

**Figure 3.** %N of incubated meristems in response to average illuminance (lux) during incubation. Error bars are SE.

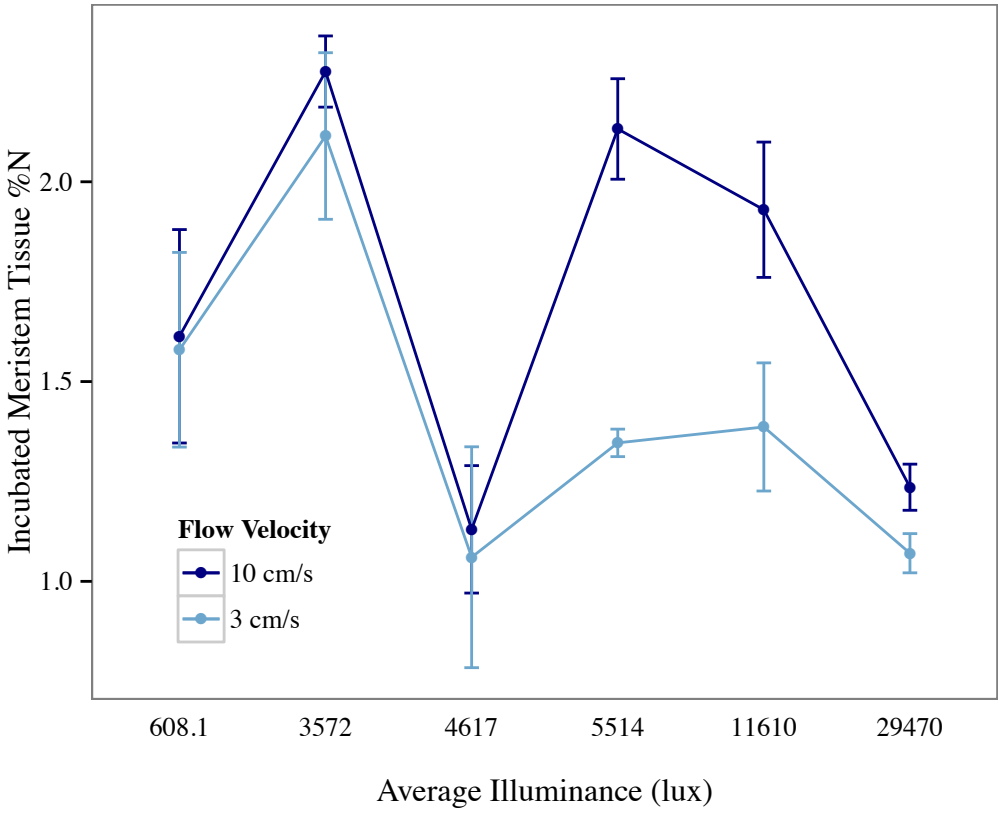

**Figure 4**. Change in $\partial^{13}C$ of incubated meristems as a function of their initial (field collected) $\partial^{13}C$ signature, plotted by irradiance treatment. Meristems incubated in high irradiance generally became more enriched over the course of the incubation, unless they were initially more enriched than -15‰. Meristems incubated in low irradiance became more depleted over the course of their incubation, unless they began very depleted (~23‰), in which case there was no change (dashed black line).

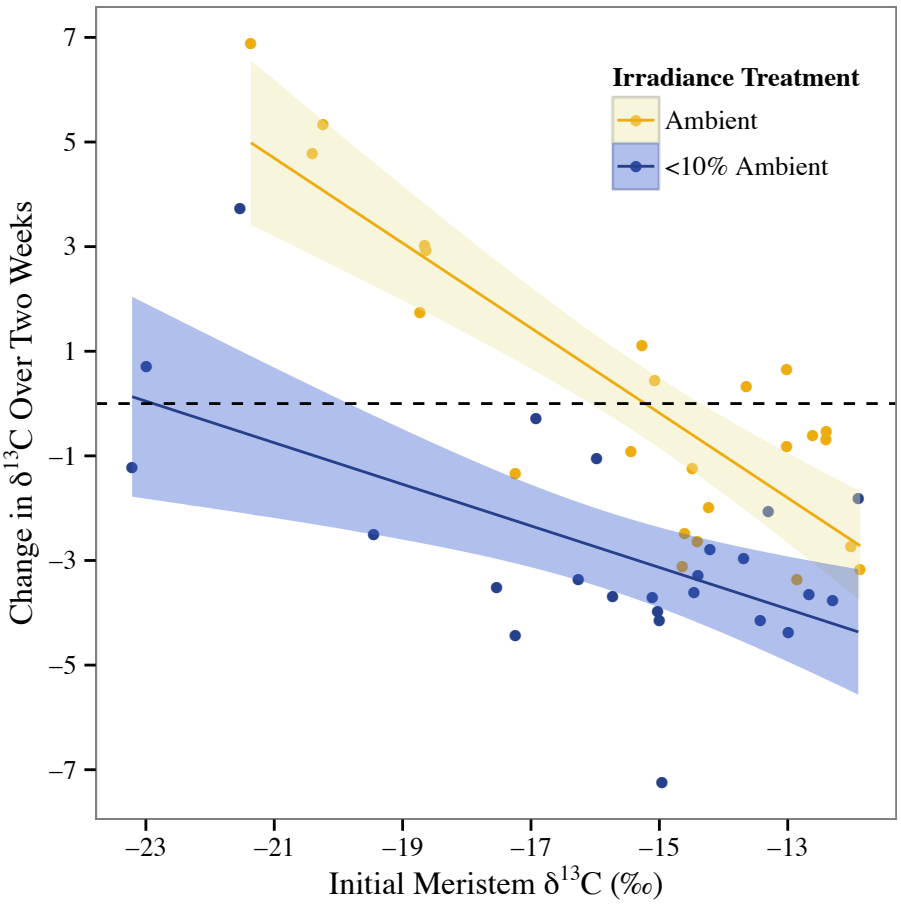

**Figure 5**. $\partial^{13}C$ of field collected blades from two depth categories (surface and 10 m deep), plotted as a function of their position relative to the kelp bed (inside or offshore edge), in two different seasons (panels represent April and September collections). Error bars are 95% confidence intervals.

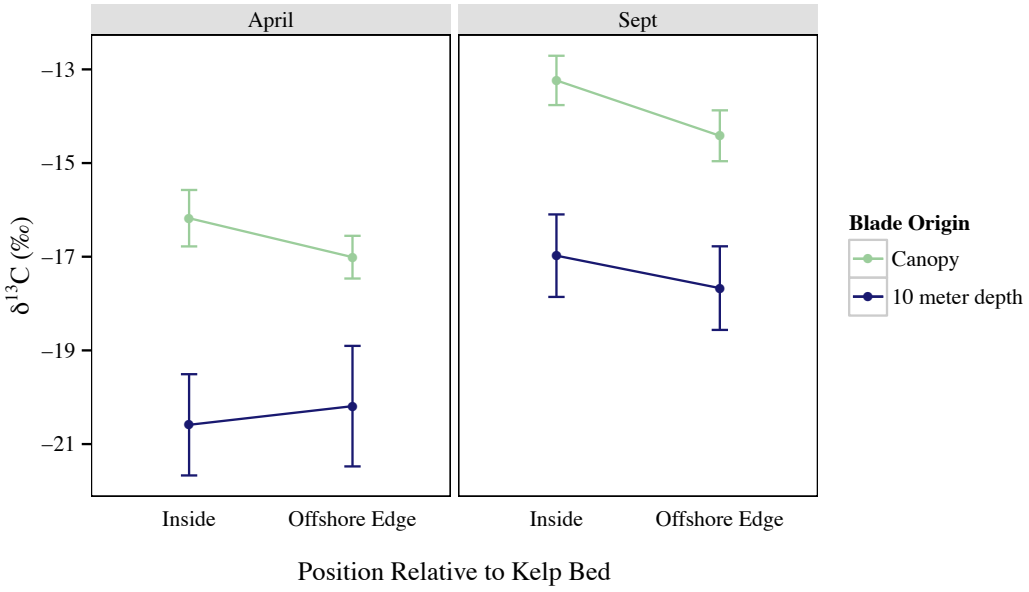

**Figure 6**. $\partial^{13}$C signatures of two tissue types (liquid sieve tube sap and adjacent blades) plotted by position along a mature *M. pyrifera* frond. Error bars are SE.

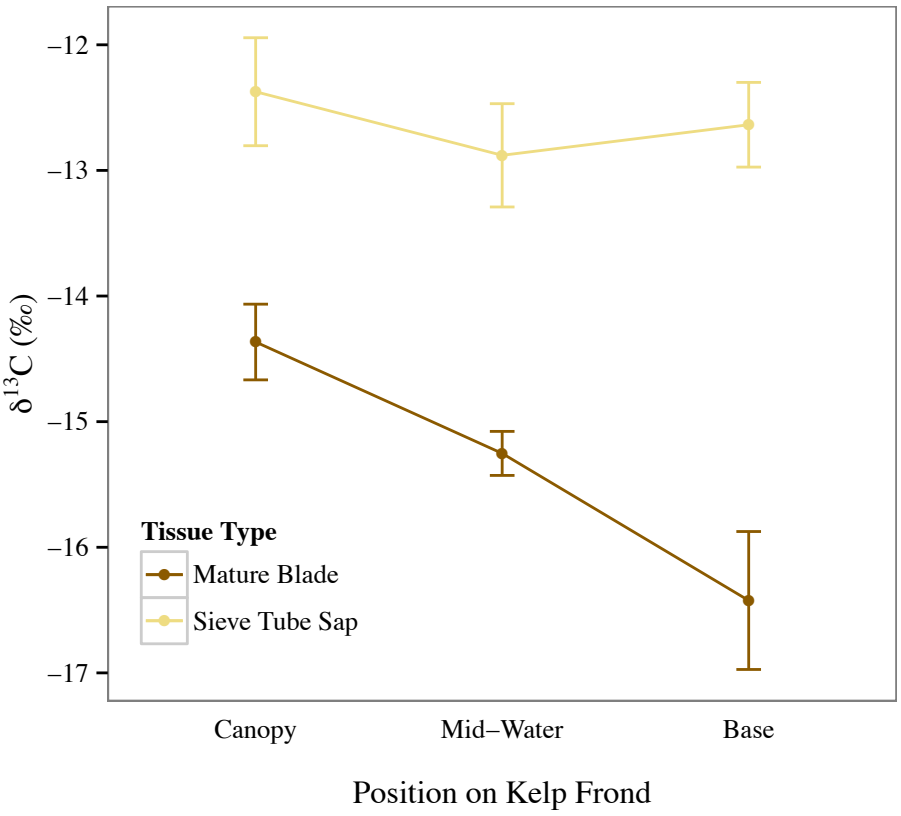

## Conclusion

This dissertation represents an effort to understand how the physiological traits of kelps are shaped by their abiotic environment, and in particular by exposure to gradients of resources and stress. **In Chapter 1**, I sought to elucidate the design and constraints of long distance transport vasculature in kelps. In terrestrial plants, researchers have spent the last few decades quantifying and modeling the structure and function of resource transport networks (i.e. xylem, phloem). In modeling the scaling of transport networks and in observing deviations from those models, these same researchers have been able to hypothesize many of the ecological and evolutionary factors that shape these networks. In macroalgae, which possess transport networks and support ecosystems of great value, none of these advances have been made. Thus, I set out to model and empirically measure the network structure and scaling of a variety of canopy-forming brown macroalgae. I investigated the architecture and presence/absence of allometric scaling and optimization in kelps from a broad array of habitats and possessing diverse life history traits. I observed that only the giant kelp *Macrocystis pyrifera* possesses tapered phloem conduit with scaling relationships that agree with my developed model of transport optimization. The remaining five species possessed sieve elements were largely invariant in size, with little relationship to body size or habitat, and did not display clear scaling patterns. These observations beg the following questions: What attributes or drivers are unique to *M. pyrifera* and give rise to phloem optimization? Is optimized phloem

a novel, evolutionarily derived trait in algae? Additional work is required to understand whether growth habit (such as annual growth and apical branching) or light stratified environments (necessitating subsidies to light-limited organs) drive scaled transport in *M. pyrifera*. A broader search for other transport-optimized brown algae is also necessary to answer the question of whether optimized scaling is necessary and widespread within marine autotrophs, the great majority of whom are uniformly photosynthetic across all functional organs.

**In Chapter 2**, I investigated how environmental cues impact the mechanism by which carbon is acquired in *M. pyrifera.* Although the carbonate chemistry and dynamics of carbon supply and demand fluctuate on daily and seasonal scales for giant kelp, we understood little about how certain abiotic variables influence carbon uptake strategy. Furthermore, it was unknown if carbon uptake physiology is acclimated to different microenvironments experienced by *M. pyrifera,* as photosynthetic physiology and many morphological traits have been demonstrated to be. Thus I set out to measure the dynamics of external bicarbonate and $CO_2$ uptake in *M. pyrifera* in response to strong gradients of irradiance and flow velocity in the Monterey Bay, California. Flow and irradiance each have the potential to regulate the supply and utilization of DIC, thus triggering possible divergent carbon concentrating mechanisms. I found that ecologically relevant high levels of irradiance and flow velocity additively increased the proportion of bicarbonate utilized by *M. pyrifera* via external carbonic anhydrase catalysis. In relatively low levels of irradiance and flow velocity, $CO_2$ use and an unknown proportion of active bicarbonate uptake dominated

*M. pyrifera* metabolism. Interestingly, there was no evidence of acclimation of carbon uptake strategy to extreme irradiance or wave exposure habitats. From these results we can infer that *M. pyrifera* takes up measurably more bicarbonate in the surface canopy, where flow velocities and irradiances are greatest, than in basal blades near the benthos. A clear next step for future work is to understand the contribution of actively pumped bicarbonate to overall photosynthesis in *M. pyrifera* in response to environmental conditions. Once the many concurrent mechanisms of carbon uptake are accurately measured in *M. pyrifera*, we can move forward to model and measure the degree to which *M. pyrifera* determines the pH of the water column relative to the influence of ambient onshore/alongshore currents. A thorough understanding of carbon use dynamics in macroalgae is essential, especially in estimating the impacts of ocean acidification on nearshore marine communities.

**In Chapter 3**, I dug deeper into the carbon use strategies of *M. pyrifera*, and how carbon use physiology can be tracked in individuals and the broader kelp forest ecosystem. I designed a study to begin to understand the mechanisms of $^{13}C$ discrimination during carbon fixation in *M. pyrifera*. In terrestrial plants, it is rigorously understood that leaf $\partial^{13}C$ signature reflect the carbon concentrating mechanism of the organism, and to a smaller extent, its water use efficiency. In aquatic and marine organisms, however, $\partial^{13}C$ is driven by a maze of possible mechanisms and can utterly lacks the rigor to be used as a physiological biomarker. I investigated whether patterns of irradiance and flow velocity in the field (functions of DIC supply and utilization) explain the extreme variation of $^{13}C$ discrimination in *M.*

*pyrifera.* Furthermore, I asked whether differential $CO_2$/bicarbonate use, carbon supply/demand dynamics, or other physiological processes (e.g. photosynthate transport) were the physiological mechanisms underlying this $^{13}C$ discrimination. I found that $\partial^{13}C$ of *M. pyrifera* tissues in forests in the Monterey Bay can be predicted largely by their depth (a proxy for irradiance level), as well as their position within the bed and the season in which they grew (possibly indicating DIC limitation). A manipulative experiment suggested that the mechanism of high irradiance $^{13}C$ enrichment is a light-driven metabolic process unrelated to external bicarbonate use or DIC limitation. To thoroughly understand and utilize $\partial^{13}C$ as a physiological biomarker (as it is in terrestrial plants), future work must follow up and investigate the presence or absence of several light-upregulated processes related to photosynthesis, CCM's, compound-specific fractionation and nutrient limitation. From an ecologist's perspective, however, these data advance our understanding of kelp $\partial^{13}C$ variability in the field, and are a boon to future trophic studies.

Although the three chapters of this dissertation investigate quite separate physiological traits, there is a growing consensus among terrestrial plant physiologists that phloem design is intimately related to the physiology of photosynthesis and carbon fixation. The anatomy (size and number) of sieve elements in the phloem has been shown to correlate with maximum photosynthetic rates in *A. thaliana.* Since high sugar concentrations in the mesophyll cells may down-regulate photosynthetic rates, enhanced phloem transport may preclude this feedback loop and enable higher rates of productivity (Adams III et al. 2013, Cohu et al. 2013). This topic is wholly

unexplored in macroalgae. Indeed, the advanced phloem structures on display in *M. pyrifera* could be responsible for the very high photosynthetic and growth rates in canopy tissues as compared to other, smaller macroalgae. The traits explored in my dissertation—transport network anatomy, photosynthesis, and carbon uptake—are ripe for such a synthetic investigation. There remains much that we do not understand regarding the basic physiology of macroalgae, nor how this physiology interacts with and shapes their environment. I examined and made modest contributions to our understanding of carbon acquisition and transport in an ecologically important group of macroalgae, the Laminariales.

**Literature Cited**


Adams III, W.W., Cohu, C.M., Muller, O. & Demmig-Adams, B. 2013. Foliar phloem infrastructure in support of photosynthesis. *Front. Plant Sci.* 4:194.

Alonso Vega, J.M., Vásquez, J.A. & Buschmann, A.H. 2005. Population biology of the subtidal kelps *Macrocystis integrifolia* and *Lessonia trabeculata* (Laminariales, Phaeophyceae) in an upwelling ecosystem of northern Chile: interannual variability and El Niño 1997-1998. *Rev. Chil. Hist. Nat.* 78:33–50.

Arnold, K.E. & Manley, S.L. 1985. Carbon allocation in *Macrocystis pyrifera* (Phaeophyta): Intrinsic variability in photosynthesis and respiration. *J. Phycol.* 21:154–167.

Badano, E.I. & Marquet, P.A. 2009. Biogenic habitat creation affects biomass-diversity relationships in plant communities. *Perspect. Plant Ecol. Evol. Syst.* 11:191–201.

Baldauf, S.L. 2008. An overview of the phylogeny and diversity of eukaryotes. *Evolution (N. Y).* 46:263–73.

Banavar, J.R., Moses, M.E., Brown, J.H., Damuth, J., Rinaldo, A., Sibly, R.M. & Maritan, A. 2010. A general basis for quarter-power scaling in animals. *Proc. Natl. Acad. Sci. U. S. A.* 107:15816–20.

Beardall, J., Griffiths, H. & Raven, J.A. 1982. Carbon isotope discrimination and the CO2 accumulating mechanism in *Chlorella emersonii*. *J. Exp. Bot.* 33:729–37.

Berner, R.A. 1997. The Rise of Plants and Their Effect on Weathering and Atmospheric CO2. *Science (80-. ).* 276:544–6.

Bernstein, B. & Jung, N. 1979. Selective pressures and coevolution in a kelp canopy community in southern California. *Ecol. Monogr.* 49:335–55.

Britton, D., Cornwall, C.E., Revill, A.T., Hurd, C.L. & Johnson, C.R. 2016. Ocean acidification reverses the positive effects of seawater pH fluctuations on growth and photosynthesis of the habitat-forming kelp, *Ecklonia radiata*. *Sci. Rep.* 6:26036.

Brostoff, W. 1988. Taxonomic studies of *Macrocystis pyrifera* (L.) C. Agardh (Phaeophyta) in Southern California: Holdfasts and basal stipes. *Aquat. Bot.* 31:289–305.

Brown, M.B., Edwards, M.S. & Kim, K.Y. 2014. Effects of climate change on the

physiology of giant kelp, Macrocystis pyrifera, and grazing by the purple sea urchin, *Strongylocentrotus purpuratus*. *Algae*. 29:203–15.

Bruno, J.F. & Bertness, M.D. 2001. Habitat modification and facilitation in benthic marine communities. *Mar. Community Ecol.* 413:201–18.

Burkhardt, S., Riebesell, U. & Zondervan, I. 1999. Effects of growth rate, CO2 concentration, and cell size on the stable carbon isotope fractionation in marine phytoplankton. *Geochim. Cosmochim. Acta*. 63:3729–3741.

Cabello-Pasini, A., Aguirre-Von-Wobeser, E. & Figueroa, F.L. 2000. Photoinhibition of photosynthesis in *Macrocystis pyrifera* (Phaeophyceae), *Chondrus crispus* (Rhodophyceae) and *Ulva lactuca* (Chlorophyceae) in outdoor culture systems. *J. Photochem. Photobiol. B Biol.* 57:169–78.

Campbell, J. & Coxson, D.S. 2001. Canopy microclimate and arboreal lichen loading in subalpine spruce-fir forest. *Can. J. Bot.* 79:537–55.

Carr, M.H. & Reed, D.C. 2016. Shallow Rocky Reefs and Kelp Forests. *In* Mooney, H. & Zavaleta, E. S. [Eds.] *Ecosystems of California*. University of California Press, Berkeley, pp. 311–36.

Chen, H., Niklas, K.J. & Sun, S. 2012. Testing the packing rule across the twig–petiole interface of temperate woody species. *Trees*. 26:1737–45.

Clarke, J.T., Warnock, R.C.M. & Donoghue, P.C.J. 2011. Establishing a time-scale for plant evolution. *New Phytol.* 192:266–301.

Cohu, C.M., Muller, O., Stewart, J.J., Demmig-Adams, B. & Adams III, W.W. 2013. Association between minor loading vein architecture and light- and CO2-saturated rates of photosynthetic oxygen evolution among *Arabidopsis thaliana* ecotypes from different latitudes. *Front. Plant Sci.* 4:264.

Colombo-Pallotta, M.F., García-Mendoza, E. & Ladah, L.B. 2006. Photosynthetic Performance, Light Absorption, and Pigment Composition of *Macrocystis Pyrifera* (Laminariales, Phaeophyceae) Blades From Different Depths. *J. Phycol.* 42:1225–34.

Connolly, R.M. & Walthan, N.J. 2015. Spatial analysis of carbon isotopes reveals seagrass contribution to fishery food web. *Ecosphere*. 6:1–12.

Cornelisen, C.D., Wing, S.R., Clark, K.L., Bowman, M.H., Frew, R.D. & Hurd, C.L. 2007. Patterns in the ∂13C and ∂15N signature of *Ulva pertusa*: Interaction between physical gradients and nutrient source pools. *Limnol. Oceanogr.*

52:820–32.

Cornwall, C.E., Hepburn, C.D., Pilditch, C.A. & Hurd, C.L. 2013. Concentration boundary layers around complex assemblages of macroalgae: Implications for the effects of ocean acidification on understory coralline algae. *Limnol. Oceanogr.* 58:121–30.

Coyer, J.A. 1979. The invertebrate assemblage associated with Macrocystis pyrifera and its utilization as a food source by kelp forest fishes. University of Southern California, 1-203 pp.

Coyer, J.A., Smith, G.J. & Andersen, R.A. 2001. Patterns of *Macrocystis pyrifera* (Phaeophyceae) evolution and biogeography as determined by ITS1 and ITS2 sequences. *J. Phycol.* 37:574–85.

Crain, C.M. & Bertness, M.D. 2006. Ecosystem Engineering across Environmental Gradients: Implications for Conservation and Management. *Bioscience*. 56:211–8.

Delille, B., Borges, A.V. & Delille, D. 2009. Influence of giant kelp beds (*Macrocystis pyrifera*) on diel cycles of pCO2 and DIC in the Sub-Antarctic coastal area. *Estuar. Coast. Shelf Sci.* 81:114–22.

Demartini, E.E. & Roberts, D.A. 1990. Effects of Giant Kelp (*Macrocystis*) on the Density and Abundance of Fish in a Cobble-bottom Kelp Forest. *Bull. Mar. Sci.* 46:287–300.

Dethier, M., Sosik, E., Galloway, A., Duggins, D. & Simenstad, C. 2013. Addressing assumptions: variation in stable isotopes and fatty acids of marine macrophytes can confound conclusions of food web studies. *Mar. Ecol. Prog. Ser.* 478:1–14.

Dickson, A.G. 2010. Part 1 : Seawater carbonate chemistry. The carbon dioxide system in seawater : equilibrium chemistry and measurements. *Guid. to best Pract. Ocean Acidif. Res. data Report.* 1–40.

Drake, P.T., McManus, M.A. & Storlazzi, C.D. 2005. Local wind forcing of the Monterey Bay area inner shelf. *Cont. Shelf Res.* 25:397–417.

Drechsler, Z., Sharkia, R., Cabantchik, Z.I.Z. & Beer, S. 1993. Bicarbonate uptake in the marine macroalga *Ulva sp.* is inhibited by classical probes of anion exchange by red blood cells. *Planta*. 191:34–40.

Drobnitch, S.T., Nickols, K.J. & Edwards, M.S. n.d. Abiotic influences on

bicarbonate use in the giant kelp, *Macrocystis pyrifera*, in the Monterey Bay. *J. Phycol.* In Press.

Duarte, C.M., Middelburg, J.J. & Caraco, N. 2004. Major role of marine vegetation on the oceanic carbon cycle. *Biogeosciences Discuss.* 1:659–79.

Duggins, D., Simenstad, C. & Estes, J. 1989. Magnification of secondary production by kelp detritus in coastal marine ecosystems. *Science (80-. ).* 245:170–3.

Ebeling, A.W., Larson, R.J., Alevizon, W. & Williams, S. 1978. Habitat Groups and Island-Mainland Distribution of Kelp-bed Fishes off Santa Barbara, CA. 403–31.

Edwards, M.S. 1998. Effects of long-term kelp canopy exclusion on the abundance of the annual alga *Desmarestia ligulata* (Light F). *J. Exp. Mar. Bio. Ecol.* 228:309–26.

Edwards, M.S. & Kim, K.Y. 2010. Diurnal variation in relative photosynthetic performance in giant kelp *Macrocystis pyrifera* (Phaeophyceae, Laminariales) at different depths as estimated using PAM fluorometry. *Aquat. Bot.* 92:119–28.

Enquist, B.J. & Biology, E. 2003. Cope's Rule and the evolution of long-distance transport in vascular plants : allometric scaling, biomass partitioning and optimization. *Plant, Cell Environ.* 26:151–61.

Erikson, L., Storlazzi, C. & Golden, N. 2014. Wave height, peak period, and orbital velocity for the California continental shelf. U.S. Geological Survey data set.

Fernández, P., Hurd, C.L. & Roleda, M.Y. 2014. Bicarbonate uptake via an ion exchange protein is the main mechanism of inorganic carbon acquisition by the giant kelp *Macrocystis pyrifera* (Laminariales, Phaeophyceae) under variable pH. *J. Phycol.* 50:998–1008.

Fernández, P., Roleda, M.Y. & Hurd, C.L. 2015. Effects of ocean acidification on the photosynthetic performance, carbonic anhydrase activity and growth of the giant kelp *Macrocystis pyrifera*. *Photosynth. Res.* 124:293–304.

Figurski, J. 2010. Patterns and sources of variation in drift algae and the ecological consequences for kelp forests. University of California, Santa Cruz.

Finlay, J.C., Power, M.E. & Cabana, G. 1999. Effects of water velocity on algal carbon isotope ratios: Implications for river food web studies. *Limnol. Oceanogr.* 44:1198–203.

Foley, M.M. & Koch, P. 2010. Correlation between allochthonous subsidy input and

isotopic variability in the giant kelp *Macrocystis pyrifera* in central California, USA. *Mar. Ecol. Prog. Ser.* 409:41–50.

Fox, M.D. 2013. Resource translocation drives δ 13 C fractionation during recovery from disturbance in giant kelp, *Macrocystis pyrifera*. *J. Phycol.* 49:811–5.

Franco, A.C. & Nobel, P.S. 1989. Effect of Nurse Plants on the Microhabitat and Growth of Cacti. *Ecology*. 77:870–86.

Fredriksen, S. 2003. Food web studies in a Norwegian kelp forest based on stable isotope analysis. *Mar. Ecol. Prog. Ser.* 260:71–81.

Frieder, C.A., Nam, S.H., Martz, T.R. & Levin, L.A. 2012. High temporal and spatial variability of dissolved oxygen and pH in a nearshore California kelp forest. *Biogeosciences*. 9:3917–30.

Fritz, K.M., Gangloff, M.M. & Feminella, J.W. 2004. Habitat modification by the stream macrophyte *Justicia americana* and its effects on biota. *Oecologia*. 140:388–97.

Gaylord, B., Denny, M.W. & Koehl, M. a. R. 2003. Modulation of wave forces on kelp canopies by alongshore currents. *Limnol. Oceanogr.* 48:860–71.

Gaylord, B., Rosman, J.H., Reed, D.C., Koseff, J.R., Fram, J., MacIntyre, S., Arkema, K. et al. 2007. Spatial patterns of flow and their modification within and around a giant kelp forest. *Limnol. Oceanogr.* 52:1838–52.

Gerard, V.A. 1982. Growth and Utilization of Internal Nitrogen Reserves by the Giant Kelp *Macrocystis pyrifera* in a Low-Nitrogen Environment. *Mar. Biol.* 66:27–35.

Gerard, V.A. 1984. The light environment in a giant kelp forest: influence of *Macrocystis pyrifera* on spatial and temporal variability. *Mar. Biol.* 84:189–95.

Gillies, C.L., Stark, J.S. & Smith, S.D. a. 2011. Research article: small-scale spatial variation of δ13C and δ15N isotopes in Antarctic carbon sources and consumers. *Polar Biol.* 35:813–27.

Giordano, M., Beardall, J. & Raven, J.A. 2005. CO2 concentrating mechanisms in algae: mechanisms, environmental modulation, and evolution. *Annu. Rev. Plant Biol.* 56:99–131.

Gowell, M.R., Coombes, M.A. & Viles, H.A. 2015. Rock-protecting seaweed? Experimental evidence of bioprotection in the intertidal zone. *Earth Surf.*

*Process. Landforms*. 40:1364–70.

Graham, M.H. 1997. Factors determining the upper limit of giant kelp, *Macrocystis pyrifera* Agardh, along the Monterey Peninsula, central California, USA. *J. Exp. Mar. Bio. Ecol.* 218:127–149.

Graham, M.H., Harrold, C., Lisin, S., Light, K., Watanabe, J.M. & Foster, M.S. 1997. Population dynamics of giant kelp *Macrocystis pyrifera* along a wave exposure gradient.

Graham, M.H., Vasquez, J.A. & Buschmann, A.H. 2007. Global ecology of the giant kelp *Macrocystis*: from ecotypes to ecosystems. *In* Gibson, R. N., Atkinson, R. J. A. & Gordon, J. D. M. [Eds.] *Oceanography and Marine Biology: An Annual Review*. CRC Press, pp. 39–88.

Grice, A.M., Loneragan, N.R. & Dennison, W.C. 1996. Light intensity and the interactions between physiology, morphology and stable isotope ratios in five species of seagrass. *J. Exp. Mar. Bio. Ecol.* 195:91–110.

Hansen, A.T., Hondzo, M. & Hurd, C.L. 2011. Photosynthetic oxygen flux by *Macrocystis pyrifera*: a mass transfer model with experimental validation. *Mar. Ecol. Prog. Ser.* 434:45–55.

Hartney, K.B. 1996. Site fidelity and homing behaviour of some kelp-bed fishes. *J. Fish Biol.* 49:1062–9.

Helmuth, B. 1998. Intertidal mussle microclimates: Predicting the body temperature of a sessile invertebrate. *Ecol. Monogr.* 68:51–74.

Hemminga, M. A. & Mateo, M. 1996. Stable carbon isotopes in seagrasses: variability in ratios and use in ecological studies. *Mar. Ecol. Prog. Ser.* 140:285–98.

Henkel, S.K. & Hofmann, G.E. 2008. Thermal ecophysiology of gametophytes cultured from invasive *Undaria pinnatifida* (Harvey) Suringar in coastal California harbors. *J. Exp. Mar. Bio. Ecol.* 367:164–73.

Hennon, G.M.M., Ashworth, J., Groussman, R.D., Berthiaume, C., Morales, R.L., Baliga, N.S., Orellana, M. V. et al. 2015. Diatom acclimation to elevated CO2 via cAMP signalling and coordinated gene expression. *Nat. Clim. Chang.* 5:761–6.

Hölttä, T., Mencuccini, M. & Nikinmaa, E. 2009. Linking phloem function to structure: analysis with a coupled xylem-phloem transport model. *J. Theor. Biol.*

259:325–37.

Hurd, C.L. & Pilditch, C. A. 2011. Flow-Induced Morphological Variations Affect Diffusion Boundary-Layer Thickness of *Macrocystis pyrifera* (Heterokontophyta, Laminariales)1. *J. Phycol.* 47:341–51.

Huston, M. & Wolverton, S. 2009. The global distribution of net primary production: resolving the paradox. *Ecol. Monogr.* 79:343–77.

Jensen, K.H., Lee, J., Bohr, T., Bruus, H., Holbrook, N.M. & Zwieniecki, M.A. 2011. Optimality of the Münch mechanism for translocation of sugars in plants. *J. R. Soc. Interface*. 8:1155–65.

Jensen, K.H., Liesche, J., Bohr, T. & Schulz, A. 2012. Universality of phloem transport in seed plants. *Plant, Cell Environ.* 35:1065–76.

Johnston, A.M. & Raven, J.A. 1990. Effects of culture in high CO2 on the photosynthetic physiology of *Fucus serratus*. *Eur. J. Phycol.* 25:75–82.

Jones, C., Lawton, J. & Shachak, M. 1994. Organisms as ecosystem engineers. *Oikos*. 69:373–86.

Kaehler, S., Pakhomov, E.A., Kalin, R. & Davis, S. 2006. Trophic importance of kelp-derived suspended particulate matter in a through-flow sub-Antarctic system. *Mar. Ecol. Prog. Ser.* 316:17–22.

Kapsenberg, L. & Hofmann, G.E. 2016. Ocean pH time-series and drivers of variability along the northern Channel Islands, California, USA. *Limnol. Oceanogr.*

Kassab, G.S. 2006. Scaling laws of vascular trees: of form and function. *Am. J. Physiol. Heart Circ. Physiol.* 290:H894-903.

Klenell, M., Snoeijs, P. & Pedersén, M. 2004. Active carbon uptake in *Laminaria digitata* and *L. saccharina* (Phaeophyta) is driven by a proton pump in the plasma membrane. *Hydrobiologia*. 514:41–53.

Knoblauch, J., Tepler Drobnitch, S., Peters, W.S. & Knoblauch, M. 2016. In situ-microscopy reveals reversible cell wall swelling in kelp sieve tubes: one mechanism for turgor generation and flow control? *Plant. Cell Environ*.

Koehl, M.A.R. & Alberte, R.R.S. 1988. Flow, flapping, and photosynthesis of *Nereocystis luetkeana*: a functional comparison of undulate and flat blade morphologies. *Mar. Biol.* 99:435–44.

Komatsu, T., Ariyama, H., H, N. & Sakamoto, W. 1982. Spatial and Temporal Distributions of Water Temperature in a Sargassum forest. *J. Oceanogr. Soc. Japan*. 38:63–72.

Kopczak, C.D., Zimmerman, R.C. & Kremer, J.N. 1991. Variation in nitrogen physiology and growth among geographically isolated populations of the giant kelp, *Macrocystis pyrifera* (Phaeophyta). *J. Phycol.* 27:149–58.

Kubler, J.E. & Raven, J.A. 1995. The interaction between inorganic carbon acquisition and light supply in *Palmaria palmata* (Rhodophyta). *J. Phycol.* 31:369–75.

Lapointe, B.E., Rice, D.L. & Lawrence, J.M. 1984. Responses of photosynthesis, respiration, growth and cellular constituents to hypo-osmotic shock in the red alga *Gracilaria tikvahiae*. *Comp. Biochem. Physiol. -- Part A Physiol.* 77:127–32.

Larsson, C. & Axelsson, L. 1999. Bicarbonate uptake and utilization in marine macroalgae. *Eur. J. Phycol.* 34:79–86.

Laws, E.A.E., Popp, B., Bidigare, R., Kennicutt, M.M.C., Macko, S.S.A. & Bidigare, J.R.R. 1995. Dependence of phytoplankton carbon isotopic composition on growth rate and [CO2]aq: Theoretical considerations and experimental results. *Geochim. Cosmochim. Acta*. 59:1131–8.

Lee, K.S. & Dunton, K.H. 2000. Diurnal changes in pore water sulfide concentrations in the seagrass *Thalassia testudinum* beds: The effects of seagrasses on sulfide dynamics. *J. Exp. Mar. Bio. Ecol.* 255:201–14.

Lobban, C. 1978. Translocation of C in *Macrocystis pyrifera* (Giant Kelp). *Plant Physiol.* 61:585–9.

Mackey, A.P., Hyndes, G. a., Carvalho, M.C. & Eyre, B.D. 2015. Physical and biogeochemical correlates of spatio-temporal variation in the δ13C of marine macroalgae. *Estuar. Coast. Shelf Sci.* 1–12.

MacLeod, N. a & Barton, D.R. 1998. Effects of light intensity, water velocity, and species composition on carbon and nitrogen stable isotope ratios in periphyton. *Can. J. Fish. Aquat. Sci.* 55:1919–25.

Manley, S.L. 1983. Composition of sieve tube sap from *Macrocystis pyrifera* (Phaeophyta) with emphasis on the inorganic constituents. *J. Phycol.* 19:118–121.

Mann, K.H. 1982. Ecology of coastal waters: a systems approach. Univ. of California Press.

Marconi, M., Giordano, M. & Raven, J.A. 2011. Impact of Taxonomy, Geography, and Depth on Δ13C and Δ15N Variation in a Large Collection of Macroalgae. *J. Phycol.* 47:1023–35.

Mass, T., Genin, A., Shavit, U., Grinstein, M. & Tchernov, D. 2010. Flow enhances photosynthesis in marine benthic autotrophs by increasing the efflux of oxygen from the organism to the water. *Proc. Natl. Acad. Sci. U. S. A.* 107:2527–31.

McAfee, D., Cole, V.J. & Bishop, M.J. 2016. Latitudinal gradients in ecosystem engineering by oysters vary across habitats. *Ecology*. 97:929–39.

Mcginn, P.J., Price, G.D. & Badger, M.R. 2004. High light enhances the expression of low-CO2-inducible transcripts involved in the CO2-concentrating mechanism in *Synechocystis sp. PCC6803*. *Plant, Cell Environ.* 27:615–26.

Mcmahon, K.W., Thorrold, S.R., Houghton, L.A. & Berumen, M.L. 2015. Tracing carbon flow through coral reef food webs using a compound-specific stable isotope approach. *Oecologia*.

McPherson, M.L., Zimmerman, R.C. & Hill, V.J. 2015. Predicting carbon isotope discrimination in Eelgrass (*Zostera marina* L.) from the environmental parameters-light, flow, and [DIC]. *Limnol. Oceanogr.* 60:1875–89.

Mercado, J.M., Andría, J.R., Pérez-Llorens, J.L., Vergara, J.J. & Axelsson, L. 2006. Evidence for a plasmalemma-based CO2 concentrating mechanism in *Laminaria saccharina*. *Photosynth. Res.* 88:259–68.

Middelburg, J.J., Duarte, C.M. & Gattuso, J.P. 2007. Respiration in coastal benthic communities. *Respir. Aquat. Ecosyst.* 206–24.

Miller, R.J. & Page, H.M. 2012. Kelp as a trophic resource for marine suspension feeders: a review of isotope-based evidence. *Mar. Biol.* 159:1391–402.

Miller, R.J., Page, H.M. & Reed, D.C. 2015. Trophic versus structural effects of a marine foundation species, giant kelp (*Macrocystis pyrifera*). *Oecologia*. 179:1199–209.

Mook, W.G., Bommerson, J.C. & Staverman, W.H. 1974. Carbon isotope fractionation between dissolved bicarbonate and gaseous carbon dioxide. *Earth Planet. Sci. Lett.* 22:169–76.

Nielsen, K.J., Blanchette, C.A., Menge, B.A. & Lubchenco, J. 2006. Physiological snapshots reflect ecological performance of the sea palm, *Postelsia palmaeformis* (Phaeophyceae) across intertidal elevation and exposure gradients. *J. Phycol.* 42:548–59.

Niklas, K.J. 1993. The allometry of plant reproductive biomass and stem diameter. *Am. J. Bot.* 80:461–7.

Nishihara, G.N. & Ackerman, J.D. 2009. Diffusive boundary layers do not limit the photosynthesis of the aquatic macrophyte, *Vallisneria americana*, at moderate flows and saturating light levels. *Limnol. Oceanogr.* 54:1874–82.

O'Leary, M. 1988. Carbon isotopes in photosynthesis. *Bioscience*. 38:328–36.

Petit, G. & Crivellaro, A. 2014. Comparative axial widening of phloem and xylem conduits in small woody plants. *Trees*.

Phillips, D.L. & Gregg, J.W. 2003. Source partitioning using stable isotopes: coping with too many sources. *Oecologia*. 136:261–9.

Pierrot, D., Lewis, E. & Wallace, D. 2006. MS Excel Program Developed for CO2 System Calculations. ORNL/CDIAC-105a.

Pointing, S.B. & Belnap, J. 2012. Microbial colonization and controls in dryland systems. *Nat. Rev. Microbiol.* 10:654.

Popp, B., Laws, E., Bidigare, R. & Dore, J. 1998. Effect of phytoplankton cell geometry on carbon isotopic fractionation. *Geochim. Cosmochim. Acta*. 62:69–77.

Post, D.M. 2002. Using stable isotopes to estimate trophic position: Models, methods, and assumptions. *Ecology*. 83:703–18.

Rambo, T.R. & North, M.P. 2009. Forest Ecology and Management Canopy microclimate response to pattern and density of thinning in a Sierra Nevada forest. 257:435–42.

Raven, J.A., Beardall, J. & Giordano, M. 2014. Energy costs of carbon dioxide concentrating mechanisms in aquatic organisms. *Photosynth. Res.* 121:111–24.

Raven, J.A., Giordano, M., Beardall, J. & Maberly, S.C. 2012. Algal evolution in relation to atmospheric CO2: carboxylases, carbon-concentrating mechanisms and carbon oxidation cycles. *Philos. Trans. R. Soc. B Biol. Sci.* 367:493–507.

Raven, J.A. & Hurd, C.L. 2012. Ecophysiology of photosynthesis in macroalgae. *Photosynth. Res.* 113:105–25.

Reed, D.C. & Brzezinski, M. 2009. Kelp forests. *In* Laffoley, D. & Grimsditch, G. [Eds.] *The Management of Natural Coastal Carbon Sinks*. IUCN, Gland, Switzerland.

Riisberg, I., Orr, R.J.S., Kluge, R., Shalchian-Tabrizi, K., Bowers, H.A., Patil, V., Edvardsen, B. et al. 2009. Seven gene phylogeny of heterokonts. *Protist*. 160:191–204.

Ronellenfitsch, H., Liesche, J., Jensen, K.H., Holbrook, N.M., Schulz, A. & Katifori, E. 2015. Scaling of phloem structure and optimality of photoassimilate transport in conifer needles. *Proc. R. Soc. B*. 282:20141863.

Royal Society, T. 2005. Ocean acidification due to increasing atmospheric carbon dioxide.

Savage, V.M., Bentley, L., Enquist, B.J., Sperry, J.S., Smith, D.D., Reich, P.B. & Allmen, E.I. Von 2010. Hydraulic trade-offs and space filling enable better predictions of vascular structure and function in plants. *PNAS*. 107:22722–7.

Schiel, D.R. & Foster, M.S. 2015. The biology and ecology of giant kelp forests. University of California Press.

Schindelin, J., Arganda-Carreras, I., Frise, E., Kaynig, V., Longair, M., Pietzsch, T., Preibisch, S. et al. 2012. Fiji: an open-source platform for biological-image analysis. *Nat. Methods*. 9:676–82.

Schmitz, K. 1981. Translocation. *In* Lobban, C. & Wynne, M. [Eds.] *The Biology of Seaweeds*. Botanical Monographs 17, pp. 534–58.

Schmitz, K. & Lobban, C. 1976. A Survey of Translocation in Laminariales (Phaeophyceae). *Mar. Biol.* 36:207–16.

Seely, G., Duncan, M. & Vidaver, W. 1972. Preparative and analytical extraction of pigments from brown algae with dimethyl sulfoxide. *Mar. Biol.* 12:184–8.

Sharkey, T.D., Stitt, M., Heineke, D., Gerhardt, R., Raschke, K. & Heldt, H.W. 1986. Limitation of Photosynthesis by Carbon Metabolism II. O2-Insensistive CO2 Uptake Results from Limitation of Triose Phosphate Utilization. *Plant Physiol.* 81:1123–9.

Silberfeld, T., Leigh, J.W., Verbruggen, H., Cruaud, C., de Reviers, B. & Rousseau, F. 2010. A multi-locus time-calibrated phylogeny of the brown algae (Heterokonta, Ochrophyta, Phaeophyceae): Investigating the evolutionary nature of the "brown algal crown radiation". *Mol. Phylogenet. Evol.* 56:659–74.

Skriptsova, A. V. & Titlyanov, E.A. 2003. Effect of the Meristem on Sporification of *Laminaria cichorioides*. *Russ. J. Mar. Biol.* 29:372–7.

Smith, B.M. & Melis, A. 1987. Photosystem Stoichiometry and Excitation Distribution in Chloroplasts from Surface and Minus 20 Meter Blades of *Macrocystis pyrifera*, the Giant Kelp. *Plant Physiol.* 84:1325–30.

Steneck, R.S., Graham, M.H., Bourque, B.J., Corbett, D., Erlandson, J.M., Estes, J.A. & Tegner, M.J. 2002. Kelp forest ecosystems: biodiversity, stability, resilience and future. *Environ. Conserv.* 29:436–59.

Stewart, H.L., Fram, J. & Reed, D.C. 2009. Differences in growth, morphology and tissue carbon and nitrogen of *Macrocystis pyrifera* within and at the outer edge of a giant kelp forest in California, USA. *Mar. Ecol. Prog. Ser.* 375:101–12.

Storlazzi, C., McManus, M. & Figurski, J. 2003. Long-term, high-frequency current and temperature measurements along central California: insights into upwelling/relaxation and internal waves on the inner shelf. *Cont. Shelf Res.* 23:901–18.

Surif, M.B. & Raven, J.A. 1990. Photosynthetic gas exchange under emersed conditions in eulittoral and normally submersed members of the Fucales and the Laminariales: interpretation in relation to C isotope ratio and N and water use efficiency. *Oecologia*. 82:68–80.

Tokoro, T., Hosokawa, S., Miyoshi, E., Tada, K., Watanabe, K., Montani, S., Kayanne, H. et al. 2014. Net uptake of atmospheric CO2 by coastal submerged aquatic vegetation. *Glob. Chang. Biol.* 20:1873–84.

Trudeau, V. & Rasmussen, J.B. 2003. The effect of water velocity on stable carbon and nitrogen isotope signatures of periphyton. *Limnol. Oceanogr.* 48:2194–9.

Utter, B. & Denny, M.W. 1996. Wave-induced forces on the giant kelp *Macrocystis pyrifera* (Agardh): field test of a computational model. *J. Exp. Biol.* 199:2645–54.

Vanderklift, M.A. & Bearham, D. 2014. Variation in δ13C and δ15N of kelp is explained by light and productivity. *Mar. Ecol. Prog. Ser.* 515:111–21.

Walker, L.R., Clarkson, B.D., Silvester, W.B. & Clarkson, B.R. 2003. Colonization dynamics and facilitative impacts of a nitrogen-fixing shrub in primary succession. *J. Veg. Sci.* 14:277–90.

Ward, B.B. 2005. Temporal variability in nitrification rates and related biogeochemical factors in Monterey Bay, California, USA. *Mar. Ecol. Prog. Ser.* 292:97–109.

Watanabe, J. 1984. The influence of recruitment, competition, and benthic predation on spatial distributions of three species of kelp forest gastropods (Trochidae: *Tegula*). *J. Ecol.* 65:920–36.

Wefer, G. & Killingley, J.S. 1986. Carbon isotopes in organic matter from a benthic alga *Halimeda incrassata* (Bermuda): Effects of light intensity. *Chem. Geol. Isot. Geosci. Sect.* 59:321–6.

Wernberg, T., Kendrick, G.A. & Toohey, B.D. 2005. Modification of the physical environment by an *Ecklonia radiata* (Laminariales) canopy and implications for associated foliose algae. *Aquat. Ecol.* 39:419–30.

Wernberg, T., Thomsen, M.S., Tuya, F. & Kendrick, G.A. 2011. Biogenic habitat structure of seaweeds change along a latitudinal gradient in ocean temperature. *J. Exp. Mar. Bio. Ecol.* 400:264–71.

West, G.B., Brown, J.H. & Enquist, B.J. 1997. A General Model for the Origin of Allometric Scaling Laws in Biology. *Science.* 276:122–6.

West, G.B., Brown, J.H. & Enquist, B.J. 1999. The fourth dimension of life: fractal geometry and allometric scaling of organisms. *Science.* 284:1677–9.

Wheeler, P.A. & North, W.J. 1981. Nitrogen supply, tissue composition and frond growth rates for *Macrocystis pyrifera* off the coast of southern California. *Mar. Biol.* 64:59–69.

Wheeler, W.N. 1980. Effect of boundary layer transport on the fixation of carbon by the giant kelp *Macrocystis pyrifera*. *Mar. Biol.* 56:103–10.

Wiencke, C. & Fischer, G. 1990. Growth and stable carbon isotope composition of cold-water macroalgae in relation to light and temperature. *Mar. Ecol. Prog. Ser.* 65:283–92.

Woodson, C.B., Eerkes-Medrano, D.I., Flores-Morales, A., Foley, M.M., Henkel, S.K., Hessing-Lewis, M., Jacinto, D. et al. 2007. Local diurnal upwelling driven by sea breezes in northern Monterey Bay. *Cont. Shelf Res.* 27:2289–302.

Young, J., Kranz, S., Goldman, J., Tortell, P. & Morel, F. 2015. Antarctic phytoplankton down-regulate their carbon-concentrating mechanisms under high CO2 with no change in growth rates. *Mar. Ecol. Prog. Ser.* 532:13–28.

Zou, D., Gao, K. & Xia, J. 2003. Photosynthetic utilization of inorganic carbon in the economic brown alga, *Hizikia fusiforme* (Sargassaceae) from the South China Sea. *J. Phycol.* 39:1095–100.

Zwieniecki, M.A., Stone, H., Leigh, A., Boyce, C. & Holbrook, N.M. 2006. Hydraulic design of pine needles: one-dimensional optimization for single-vein leaves. *Plant, Cell Environ.* 29:803–9.

# Appendix 1:

## Supplementary Data and Methods for Chapter 1

Table S1. Scaling parameters for the log-log relationship between average SE diameter and various functional anatomy traits.

| Independent variable | species | slope | intercept | R^2 | P-value |
|---|---|---|---|---|---|
| Stipe diameter (cm) | *A. marginata* | 0.963 | 0.599 | 0.01 | 0.4156 |
| | *E. menziesii* | 0.389 | 1.230 | 0.01 | 0.5038 |
| | *L. setchellii* | 0.147 | 1.128 | 0.28 | 0.0003 |
| | *M. pyrifera* | 0.871 | 1.660 | 0.89 | <0.0001 |
| | *N. luetkeana* | 0.302 | 1.448 | 0.23 | 0.0007 |
| | *P. californica* | 0.197 | 1.137 | 0.11 | 0.0304 |
| Conduit packing (SE/$\mu m^2$) | *A. marginata* | 0.304 | -1.953 | 0.06 | 0.1108 |
| | *E. menziesii* | -0.550 | -0.395 | 0.00 | 0.7414 |
| | *L. setchellii* | 0.749 | 3.156 | 0.00 | 0.8316 |
| | *M. pyrifera* | -0.676 | -0.955 | 0.95 | <0.0001 |
| | *N. luetkeana* | -0.536 | -0.554 | 0.04 | 0.1708 |
| | *P. californica* | -0.800 | -1.165 | 0.08 | 0.0751 |
| Vascular fraction | *A. marginata* | 0.346 | 1.346 | 0.40 | <0.0001 |
| | *E. menziesii* | 0.558 | 1.503 | 0.22 | <0.0001 |
| | *L. setchellii* | 0.526 | 1.517 | 0.32 | 0.0001 |
| | *M. pyrifera* | 1.597 | 2.608 | 0.68 | <0.0001 |
| | *N. luetkeana* | 0.735 | 1.991 | 0.46 | <0.0001 |
| | *P. californica* | 0.601 | 1.568 | 0.49 | <0.0001 |
| Cumulative blade area ($cm^2$) | *A. marginata* | 0.108 | 0.833 | 0.37 | <0.0001 |
| | *E. menziesii* | -0.178 | 1.660 | 0.00 | 0.7740 |
| | *L. setchellii* | 0.229 | 0.366 | 0.46 | <0.0001 |
| | *M. pyrifera* | 0.193 | 0.803 | 0.88 | <0.0001 |
| | *N. luetkeana* | 0.182 | 0.777 | 0.03 | 0.2430 |
| | *P. californica* | 0.184 | 0.473 | 0.07 | 0.1072 |
| Path length (m) | *A. marginata* | -0.168 | 1.064 | 0.01 | 0.5633 |
| | *E. menziesii* | 0.171 | 1.045 | 0.01 | 0.3867 |
| | *L. setchellii* | -0.215 | 0.969 | 0.00 | 0.6835 |
| | *M. pyrifera* | 0.280 | 1.427 | 0.85 | <0.0001 |
| | *N. luetkeana* | -0.278 | 1.542 | 0.05 | 0.1402 |
| | *P. californica* | -0.335 | 0.958 | 0.01 | 0.4735 |
| Cumulative biomass (g) | *A. marginata* | 0.129 | 1.031 | 0.03 | 0.1985 |
| | *E. menziesii* | 0.121 | 0.861 | 0.00 | 0.8301 |
| | *L. setchellii* | 0.239 | 0.747 | 0.25 | 0.0006 |
| | *M. pyrifera* | 0.188 | 1.204 | 0.89 | <0.0001 |
| | *N. luetkeana* | 0.187 | 1.188 | 0.08 | 0.0569 |
| | *P. californica* | 0.167 | 0.819 | 0.03 | 0.2878 |

# Supplemental Material
# Convergent evolution of vascular optimization in kelp (Laminariales)

Sarah Tepler, Kaare H. Jensen, Paige Prentice, and Jarmila Pittermann
(Dated: July 10, 2015)

## I. MATHEMATICAL MODEL OF CARBOHYDRATE LOADING AND UNLOADING IN MACROALGAE

We model sugar transport by considering the movement of sap through collection of parallel conduits along the $x$-axis. We denote the flow velocity $u(x)$ and the total conduit cross-section area $A(x)$, while $c$ is the total carbohydrate concentration. Phloem loading and unloading is included via a loading function $\phi$ in the sap conservation equation [1]

$$c\frac{d}{dx}\left(Au\right) = \phi. \tag{1}$$

Here, $\phi$ is amount of carbohydrate loaded into or unloaded from the phloem per unit time. We can express it as $\phi = qc$, where $q$ is the sap volume entering or leaving the stipe phloem per unit length and time. Note that the sign of $q$ reflects the direction of the sap flow leaving or entering the conduit system; $q > 0$ is used in a source while $q < 0$ applies in a sink organ. The coordinate $x$ is measured from the start of the zone. For the unloading zone relevant to *M. pyrifera*, it is given by $x = \ell + x^* - H$, where $x^*$ is the distance from the holdfast, $H$ is the organism height, and $\ell = 1$ m is the length of the unloading zone. Here we assume that $\phi = qc$ is constant throughout either the loading or unloading zone. This assumption is supported by observations by Lobban, who found that the unloading rate reached a plateau near the apex in *M. pyrifera* [2]. Outside the transfer zones the loading factor $\phi = 0$. In that case (1) implies conservation of sugar mass flow $cAu = \text{const}$.

Equation (1) can be integrated to yield

$$Au = qx + c_1. \tag{2}$$

Imposing a no-flow boundary condition at the apex ($Au = 0$ at $x = \ell$) leads to

$$Au = q(x - \ell). \tag{3}$$

We now use Darcy's law for the relationship between the velocity $u$ and the pressure gradient $dp/dx$

$$\frac{dp}{dx} = -\frac{\eta u}{k}, \tag{4}$$

where $\eta$ is the viscosity of the phloem sap and $k(x)$ is the permeability of a single phloem tube. For a cylindrical pipe, the permeability is given by

$$k = \frac{r(x)^2}{8} = \frac{a(x)}{8\pi}, \tag{5}$$

where we have substituted the cross section area $a(x) = \pi r(x)^2$ of a single conduit. Using the expression for velocity found in Eq. (3) in Eq. (4) leads to

$$\frac{dp}{dx} = -\frac{\eta q(x-\ell)}{k(x)A(x)} = -8\pi\frac{\eta q(x-\ell)}{a(x)^2 N(x)} \tag{6}$$

where we have written the total transport area as $A(x) = a(x)N(x)$ where $N(x)$ is the number of sieve elements at the position $x$. Experimental data suggest that the sieve tube number is approximately constant in the species we consider. For instance, $N(x) \approx 500$ in *M. pyrifera* (Fig. 1). With these assumptions, Eq. (6) can be integrated to yield the pressure drop along the collection of conduits $\Delta p = p(\ell) - p(0)$

$$\Delta p = 8\pi\frac{\eta q}{N}\int_0^\ell \frac{\ell - x}{a(x)^2}\,\mathrm{d}x \tag{7}$$

We now ask the question: what is the distribution of sieve tube area $a(x)$ which minimizes the pressure drop $\Delta p$ along the length $\ell$ subject to the constraint that the total volume of conduits remains constant? In other words, we minimize

$$\frac{1}{8\pi}\frac{\Delta p N}{\eta q} = \int_0^\ell \frac{\ell - x}{a(x)^2}\,\mathrm{d}x \text{ subject to } N\int_0^\ell a(x)\,\mathrm{d}x = V_0. \tag{8}$$

A more convenient form of the equations are obtained when rescaling the axial coordinate by the apex distance to obtain the non-dimensional coordinate $z = x/\ell$. This leads to

$$\min \int_0^1 \frac{1-z}{a(z)^2}\,\mathrm{d}z \text{ subject to } \int_0^1 a(z)\,\mathrm{d}z = \text{const}. \tag{9}$$

The Euler-Lagrange equation for this minimization problem is

$$\frac{\partial}{\partial a}\left(\frac{1-z}{a(z)^2}\right) = \lambda \tag{10}$$

where $\lambda$ is a Lagrange multiplier to be determined from the boundary conditions. Equation (10) leads to

$$a(z) = \bar{a}(1-z)^{1/3} = \bar{a}\left(1 - \frac{x}{\ell}\right)^{1/3} \tag{11}$$

where $\bar{a} = a(0)$ is the area at $x = 0$. Equation (11) represents the optimized phloem tube cross section area distribution along the stipe. We can now compute the pressure drop (Eq. (7)) along the stipe

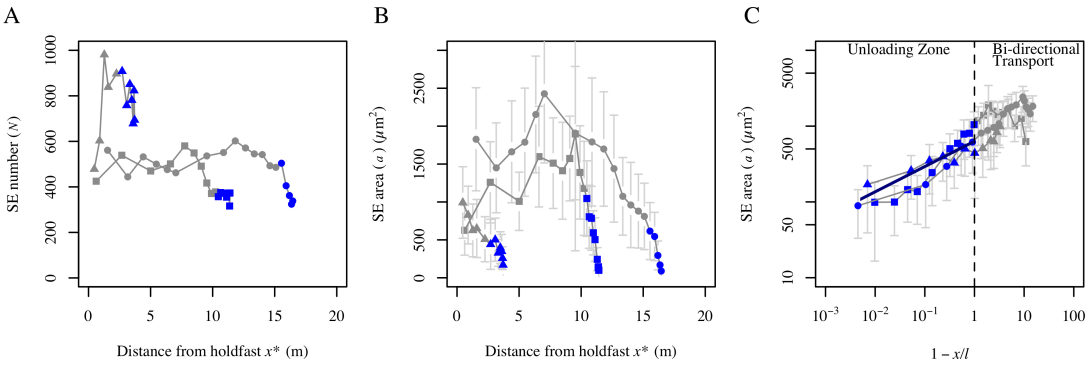


FIG. 1. The area of sieve elements vary along the stipe in *M. pyrifera*, while the number of conduits is approximately constant. (A) Number of sieve element conduits $N$ and (B) sieve element cross-section area $a$ plotted as a function of distance $x^*$ from the holdfast. (C) Sieve tube area $a$ plotted as a function of inverse distance $1 - x/\ell$ using data from (B). Only data points within the unloading zone identified by Lobban of length $\ell = 1$ m are used. The data are in reasonable agreement with the predicted optimum scaling ($a(x) \sim (1 - x/\ell)^{1/3}$, see Eq. (11)) indicated by solid black line.

$$\Delta p_{\rm opt} = 8\pi \frac{q\eta\ell}{N\bar{a}^2} \int_0^1 \frac{1-z}{(1-z)^{2/3}}\,{\rm d}z = 6\pi \frac{q\eta\ell}{N\bar{a}^2} \tag{12}$$

We may contrast this pressure drop with that calculated assuming a uniform sieve element cross-section area $a_0$. Requiring that the two conduit populations have identical volumes leads to the identity

$$N\ell\bar{a} \int_0^1 (1-z)^{1/3}\,{\rm d}z = N\ell a_0. \tag{13}$$

This can be conveniently expressed in the form

$$a_0 = \frac{3}{4}\bar{a}. \tag{14}$$

The pressure drop for a bundle uniform tubes is calculated from Eq. (7) by setting $a(x) = a_0$

$$\Delta p_{\rm unif} = 8\pi \frac{\eta q\ell}{N a_0^2} \int_0^1 (1-z)\,{\rm d}z \tag{15}$$

$$= 4\pi \frac{\eta q\ell}{N a_0^2} = \frac{64\pi}{9} \frac{\eta q\ell}{N\bar{a}^2} \tag{16}$$

Taking the ratio of the optimized to the uniform pressure drop leads to

$$\frac{\Delta p_{\rm unif}}{\Delta p_{\rm opt}} = \frac{32}{27} \approx 1.19 \tag{17}$$

This result shows that the optimal size distribution of sieve elements along the stipe reduces the required pressure drop by about 20%. We use size-invariant sieve elements as null hypotheses to test for optimality in M. pyrifera.

To further elucidate the sensitivity of the pressure ratio in Eq. (17) to the value of the exponent $n$, we consider a general, power-law area dependence given by

$$a_n(x) = \bar{a}_n \left(1 - \frac{x}{\ell}\right)^n. \tag{18}$$

Here, $n = 0$ corresponds to the uniform area distribution and $n = 1/3$ is the optimal distribution found above. The general constant volume constraint is

$$\frac{3}{4} N\ell\bar{a} = N\ell\bar{a}_n \frac{1}{n+1}. \tag{19}$$

This gives a relationship between the individual conduit areas

$$\bar{a}_n = \frac{3(n+1)}{4}\bar{a}, \tag{20}$$

that allows us to compare the pressure drops required to drive flow given a constant conduit volume. The pressure drop is

$$\Delta p_n = 8\pi \frac{q\eta\ell}{N\bar{a}_n^2} \int_0^1 (1-z)^{1-2n}\,{\rm d}z, \tag{21}$$

$$= 8\pi \frac{q\eta\ell}{N\bar{a}_n^2} \frac{1}{2(1-n)}, \tag{22}$$

$$= \frac{64\pi}{9} \frac{q\eta\ell}{N\bar{a}^2} \frac{1}{(1-n)(1+n)^2}. \tag{23}$$

Finally, we find for the general pressure ratio

$$\frac{\Delta p_n}{\Delta p_{\rm opt}} = \frac{32}{27} \frac{1}{(n-1)(n+2)^2}. \tag{24}$$

The pressure ratio given in Eq. (24) is plotted in Fig. 2. While the required pressure increases substantially when $n \to 0, 1$ a range of values around the optimum $n =$

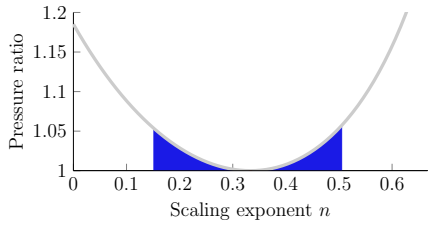


FIG. 2. The energy efficiency of phloem transport depends on the tapering of conduit area. Pressure ratio (Eq. (24)) plotted as a function of power law exponent $n$ (Eq. (18)). Exponents in the range $0.15 < n < 0.5$ (shaded area) are within 5% of the efficiency of the optimum value $n = 1/3$.

1/3 require nearly the same pressure to drive flow. For instance, values in the range $0.15 < n < 0.5$ are within 5% of the optimum, shown as the red shaded area in Fig. 2.

Figure 1(C) shows the sieve tube area $a$ plotted as a function of inverse distance $1 - x/\ell$. The data are consistent with the predicted optimum scaling (Eq. (11)).

[1] Leonard Horwitz. Some simplified mathematical treatments of translocation in plants. *Plant physiology*, 33(2):81, 1958.

[2] Christopher S. Lobban. Translocation of 14c in macrocystis pyrifera (giant kelp). *Plant physiology*, 61(4):585–589, 1978.

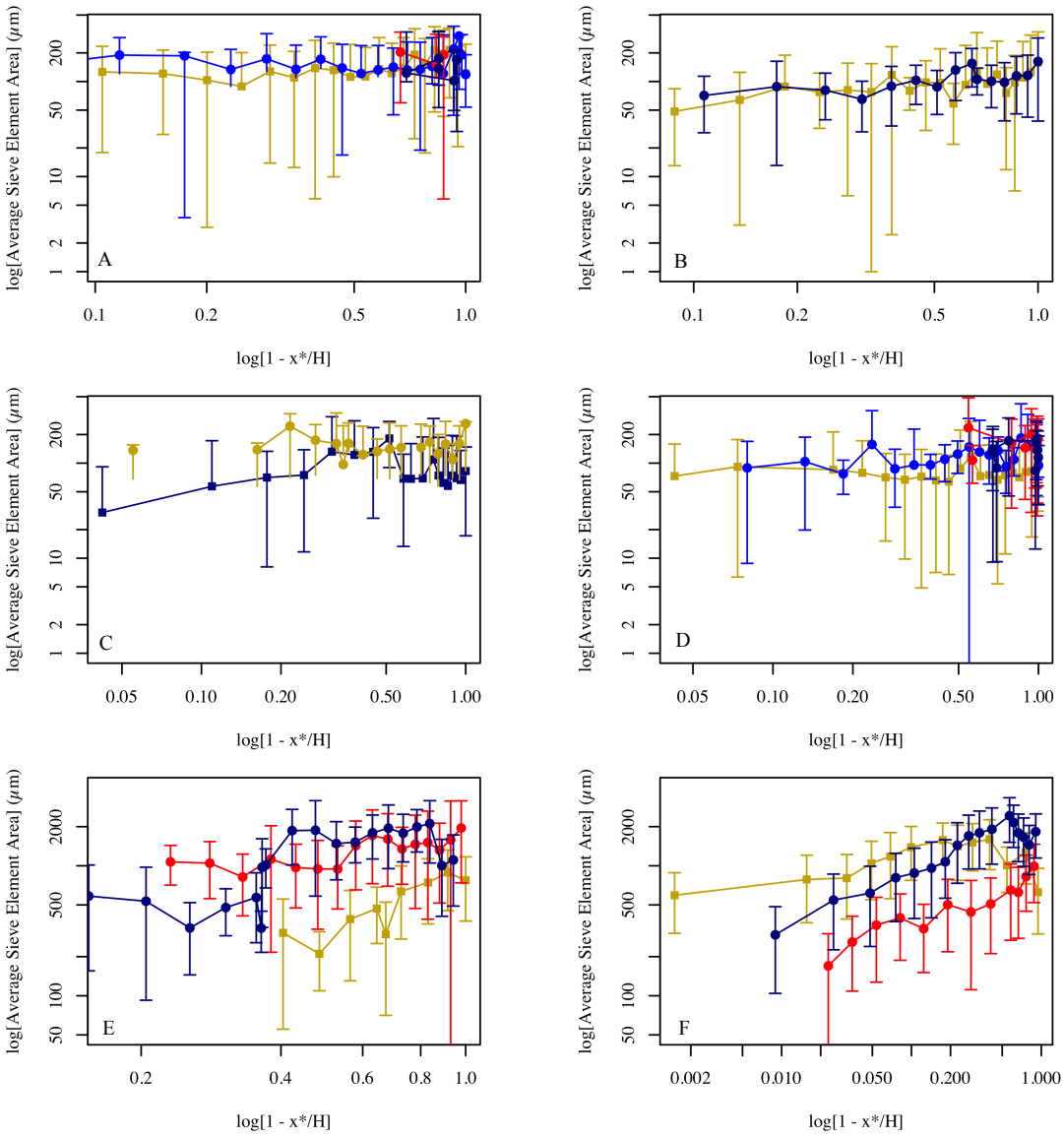


Figure S3. Log-log plot of average sieve element area vs. inverse relative plant height (1 - x*/H) for (A) *Alaria marginata*; (B) *Laminaria setchellii*; (C) *Pterygophora californica*; (D) *Egregia menziesii*; (E) *Nereocystis luetkeana* (note larger y-axis); (F) *Macrocystis pyrifera*. Segments (points) from an individual sampled sporophyte are joined by lines; each individual is a different color. Error bars are one standard deviation.

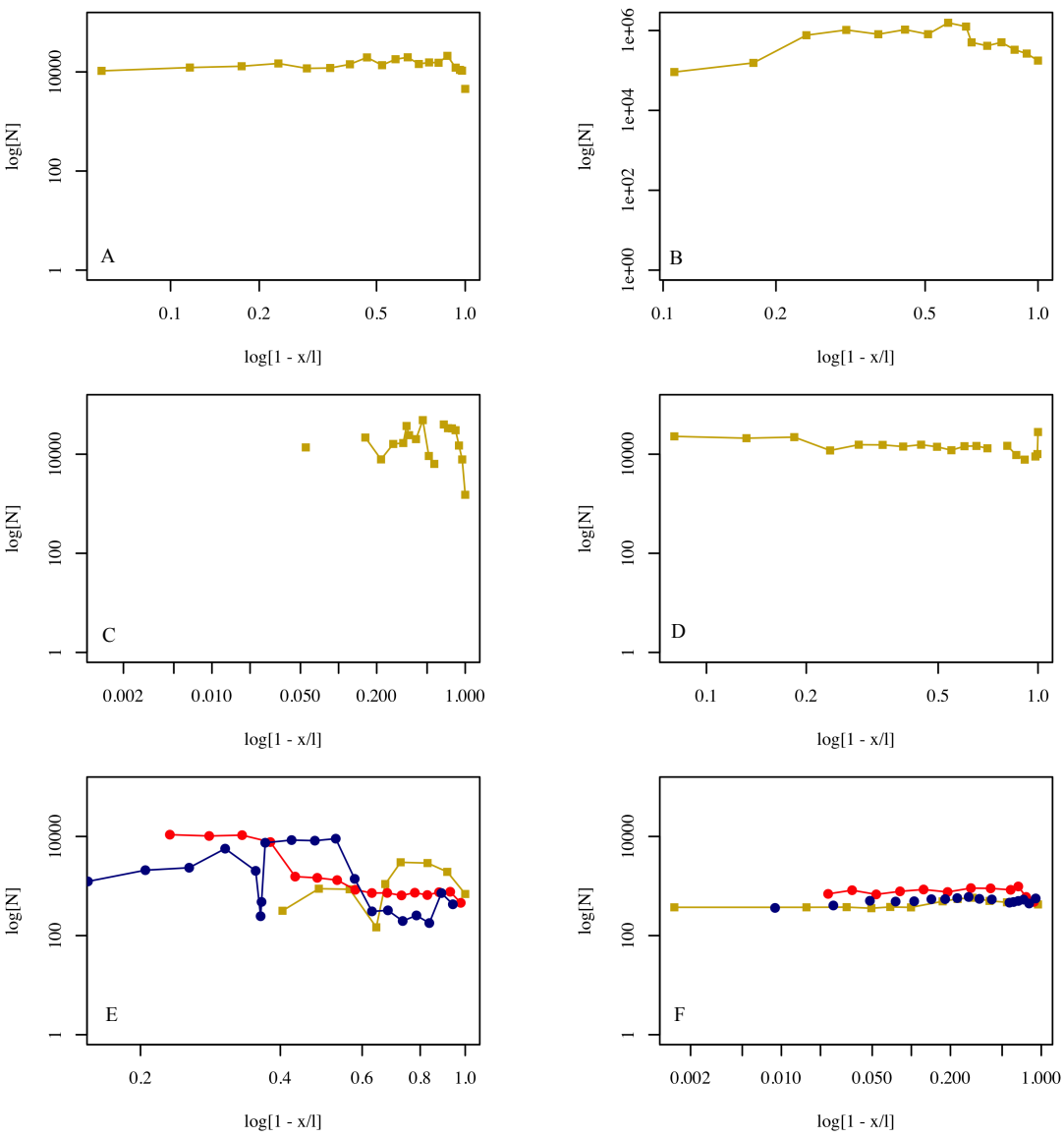


Figure S4. Log-log plot of total estimated SE count (N) vs. inverse relative plant height (1 - x/l) for (A) *Alaria marginata*; (B) *Laminaria setchellii* (note larger y-axis); (C) *Pterygophora californica*; (D) *Egregia menziesii*; (E) *Nereocystis luetkeana* ; (F) *Macrocystis pyrifera.* Segments (points) from an individual sampled sporophyte are joined by lines; each individual is a different color.

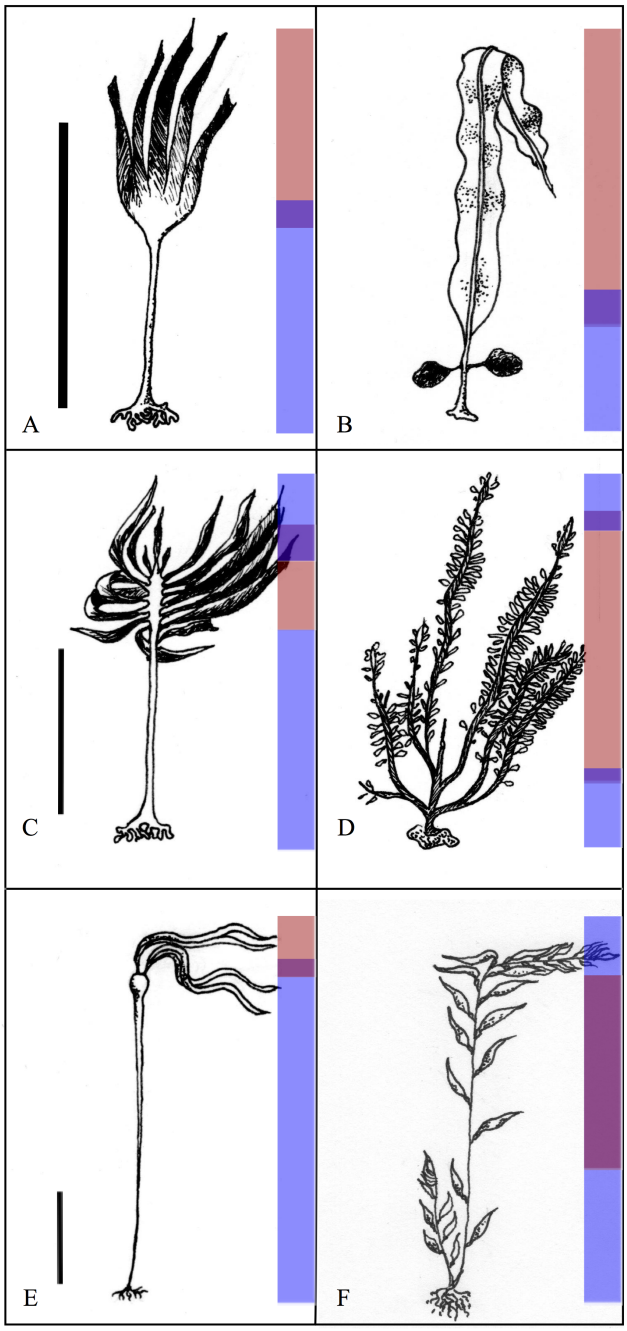


Figure S5. Illustrations of study species. (A,B,C,D) *Laminaria setchelli, Alaria marginata, Egregia menziesii, Pterygophora californica*. Scale bar = 1m. (E,F) *Nereocystis luetkeana, Macrocystis pyrifera*. Scale bar = 5m. Colored bars show approximate loading/unloading zones. Red zones are loading photoassimilate from the phloem, blue zones are unloading from the phloem, and purple zones are transporting bi-directionally.

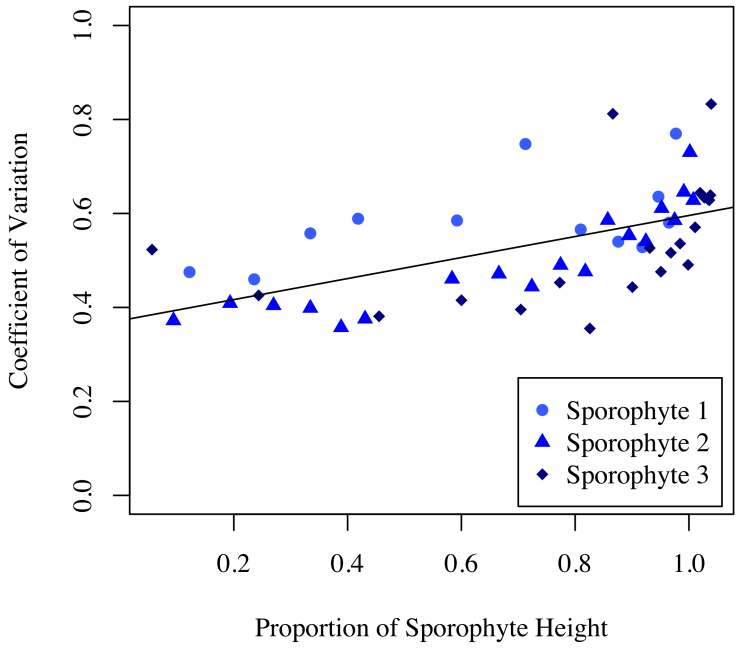


Figure S6. Increase in normalized variation in sieve element (SE) area (coefficient of variation) with height in *M. pyrifera*. Variance in cell size increases in the distal segments of each sampled *M. pyrifera* frond ($p < 0.0001$, $R2 = 0.33$); distal segments possess SE's that are an order of magnitude larger than the (~12 $\mu$m diameter) mean.

## Appendix 2:
## Supplemental Data for Chapter 2

**Figure S1**. Irradiance spectrum of wavelengths emitted by the combination of a blue bulb and sodium halide lamp during oxygen evolution trials. Spectrum was measured as the reflection off a white standard spectralon plate with an ASD Inc. field spectroradiometer with a 3.5 degree fore-optic at a 40˚ angle.

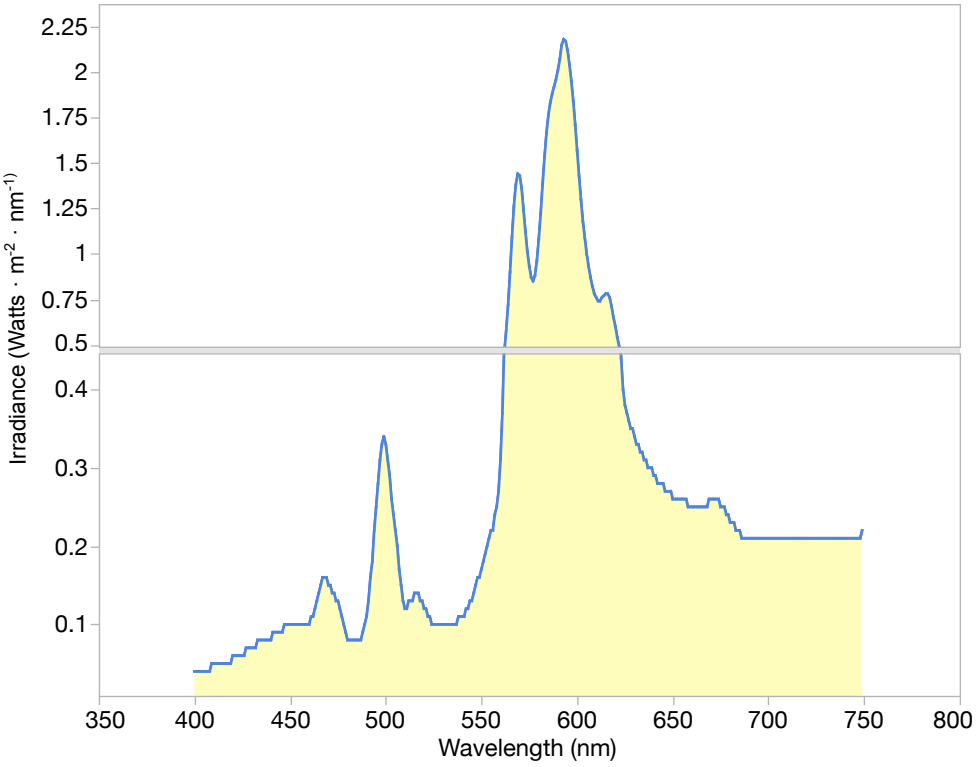


**Table S1**. Decimal bearing, wave-exposure classification, and annual orbital wave velocity for each collection site. Average annual orbital wave velocity was predicted using the CDIP model in ArcGIS (Erikson et al. 2014). Values represent average of "annual average velocity" raster pixels + standard deviation of averaged pixels within a 200m radius of the locality bearing. Locality bearings were chosen as the raster pixel on the10 meter depth contour closest to each collection site bearing.

| Site | Bearing | Habitat | Annual orbital wave velocity (m/s) |
|---|---|---|---|
| McAbee | N 36.61485 W 121.89706 | Protected | 0.167 + 0.0214 |
| Hopkins Marine Station | N 36.62365 W 121.90512 | Protected | 0.240 + 0.0489 |
| Stillwater Cove | N 36.56173 W 121.95091 | Protected | 0.345 + 0.0521 |
| Otter Pt. | N 36.63879 W 121.93328 | Exposed | 0.744 + 0.117 |
| Pt. Piños | N 36.63967 W 121.93600 | Exposed | 0.706 + 0.0846 |
| Sunset Pt. | N 36.56210 W 121.96477 | Exposed | 0.605 + 0.163 |

**Figure S2**. Boxplot of A) measurements of pCO2 of experimental seawater for 16 trials in the 2014 experiment and all trials in the 2015 experiment and B) measurements of pH during of experimental seawater for 16 trials in the 2014 experiment and all trials in the 2015 experiment.

**A)**

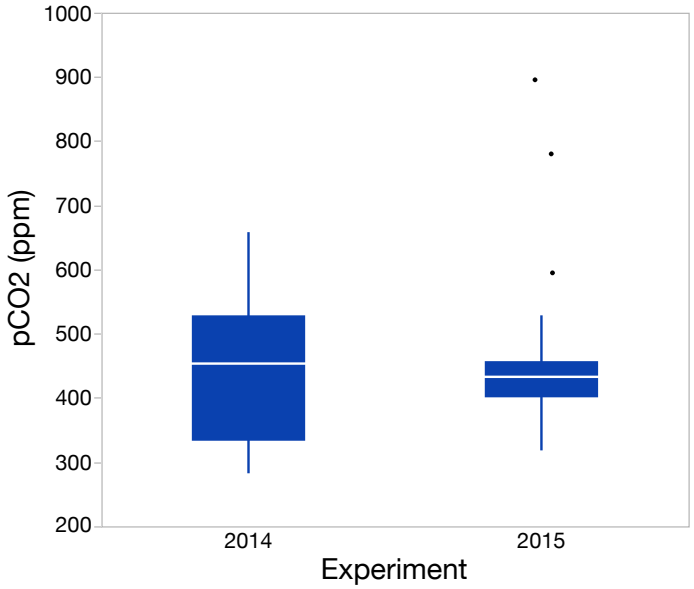


**B)**

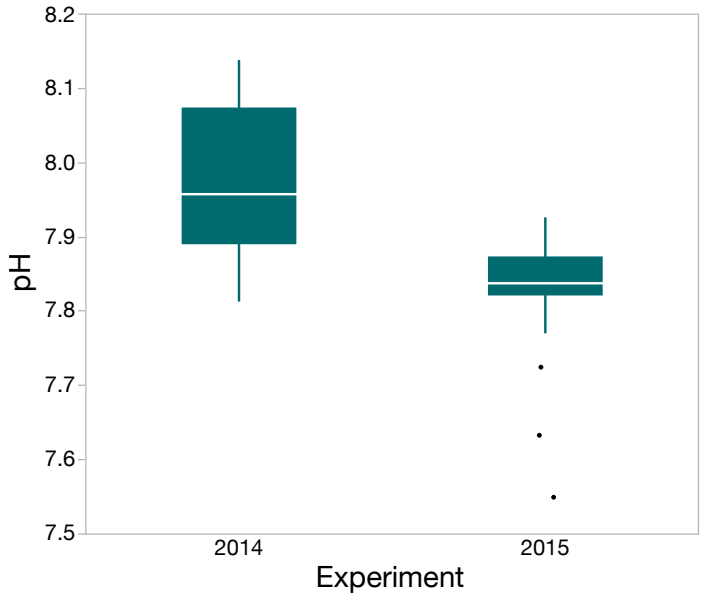

**Figure S3**. Percentages of 15 minute periods (A,B) and 60 minute periods (C,D) each day in October when velocities were less than or equal to 3 cm · $s^{-1}$ (blue), between 3 and 10 cm · $s^{-1}$ (teal) or greater than 10 cm · $s^{-1}$ (yellow) at the closest ADCP bin to the bottom (1.5 m above bottom; A,C) and the closest ADCP bin to the surface (8.5 m above bottom; B,D).

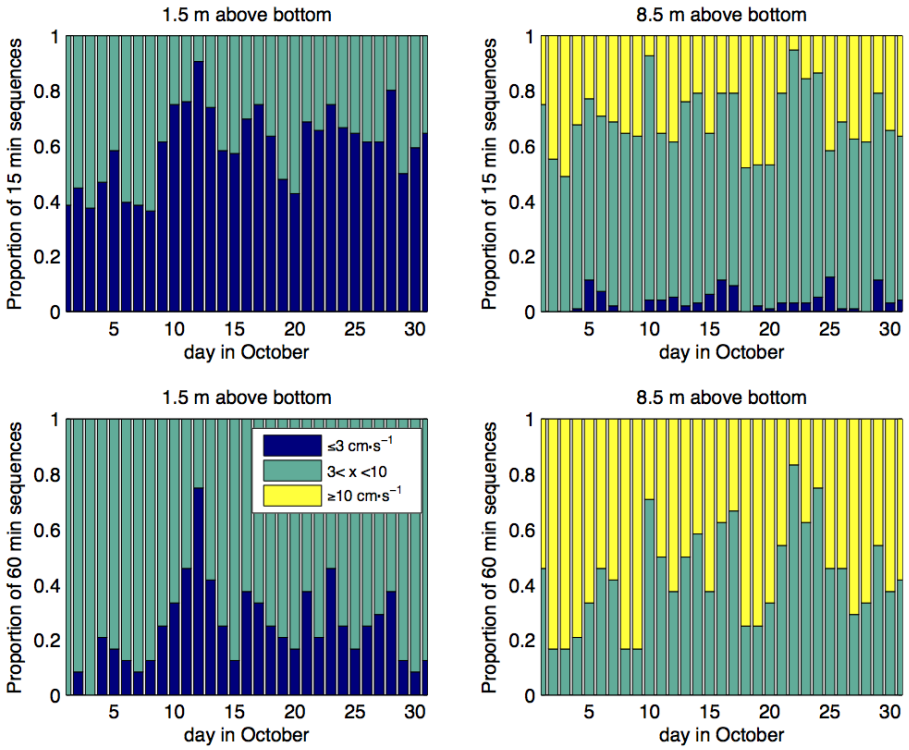

**Figure S4.** Average oxygen evolution rates for the four measurement phases (full photosynthesis (PS), acetazolamide-inhibited photosynthesis (AZPS), respiration period 1 (R1), and respiration period 2 (R2) for all trials over two measurement years (2014 and 2015). Error bars represent standard error.

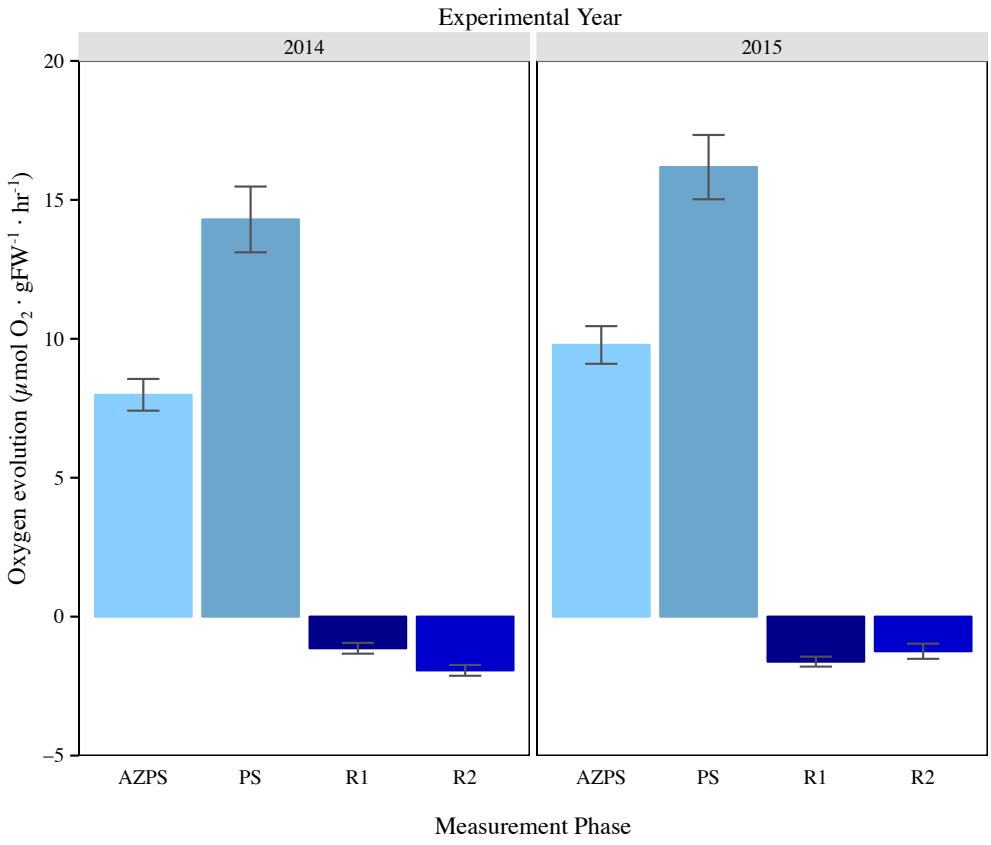

**Figure S5**. Gross photosynthetic rate of full (uninhibited photosynthesis, PS) and AZ-inhibited photosynthesis (AZPS) as a function of PAR level (1000 or 80 $\mu$mol photons · $m^{-2}$ · $s^{-1}$) and blade depth (surface and 10 meter depth). Each bar represents 4 replicate trials. The dashed line represents the maximum photosynthetic rate supported solely by $CO_2$ and an unknown proportion of bicarbonate (via active uptake). Error bars represent SE.

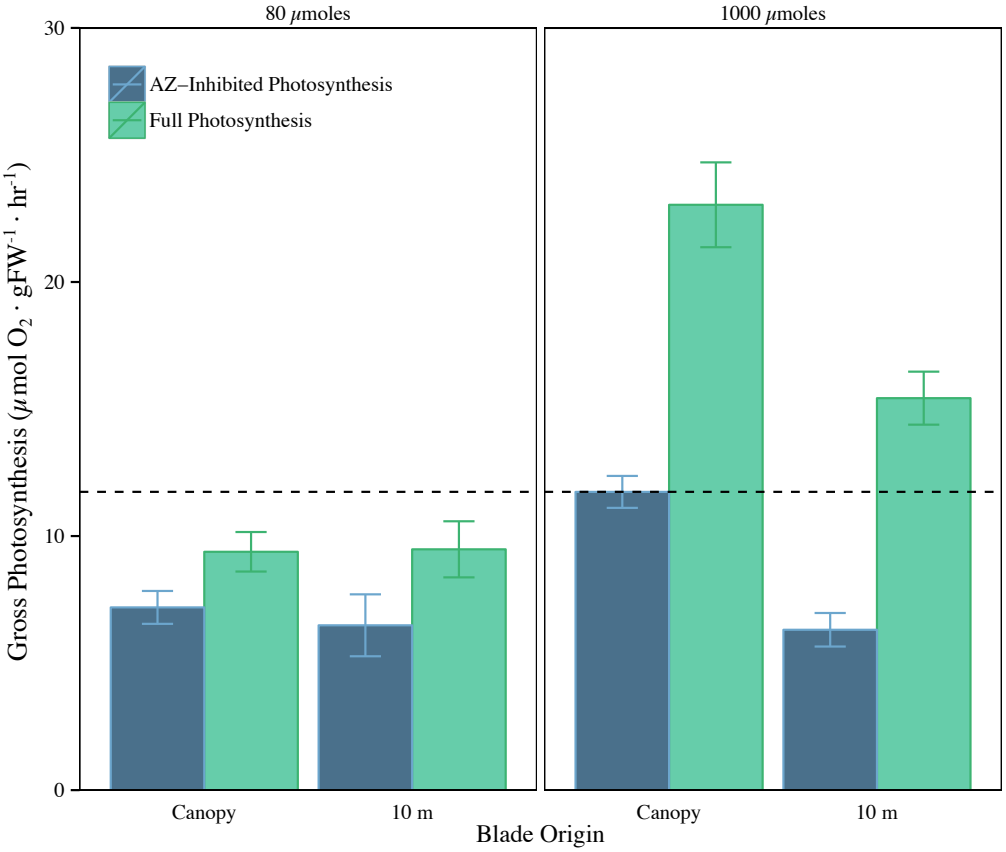

**Figure S6.** Gross photosynthetic rate of full (uninhibited photosynthesis, PS) and AZ-inhibited photosynthesis (AZPS) as a function of PAR level (800 or 100 $\mu$mol photon · $m^{-2}$ · $s^{-1}$) and flow velocity (3 and 10 cm/s). Each bar represents 4 replicate trials. The dashed line represents the maximum photosynthetic rate supported solely by $CO_2$ and an unknown proportion of bicarbonate (via active uptake). Error bars represent SE.

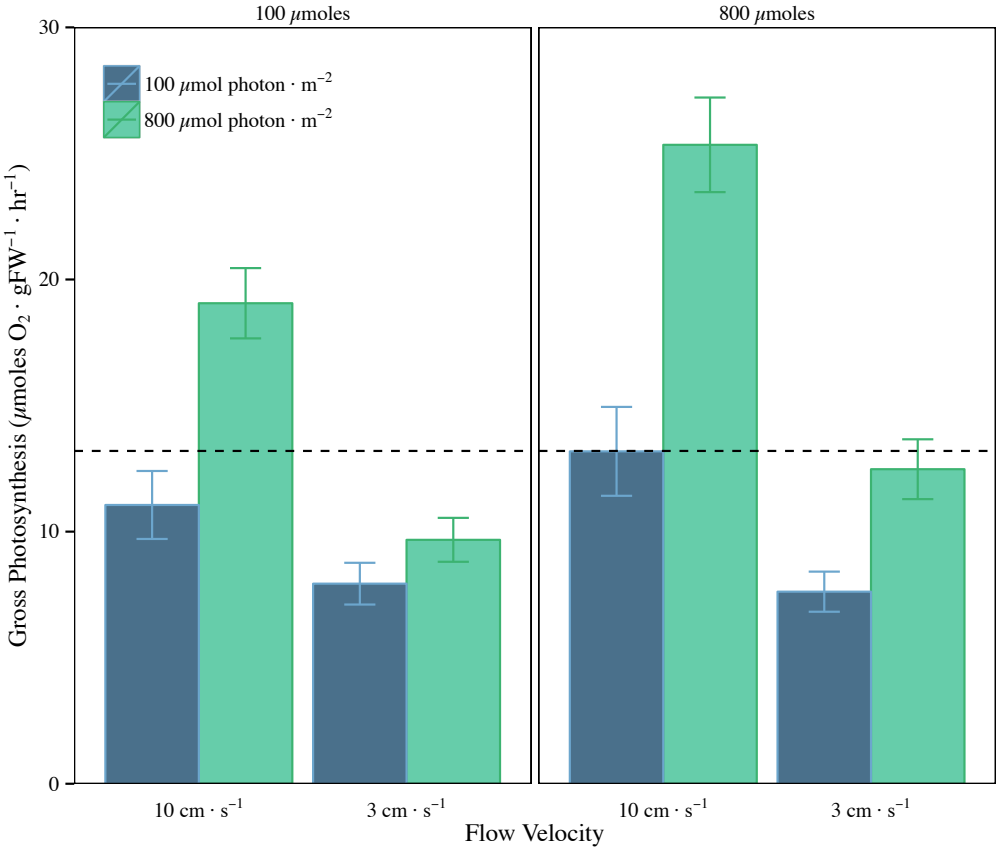

## Appendix 3:

## Supplemental Data for Chapter 3

**Table S1.**

| Site | Data | Coordinates | Mean orbital velocity | Exposure |
|---|---|---|---|---|
| Monterey Harbor | FLAVI | N 36.60890, W -121.89328 | NA | Protected |
| Steamer's Lane | FLAVI | N 36.95315, W -122.02174 | NA | Protected |
| The Breakwater | FLAVI | N 36.61079, W -121.89365 | NA | Protected |
| Hopkins Marine Station | Field study | N 36.62365 W -121.90512 | 0.24 + 0.049 | Protected |
| McAbee | Field study | N 36.61485 W -121.89706 | 0.17 $\pm$ 0.021 | Protected |
| Stillwater Cove | Field study | N 36.56173 W -121.95091 | 0.35 + 0.052 | Protected |
| Otter Pt. | Field study | N 36.63879 W -121.93328 | 0.74 + 0.12 | Exposed |
| Pt. Piños | Field study | N 36.63967 W -121.93600 | 0.71 + 0.085 | Exposed |
| Cypress Pt. | Field study | N 36.56210 W -121.96477 | 0.61 + 0.16 | Exposed |

**Methods for Pulse Amplitude Modulated Fluorometry of *Macrocystis pyrifera***

FvFm ratio and Rapid Light Curves (RLC) were measured using an Opti-Sciences OS1p fluorometer with a PAR clip on incubated *M. pyrifera* meristems. Measurements were carried out at dawn (low irradiance stress) and at 1 PM (high irradiance stress). For FvFm measurement, tissue was dark-adapted using dark clips (1 cm radius) for 20 minutes. Prior to measurement, proper effective fiber optic light intensity was set using the Auto Gain feature. Saturating Flash Duration was set to 1.2 seconds. For RLC measurments, response curves were measured on tissue clamped within a portable waterproof dark box. Tissue was dark-acclimated for 10 seconds prior to initiation of the RLC sequence. Actinic flashes were delivered in ten steps, increasing in intensity (Steps: 1, 3, 5, 7, 10, 20, 30, 50, 70, and 100% of full fiber optic intensity). Step 1 emitted 8-12 μmoles photons/$m^2$ PAR and 100% flash was ~1200 μmoles photons/$m^2$ PAR). The Absorption factor for calculating electron transport rate (ETR) was set at 0.80, and the saturating flash duration set to 0.8 seconds.

Figure S1. PAM fluorometry from Incubation 2. FvFm measurements of *M. pyrifera* meristems under high and low irradiance treatments in Week 1 (immediately following collection) and Week 2 (after incubation in FLAVI). Measurements were made at dawn (low light stress, top panels) and 13:00 (high light stress, bottom panels).

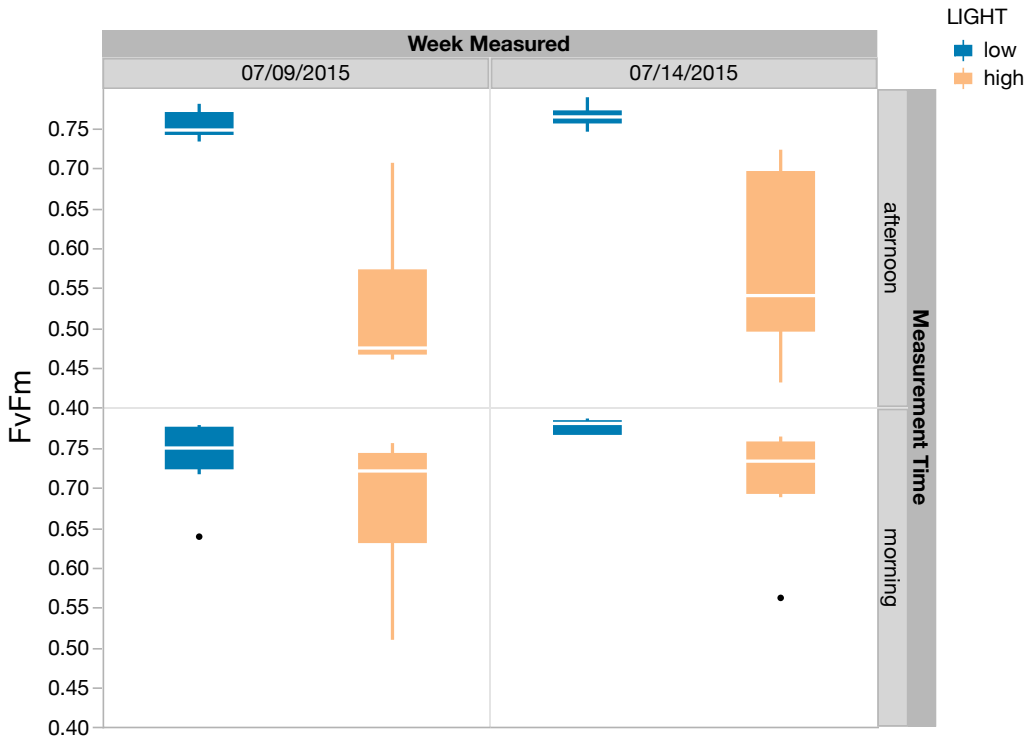

Figure S1. PAM fluorometry from Incubation 2. RLC measurements of *M. pyrifera* meristems under high and low irradiance treatments at dawn (left panel) and at 13:00 (right panel).